Characterisation of Glass Fibre Reinforced Epoxy (GRE) Composites in hot/wet Conditions

Hybrid Design

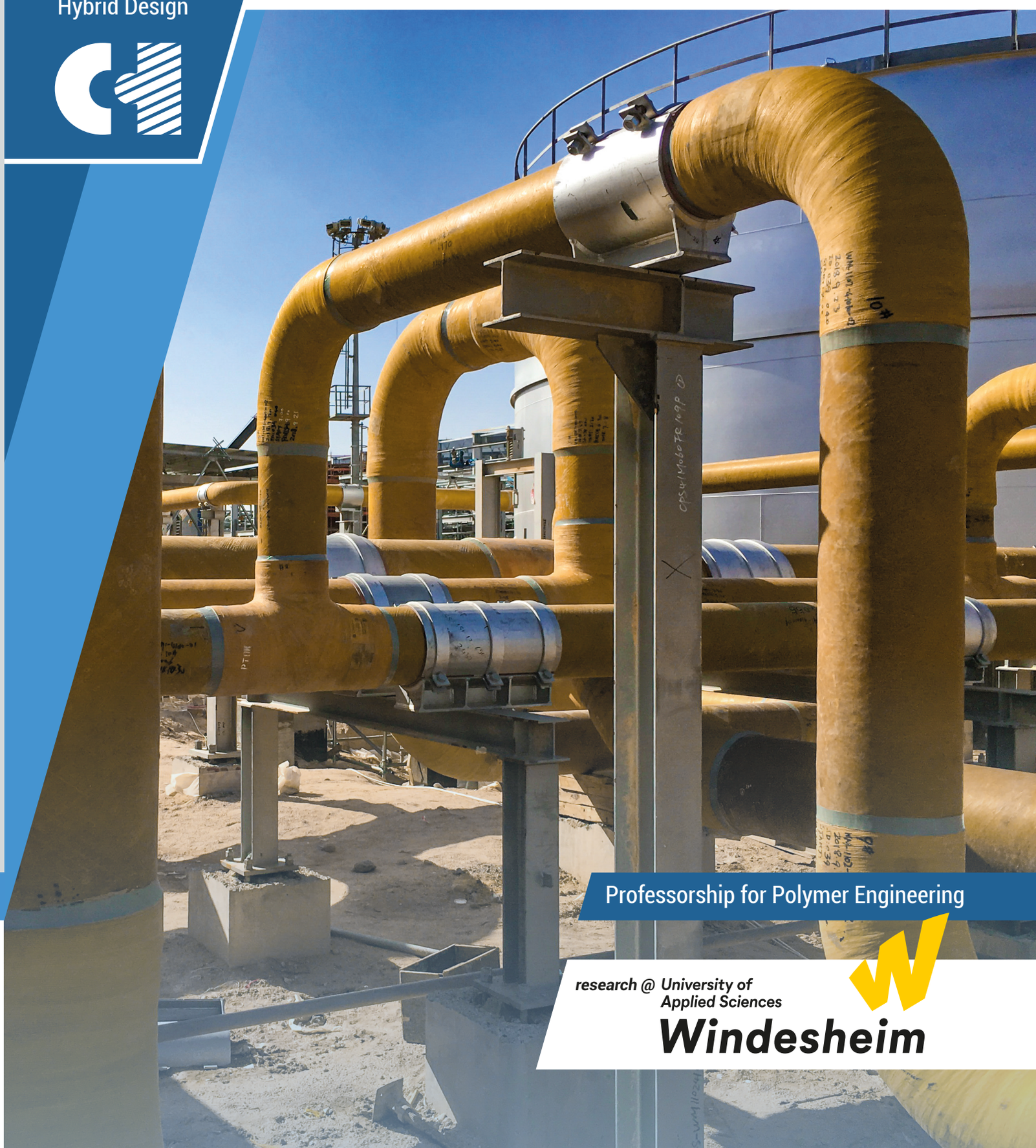

Professorship for Polymer Engineering

research @ University of Applied Sciences

Windesheim

Colophon

Title:	Characterisation of Glass Fibre Reinforced Epoxy (GRE) Composites in hot/wet Conditions
ISBN/EAN:	978-94-93243-00-2
Publication date:	July 2020

Authors: Dr. Ir. Albert ten Busschen (editor and researcher, Windesheim)
Dr. Ir. Martin Bennink (project leader and researcher, Saxion)

Participants:
Future Pipe Industries, Hardenberg
Ing. Kees Rookus, Ing. Jan ten Brinke, Henry Dubbink
Saxion University of Applied Sciences, NanoBio research group
Dr. Martin Bennink, Dr. Peter Schön, Ing. Rick Veenstra, Ing. Rick Baldenhofer, Michelle Fleermann MSc.
Windesheim University of Applied Sciences, Professorship of Polymer Engineering
Dr. Ir. Albert ten Busschen, Ing. Koen Hermans

Funded by: Tech for Future

Preface

This report describes the activities and results of the TFF-project 'Characterisation of glass-reinforced epoxy (GRE) composites'. The project has been carried out from October 2017 until December 2019 and was coordinated by the NanoBio Research Group of the Saxion University of Applied Sciences. Future Pipe Industries has been the client for the project. The project followed upon a TFF-project on the ageing aspects of glass fibres for GRE composites in the period 2014 – 2016, also commissioned by Future Pipe Industries.

This report is a non-confidential version of the original confidential report. In view of the non-confidentiality the glass fibre products that have been investigated are indicated with GF1, GF2, etc. Sometimes different supplies of the glass products have an extra 'A' or 'B' to indicate the difference. The carbon fibre product that has been investigated is indicated with CF1. Suppliers of the different reinforcement products are indicated with SUP1, SUP2, etc.

The participants of the project express their thankfulness for the funding of this project by the Centre of Expertise HTSM Oost: Tech For Future. This funding enabled this project and resulted in its valuable outcomes. We are much indebted for this.

The authors: Dr. Ir. Martin Bennink, Dr. Ir. Albert ten Busschen

Enschede, March 2020

Executive Summary

The report describes the development of test methods and the investigation of hot/wet-performance of glass fibre reinforced (GRE) composites combined with the effects of ageing of the glass fibre. This is of importance for the application of GRE in industrial piping systems at higher temperatures and in wet conditions. Future Pipe Industries (FPI) has good internal 'finger-print tests' to determine the hot/wet-performance of GRE, but these tests are labour intensive and require the use of a helical pipe winder along with a considerable amount of glass roving bobbins, both of which are sometimes not available. Moreover, the 'finger-print tests' do not provide insights on the failure mechanisms on micro-scale or on nano-scale. The assignment of the project consists of two parts: 1) development of test methods and 2) investigation of GRE-performance at hot/wet conditions.

For a macroscopic test method, a test specimen build up has been developed based on 'cross-ply' reinforcement. The test method to test this specimen is called short beam 0/90 (SB-0/90). It is performed as a bending test on a specimen with layers in 0 and 90 degree direction. The comparison with the 'finger-print tests' showed a good correlation, both for the effect of glass ageing and for the effect of hot/wet-treatment of the GRE system. Making specimens requires only one or two roving bobbins and a rotating device like a lathe.

The performance at hot/wet condition of various glass fibre roving types in an epoxy matrix has been investigated both at macro-scale (using the newly developed cross-ply SB-0/90 test) and at microscopic/nano scale. A special polishing procedure was developed to obtain a surface of the sample that was sufficiently smooth on nano-level. This enabled Atomic Force Microscopy (AFM). With optical microscopy (DIC), a cross-section of a specimen could be investigated on occurrence of cracks. By quantifying the number of cracks observed in the cross-section a good correlation was found with the macroscopic SB-0/90 test. Moreover, good correlation was found with FPI's fingerprint test. In addition to the research on fibre glass rovings, a limited comparative research was done on carbon tow in an epoxy matrix.

With the test methods developed, eight glass roving types were investigated on performance of GRE in hot/wet-conditions both with fresh rovings and with rovings that are aged for 6 weeks at 50 °C. Two rovings, GF1 and GF7 were found to give significantly lower values when the rovings were aged but not subjected to hot/wet treatment. After hot/wet-treatments for 250 hours at 100 °C, 115 °C and 125 °C it was found that GRE made with rovings GF1 and GF2 show the strongest drop in properties (over 50%) when compared to the initial results. The roving GF3 showed the best retention. When aged rovings were subjected to hot/wet treatments between 100 °C and 125 °C the same ranking of performance of the glass fibre products was found.

Microscopic evaluation of the cross-sections of the cross-ply laminates revealed dark spots in between the glass fibres. As conditions applied in the hot/wet treatment become more severe (longer times and higher temperatures), the number of the dark spots increased. Based on the observations, the dark spots are thought to grow into cracks, which ultimately lead to a lower strength of the material.

The best-performing roving, GF3 and carbon fibre rovings CF1 have been evaluated at hot/wet-exposure of 250 hours to 100 °C and 150 °C, respectively. After an exposure at 150 °C the carbon fibre composites showed a retention of properties of 50% or more, whereas the glass fibre composite dropped to less than 20% retention.

In conclusion the project has resulted in the development of both a macroscopic and a microscopic test method for characterizing GRE after hot/wet treatment for fresh and aged glass fibre roving. AFM and SEM-evaluation did not reveal interphase degradation mechanisms on atomic level. Eight commercially glass fibres have been evaluated on resistance to ageing and performance in GRE after hot/wet treatment. At temperatures as high as 150 °C glass fibres do not seem suitable for hot/wet-environment but carbon fibre composites seem promising under these conditions.

Table of Contents

Glossary

Aged	Conditioning glass roving or carbon tow in an oven at 50 °C for 6 weeks to simulate storage.
Fresh	Not-aged roving or carbon tow, as received from manufacturer.
Initial	Test condition of fresh or aged roving without (hot/wet) treatment.
Hot/Wet treatment	Exposure to water of laminates produced of glass fibre roving or carbon tow. In this project laminates have been exposed to water at temperatures of 100 °C, 115 °C, 121 °C, 125°C and 150 °C. Exposure times vary from 250 hrs. up to 3000 hrs.
Cross ply	Laminate, built up of layers in 0° and 90° direction.
ATS	Axial Tensile Strength
UEWS	Ultimate Elastic Wall Stress
ILSS	Inter Laminar Shear Stress
GRE	Glass Reinforced Epoxy
Matrix	Binding component in GRE (Epoxy/Hardener combination).
SB 0/90	Short Beam test for cross plies, built up of layers in 0° and 90° direction.
Fingerprint	FPI program consisting of several mechanical tests to indicate the quality of pipe laminate.
IPN	Inter Penetrating Network
DIC	Differential Interference Contrast
SEM	Scanning Electron Microscopy
AFM	Atomic Force Microscopy
AFM IR	Atomic Force Microscope InfraRed

1. Introduction

1.1. GRE pipe systems

Industrial pipe systems have been developed for the transportation of liquids and gases. For the transportation of corrosive fluids the use of steel for pipe systems is problematic. In those cases, pipe systems made of plastics are suitable. Often thermoplastic polymers like polyethylene (PE) and polyvinylchloride (PVC) are used. However, these plastics do not have high strength at elevated temperatures. In the case that a high internal pressure is applied in the pipe system it is necessary to use fibre reinforced polymers for the manufacturing of the pipe system. Both thermoplastic fibre reinforced (RTP, Reinforced Thermoplastic Pipe) and thermoset fibre reinforced (RTR, Reinforced Thermoset Resin) pipe systems are available. RTP is used successfully as small diameter spoolable high pressure line pipe whereas RTR piping has a long history in larger diameters.

Future Pipe Industries (FPI) has developed both RTP and RTR pipe systems. This report focuses on RTR or, more specifically, glass fibre reinforced epoxy (GRE) piping. These systems have been manufactured and installed by FPI world-wide successfully for decades.

Figure 1. Examples of GRE applications

The pipe systems of FPI are based on tubes and auxiliary parts that are manufactured by means of filament winding of glass fibres impregnated with epoxy resin around a rotating mould (Figure 2). By axial movement of the supply of the impregnated glass bundles (roving) along the rotating mould, the reinforcement is orientated with an angle to the rotating axis. Normally for thrust resistant pipe

Figure 2. Production of GRE pipes via winding

systems with internal pressure the winding angle is 55 degrees, which provides an optimum reinforcement for the transmission of the hoop stresses and the axial stresses in the pipe wall.

The glass fibres are manufactured by a spinning process from molten glass. In this manner bundles of filaments (roving) are formed. Individual filaments have diameters ranging from 17 to 27 micrometre, depending on the application and product type. During the spinning process a so-called sizing (or 'finish') is applied on the filaments that is crucial for the behaviour of the roving and for the interaction with the polymer in which the roving is subsequently embedded. The sizing is applied on the glass filaments by means of a water-based emulsion. Therefore, the products must be dried after forming. In the past the glass fibre bundles were formed on carton tubes, then dried and baked and finally unwound from the carton tubes and assembled into a roving bobbin (Figure 3). Now the roving bobbin is directly formed with the so-called 'direct draw' process, after which the complete bobbin is dried and baked. As compared to the fibre diameter (17-27 μm) the thickness of the final sizing on the fibres is very small in the order of 50 nm.

The glass fibres traditionally were made of so-called E-glass, which is a high-strength glass with a defined content of boron-oxide. As a result of environmental legislation, the glass composition gradually became boron-oxide free. This started with E-CR-glass of OCF in the 1990's. Nowadays most standard glass fibre products have a boron-oxide free composition. A detailed description of glass fibre reinforced plastics is given in various text-books, e.g. Composites – An Introduction by Nijssen (2015).

Figure 3. Direct roving bobbin

Markets for the GRE-based pipe systems are amongst others in the oil- and gas exploitation, (petro-) chemical plants and geothermic energy recovery. The pipe systems have proven long-term resistance to various chemicals, generally up to a temperature of 100 °C. Most of the times the fluids in the pipe systems are aqueous.

In the market there is a demand for pipe systems that can withstand long-term exposure to higher temperatures. This is a result of several trends. In the oil- and gas exploitation there is a trend to drill deeper which consequently results in higher temperatures e.g. injection fluids that have to be transported. Also, with regard to geothermal systems for energy recovery or energy storage in the soil there is a need to transport fluids with higher temperatures. Typically, there is a need for the transportation of corrosive aqueous fluids with temperatures up to 150 °C. The current GRE pipe systems, however, are not capable for the long-term use in aqueous conditions up to these temperatures.

1.2. Test methods

During the development of composite products, various test methods have been developed to characterize the behaviour and the performance. The high quality and safety standards in the aerospace industry have led to the build-up of extensive knowledge and standardization of the testing of fibre reinforced polymers (composites) during the 1960's and 1970's (Figure 4). Specially the mechanical performance (strength, stiffness, toughness) is of importance to test. Generally, this is done (quasi-) statically but also after certain conditioning (exposure to chemicals or to ageing) and prolonged loading (fatigue and creep). An overview of mechanical testing methods of composites is given in Appendix 2.

Figure 4. Example of composite testing

In particular for GRE pipe systems specific testing protocols have been developed. In this introductory chapter only a description is given of the test methods that are of relevance for this report. The most straight-forward method is to make a filament-wound pipe and subject it to mechanical loading. This is done in the so-called Ultimate Elastic Wall Stress (UEWS) test (Figure 5). In this test, a filament-wound GRE pipe is closed at its ends and loaded hydrostatically by water from the inside. This results in hoop stresses and axial stresses in the pipe wall. The internal test method of FPI (WS-TM-017) describes a cyclic loading programme with increasing maximum pressure.

Figure 5. Ultimate Elastic Wall Stress (UEWS) setup

By using strain gauges, the axial strain can be measured during loading and the deviation from a linear stress-strain relation is used to determine the maximum hoop stress for linear behaviour. The pipe is 'free hanging' during the test to obtain a biaxial loading condition by internal pressure. Normal ultimate hoop stress values for linear behaviour that are found in a UEWS test are around 170 MPa for 55° winding angle. The UEWS test can be performed on a fresh made tube sample (initial) or after conditioning (hot/wet treatment), for example after exposure of the pipe to 1500 hours in water of 80 °C.

Another test method on filament-wound pipes is the Axial Tensile Test (ATS). In this test the pipe is clamped in a testing machine and tested until failure (Figure 6, left). FPI has an internal test procedure for this test (WS TM 003), which is in line with ASTM D2105. Normal axial stress values at failure that are found in this test are around 70 MPa for 55° winding angle. Another test method based on ATS is: ATS on pipe strip. In this test, strips are cut from a pipe and clamped in a testing machine and tested until failure. This can be done with initial and hot/wet treated specimen.

Interlaminar Shear Strength (ILSS) is a classical test to determine the adhesion between fibres and the polymer (Figure 6, right). The principle of the test is a short-beam three-point bending test on a strip of a laminate. As a result of short span of the supports, shear failure by delamination occurs prior to failure as a result of normal stresses.

Figure 6. Left, Axial Tensile Test (ATS) on pipe. Right, Inter Laminar Shear Strength (ILSS) test.

ILSS tests for GRE pipe applications can be performed on pipe segments, on hoop-wound segments from so-called NOL-rings and on strips from laminates that were made of woven roving. Depending on the procedure for the ILSS test, normal shear strength values for a glass – epoxy combination range from 50 to 70 MPa. Although ILSS is a discriminative test for other composites, the results from the previous TFF project showed that the ILSS-test on NOL-ring segments and pipe segments for GRE pipes were not as distinctive as the UEWS and ATS tests. The reason for this is probably that on microscale it is a loading pure on shear. Already in the 1990's it was found that ILSS-test are sometimes not discriminative enough to characterize fibre-matrix interaction. Although the ILSS-test is known to be generally a good test for this for fibre-reinforced plastic composites, specifically for GRE-type of composite that are used in industrial pipes this test is not as discriminative as e.g. UEWS or ATS test, see the article of Ten Busschen at the AVK-Tagung of 1997

ILSS performed on woven roving laminates showed a better performance distinction because in that case partly transverse loading occurs. However, for testing a roving type in this manner first a woven roving fabric must be made of it by weaving. This requires a loom (Figure 7). Moreover, when both weft and warp of the fabric is to be made of the roving type a manifold of roving bobbins is needed to compose the weaving beam for the warp direction. When only one roving bobbin is available only the weft in the fabric can be made of the roving type to be investigated.

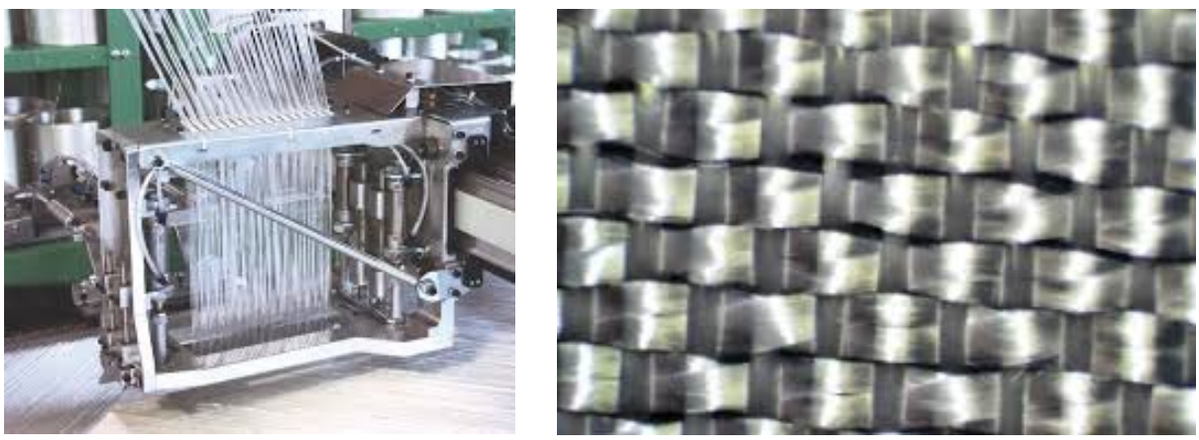

Figure 7. Left, weaving of glass fibre to make woven roving. Right, woven roving fabric

1.3. Ageing of glass fibre sizing

The sizing on the glass fibre is very important for the interaction with the polymer in which it is embedded to form the reinforced composite structure. In case of the GRE pipe systems the sizing contains components that promote the adhesion between the glass of the glass fibre and the epoxy resin. Generally, silanes are used as a component in the sizing to promote the adhesion. The adhesion between the glass fibre and the epoxy matrix is of paramount importance for the structural integrity of the GRE product and its mechanical performance. In the directions perpendicular to the fibre reinforcement (transverse directions) the strength is highly determined by this adhesion. This is explained by a micromechanical approach of the composite in Appendix 1.

Moreover, the sizing also determines the processing properties of the glass fibre roving. The sizing binds the individual filaments together to form a bundle, the actual roving. This is realized by the binder components that are in the sizing. On the other hand, the sizing must not hinder the impregnation of the filaments with the resin during the production process. When the sizing is too hard (too insoluble) or there is too much sizing present on the glass fibres it may impair the impregnation. Poor impregnation may cause air inclusions that extend along the glass fibres. This should not be confused with voids in the sense of small air bubbles. These are not a result of bad impregnation but more likely, they result from mixing, resin-return systems and turbulence in the impregnation systems themselves.

Currently, glass fibre roving for filament winding is produced by means of the so-called 'Direct Draw' technology. This implies that the roving spool (bobbin) is directly formed during the spinning process. After forming the roving bobbin is dried to remove the water that was brought in through the sizing-emulsion and then baked at a higher temperature for further curing of the sizing components. During drying however, the migration of water through the bobbin will also cause some migration of the sizing to the outside surfaces of the bobbin. This results in a sizing-rich skin on the outside of the bobbin. The content of sizing on a glass roving for filament winding generally is 0.5% by weight but can be twice as high in the sizing-rich skin of the bobbin. These sizing-rich parts of the roving may be more

difficult to impregnate than the other parts. In Figure 8 it is illustrated how the sizing-rich skin (orange) is located in the roving bobbin and how this results in sizing-rich parts along the roving when this roving is drawn from the bobbin.

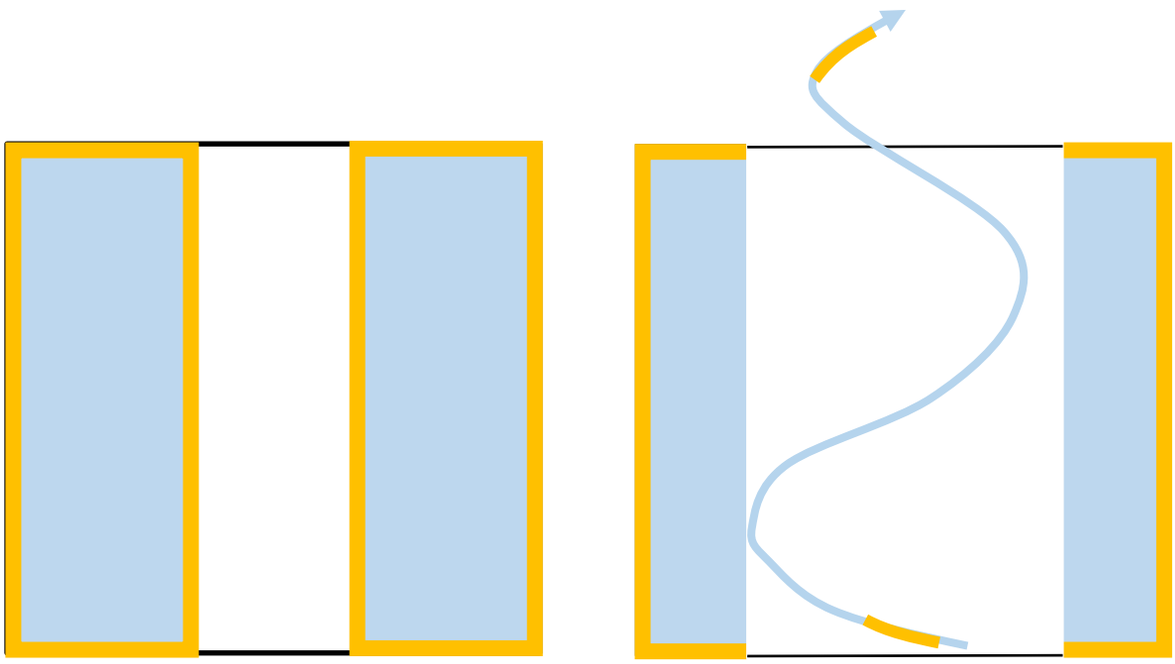

Figure 8. Left, direct draw roving bobbin, as supplied. Right, bobbin during use. The orange colour indicates the resin rich layer of the bobbin.

Specifically for glass fibre roving for the application in epoxy it has been found that the sizing of these products is sometimes susceptible to ageing during storage. Long-term storage of some glass roving products at high storage temperatures (up to 50 °C) has been found to be detrimental to the adhesion properties in GRE products. Specially at production sites at locations with climate conditions as e.g. in the Middle East this has led to problems with some glass roving products. Some aged glass fibre roving products gave a very poor performance in UEWS and ATS tests. In reaction to this problem, some glass fibre producers have developed glass roving for GRE application that suffer less from ageing during storage at high temperatures.

1.4. Results of the previous TFF-project

In the previous TFF-project for FPI the phenomenon of glass fibre ageing was investigated (see report 'Effects of aging of glass fibres on the mechanical properties of the composite pipe systems'). This study was reported in 2016 and comprised an extensive investigation of the performance in GRE pipe application of various roving products after ageing. In the report of 2016, a detailed description can be found of the research. Here the most important results of that research are given, these form the starting point for the current research.

All tests in the previous project were performed both on material with MDA as a hardener and with IPD as a hardener. In earlier days MDA was used in GRE pipe production but has been abandoned in the EU because of REACH-legislation. Nowadays, a MDA-free and a formulated IPD is used as a hardener. For the tests, the different roving products were both used as received for making test material and after ageing the roving for 6 weeks at 50 °C in a hot air oven to simulate prolonged storage at high temperatures. The test samples were tested both before and after prolonged exposure to water at

elevated temperatures (80 °C and 100 °C, depending on the test). The test programme of the previous project comprised the following six glass fibre roving types, see Table 1.

Roving type (finish)	Manufacturer
GF5-A	SUP5
GF3-A	SUP2
GF9	SUP2
GF2	SUP1
GF4	SUP3
GF10	SUP7

Table 1. Glass fibre roving types investigated in previous TFF-project

The effect of glass roving ageing on the mechanical performance was clearly seen for some roving products in the UEWS test. Of the six rovings that were investigated, two rovings GF5-A and GF9 were clearly affected by the hot-storage treatment. This was significantly more pronounced when using IPD as a hardener than with MDA as a hardener. The UEWS-values of these rovings dropped for more than 50% after ageing.

The same effect was seen with the ATS test. The effect was not so large as with the UEWS test. Again, the effect was clearly more pronounced when IPD is used as a hardener than when MDA was used. Contrary to the UEWS test the effect of hot-water treatment on the GRE-product (1500 hours in water of 80 °C) gave in the ATS an extra decrease of properties for the two rovings mentioned that are affected by the hot-storage ageing.

Because UEWS and ATS tests on laminate samples made with fresh and aged roving are both discriminative tests, they are described as 'fingerprint tests' within FPI. Moreover, the ATS test has also been adopted to test the effect of a change in raw materials in the latest version of the standard ISO 14692 'Petroleum and natural gas industries – Glass-reinforced plastics (GRP) piping (2017).

ILSS tests on helical wound pipe segments were found not to be very useful in this investigation to discriminate between the performance of roving after hot-storage ageing.

A chemical analysis with infrared spectroscopy analysis (FTIR) on the sizing of different roving products was performed to discover possible changes after long-term hot air treatment. Clearly a relation was found between the decrease of the number of epoxy groups (measured at wavelength 915 cm^{-1}) at prolonged ageing of the roving in hot air and the decrease of adhesion performance. Also, a comparison was made with rovings that were aged in hot air with a high humidity. It was found that the humidity accelerates the decrease of epoxy groups in the sizing in a hot-air environment.

Optical microscopy and Atomic Force Microscopy (AFM) did not reveal the mechanisms behind the difference in performance between the different rovings tested in the report of 2016.

1.5. Hot-wet behaviour of GRE

The performance of GRE-pipes is of particular interest in an environment that has high temperature in combination with the presence of water. These so-called hot-wet conditions occur in several applications in oil and gas exploration, chemical industry and geothermic installations. As indicated in 1.1 there is an increasing demand from the market for GRE pipe systems for hot-wet applications at higher temperatures (up to 150 °C).

The accepted method for the determination of the long-term hot-wet performance of a GRE pipe system is by the use of regression lines. The principle of this is to determine the time to failure of a pipe that is pressurized at different pressure-levels at a certain temperature. By representing the test data in a double logarithmic graph, long-term performance can be obtained by extrapolation as illustrated in the figure below (Figure 9).

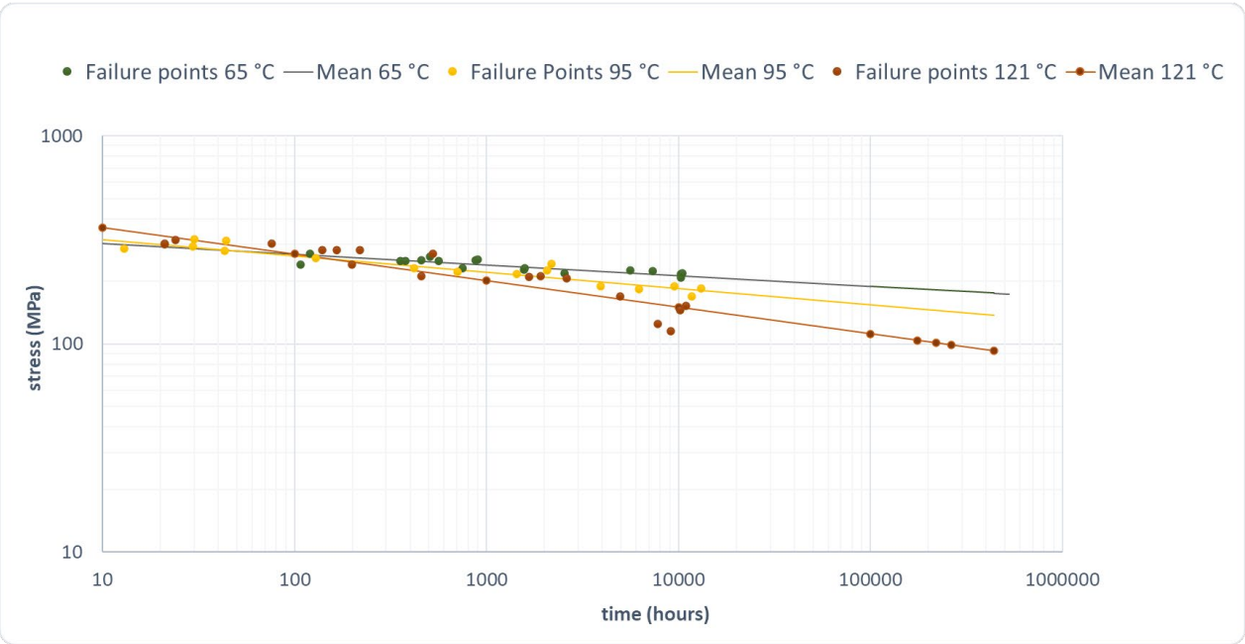

Figure 9, example of a stress-based regression line for GRE

The method for this is described in the American standard ASTM D2992 – 18 'Standard Practice for Obtaining Hydrostatic or Pressure Design Basis for 'Fiberglas' (Glass-Fiber-Reinforced Thermosetting Resin) Pipe and Fittings'

This method of determining the long-term performance of GRE-systems by testing several GRE pipes at different temperature levels involves much effort. A more small-scale test that is as discriminative would be desirable.

A critical note has to be made regarding the use of regression lines at hot-wet-conditions that are too severe. Because when these conditions already result in internal material damage even without loading the use of regression lines for long-term performance is questionable.

2. Research assignment

2.1. Macroscopic test method glass roving

As described in the previous chapter, tests on filament-wound GRE pipes like UEWS and ATS (the 'finger-print tests') are discriminative tests. However, these tests involve much work and require equipment (for example a pipe winder) for manufacturing the test material and for the test itself. Moreover, manufacturing of the pipes requires a manifold of roving bobbins (minimum 6). Therefore, the UEWS and ATS are not quick tests that a laboratory can use to investigate the expected performance of raw materials in GRE pipes when only one or two roving bobbins are available.

ILSS is a test method that can be done when only one roving bobbin is present and no facility for filament winding of GRE pipes is available. To make sample material for the ILSS test it would only require a means of impregnating the roving and forming the impregnated rovings into a plate or a rod. Testing ILSS can also be done after samples are exposed to hot water. Appendix 2 describes ILSS tests methods.

Through many years of experience by FPI it is clear that ILSS is not a discriminating test for the performance in GRE pipes as long as the specimens are tested by using only shear stresses during loading. This has already been reported by Ten Busschen in his contribution to the AVK-Tagung in 1997. In this article other methods are mentioned that are connected to the glass-epoxy adhesion. However, these tests are either not easy to perform or they are not discriminating enough. Thus there remains a task to find or to develop a macroscopic test method to evaluate the performance of a glass roving. Therefore, the research assignment was defined as follows:

- To propose a macroscopic lab-scale test method capable of detecting these effects.
- To examine the effects of hot-wet conditions on fibre glass- and carbon reinforced epoxy composite integrity.
- To find the relation between data from this proposed test method and the microscopic observed (lack of) composite integrity.

The aim of the proposed macroscopic lab-scale test is to assess GRE composite raw materials including (but not limited to) fibreglass roving. The proposed test method would therefore have to comply with following requirements:

- Discriminative for the performance in filament-wound GRE pipes at least similar to FPI's fingerprint tests based on UEWS and ATS.
- Can be performed when only one roving bobbin is available.
- Can be performed with basic specimen preparation and standard lab testing equipment.

For this part of the project the following deliverables have been identified:

- Deliver a routinely usable procedure, including description of materials and machinery needed, to fabricate test samples at a sufficiently reproducible quality.
- Deliver a routinely usable test procedure complying to the research assignments.

2.2. Microscopic and nano analysis method of glass-matrix interphase

The interphase between the bulk glass of the fibre and the bulk epoxy matrix is effectively a three-dimensional region. The glass fibres are coated with a finish (so called “sizing”) that interacts on one side with the glass and on the other side with the epoxy matrix. This creates a region of some finite thickness consisting of various phases: glass, glass-to-sizing, sizing, sizing-to-epoxy and epoxy matrix. This interphase with its various phases is pivotal for the improvement of the compatibility between the fibre and the matrix by forming a strong but tough link between all phases. This effectively determines the mechanical and thermal stability of the fibre composite material on the macroscopic scale. Therefore a better understanding of what happens at this interphase at the micro- and nanometre scale as a function of the composition of the sizing layer components, the epoxy matrix and the glass/carbon fibre materials and when the material is aged or stored at hot-wet conditions should provide profound fundamental information on the ageing mechanisms or origin of composite material failure. This in return will give pivotal input for composite fabrication.

In the framework of the first collaborative project between Future Pipe Industries (FPI) and the Saxion University of Applied Sciences in Enschede microscopic and nanoscopic characterization by atomic force microscopy (AFM), optical microscopy (phase/DIC) and SEM were introduced in proof-of-principle experiments on glass fibre (coatings) and polished glass fibre composite cross sections. These preliminary encouraging results immediately provided unique insights in the glass-fibre epoxy interphase and co-initiated the continuation of the collaboration to further explore the aging mechanism on composite samples.

The preliminary microscopic/nanoscopic characterization results from the last project shall be substantially explored and expanded within this project. Important to mention is that for the microscopic analysis, an appropriate procedure for polishing the sample surfaces is essential and will be developed during this project.

For this part of the project the following deliverables have been identified:

- Obtain a deeper understanding of the mechanism of glass fibre ageing independent of crude material and composite composition
- Explore and establish microscopic and nanoscopic characterization (optical microscopy/SEM/AFM) for analysis
- Deliver a routinely useable, systematic polishing procedure, including the necessary infrastructure with labs, instrumentation and working protocols.

2.3. Characterisation of relevant glass-matrix systems

Various glass roving products are available in the market for filament winding of GRE pipes. In the previous research six glass roving products have been investigated with UEWS and ATS (see Table 1, in the previous chapter). But other products are also interesting. For the current study, glass roving products were selected to investigate the following research aims:

A. Investigation of interphase for ageing stability with an optical microscope
B. Nano-investigation of interphase for hot-wet resistance
C. Investigation of the performance of existing products and new/improved products

2.4. Long term hot-wet exposure

To investigate the effects of long term hot/wet conditions, cross plies produced with research and test rovings have been exposed to water at a temperature of 121 °C (250 °F) for 500, 1000, 3000 and 5000 hrs and have been tested with SB 0/90.

2.5. Comparison with carbon fibre reinforced systems

FPI investigated the performance of filament-wound carbon fibre epoxy (CFRE) pipes. These tests showed superior pipe performance in hot-wet-conditions up to 150 °C. Moreover, this product does not seem to suffer from the ageing phenomenon as was encountered by some glass fibre products. Therefore, carbon fibre products were investigated further in this study.

3. Macroscopic test method

3.1. Literature search

In the sixties mechanical testing methods for fibre reinforced polymers started to develop. This development began in the aerospace industry because applications of materials in this industry directly require reliable testing methods for securing both quality and safety. Gradually the development of test methods for fibre reinforced polymers expanded in other industries. A general overview of the current state is given in Appendix 2.

In the present study the characterization of the transverse strength behaviour is of interest. As explained based on micromechanics in Appendix 1, the transverse strengths of fibre reinforced polymer is determined by several aspects: strength of the polymer itself, the interaction (adhesion) between fibre and polymer, residual stresses (e.g. due to shrinkage), fibre distribution, the occurrence of imperfections (e.g. voids), etc.

It is important to give a definition of the transverse stresses, see Figure 10.

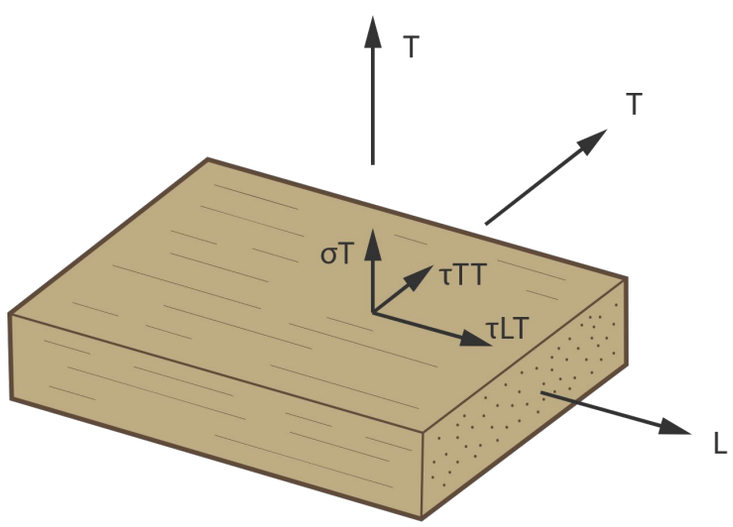

Figure 10. Transverse stresses acting on a unidirectional composite part.

Two fibre directions can be distinguished, in line along the axis (Longitudinal direction: L) and perpendicular to the fibre direction (Transverse directions: T). Three transverse stress components are defined:

Transverse normal stress:	σ_T
Longitudinal-transverse shear stress:	τ_{LT}
Transverse-transverse shear stress:	τ_{TT}

3.1.1. Transverse normal strength tests

The transverse compressive strength is not of interest for the present project because GRE-pipes with internal pressure do not contain areas of unidirectional (UD) reinforced material that are loaded in transverse compression.

Relevant for the present project is the transverse tensile strength. In literature a straight-forward testing of the transverse tensile strength is reported as the testing of a strip that is clamped in the testing machine and tested until failure (see e.g. Whitney, Daniel and Pipes, 1984). The principle of this test is depicted in Figure 11.

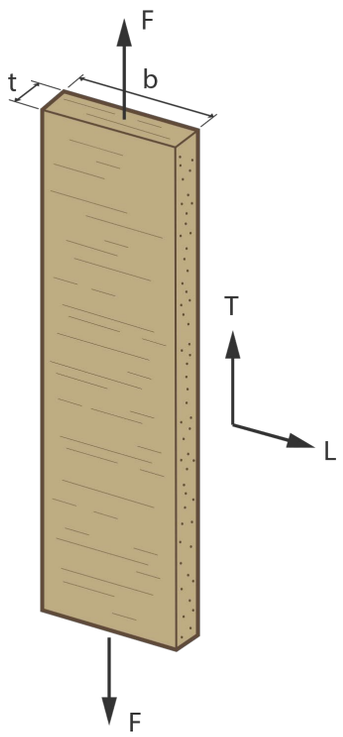

Figure 11. Principle of testing transverse normal strength with a UD-strip.

The transverse tensile strength, $\sigma_{Tt,max}$, is calculated as the maximum force at breakage of the strip, F_{max} divided by the cross-sectional area (b · t), A:

$$\sigma_{Tt,max} = \frac{F_{max}}{A} = \frac{F_{max}}{b \cdot t}$$

The low value of the accompanying rupture strain in transverse tension means that the test is very sensitive for misalignments of the test setup and for deviations in the shape of the specimen (non-straightness, variations in thickness).

The effect of the imperfections in the side-edges of the strip that is cut from a larger panel and in the laminate production (e.g. voids) are uncertain. This makes the test method sensitive to rapid crack propagation from the imperfections that result in scatter in the test outcome.

A method to determine the transverse tensile strength of UD-GRE that does not suffer from the above-mentioned uncertainties is the so-called 'ring-test' that has been proposed by Ten Busschen (see PhD-thesis of 1996 and AVK-conference of 1997). The method is based on the pulling of a thick-walled, filament-wound ring with a cut on one side. Because of the development of radial stresses at the opposite side of the cut, transverse failure occurs at this location. The principle of the test method is depicted in Figure 12.

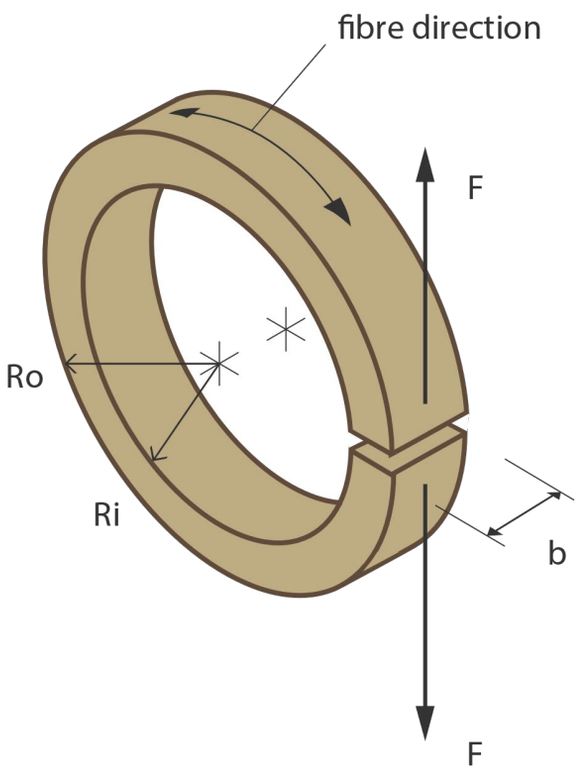

Figure 12. Principle of ring test for determination of transverse tensile strength

The transverse tensile strength can be found by the force at which transverse failure occurs and the geometric parameters of the ring using the following approximate formula.

$$\sigma_{Tt,max} \approx \frac{3 \cdot F_{max}(R_o + R_i)}{2b \cdot (R_o - R_i)(R_o \cdot R_i)^{0.5}}$$

The ring-test has in principle the potential to give more consistent results than the testing of a strip. However, in the nineties of the last century FPI has determined the transverse tensile strength of various glass-epoxy systems but the results were not consistent with UEWS and ATS tests. This may be related to imperfections in the sample production (e.g. voids) but also in that time the effect of glass fibre ageing (that was not recognized as an influence) may have played a role. Therefore, the ring-test has been abandoned as a candidate test method.

3.1.2. Longitudinal-transverse shear strength tests

This strength property is normally tested by the ILSS-test (interlaminar shear strength tests). The principle of the test is based on the three-point bending of a laminated structure with a short support span. Because the bending stresses remain low (due to the short span) the interlaminar shear stresses can develop so that delamination occurs prior to bending failure. The test method is described in various textbooks on composite testing (see e.g. Whitney, Daniel and Pipes, 1984). The test set-up is illustrated with the photo and the illustration below in Figure 13.

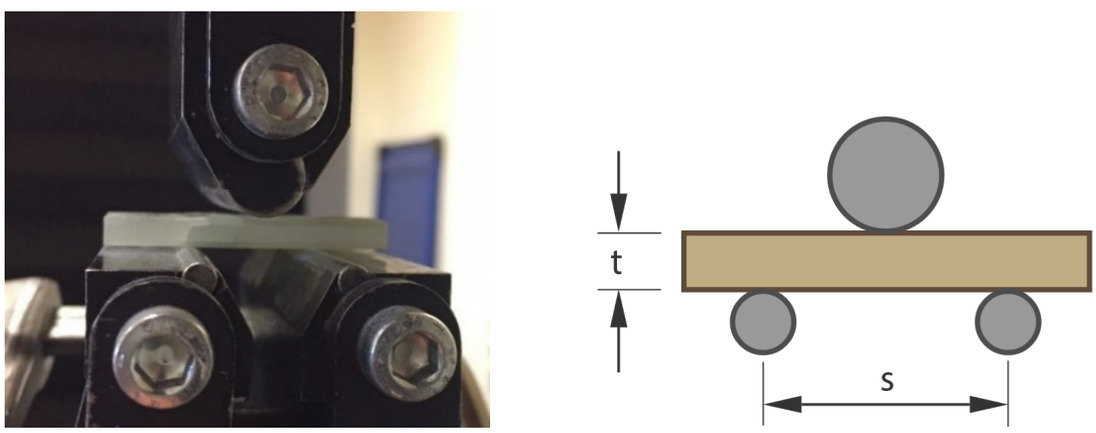

Figure 13. Photo of ILSS-test and illustration of the principle of the ILSS-test

Two well-known standards can be used for the procedure of ILSS-testing: ASTM D2344 and ISO 14130. There are differences between these standards in the way the test is carried out. This may result in a different outcome for the longitudinal-transverse shear strength. The main differences that affect the outcome concern the support length 's' with respect to the specimen thickness 't' and the radii of the support rolls, R_s , and of the load roll, R_l . The differences are summarized in Table 2.

Standard	Support length 's' (mm)	Radius support (mm)	Radius load (mm)
ASTM D2344	4 · t	3	6
ISO 14130	5 · t	2	5

Table 2. Differences between two ILSS test standards.

However, the formula for the calculation of the longitudinal-transverse shear strength , τ_L , is the same for both standards and is based on classical mechanics of the shear stress distribution of a rectangular cross-section that is loaded by a shear force:

$$\tau_{LT,max} = \frac{0.75 \cdot F_{max}}{b \cdot t}$$

Although the ILSS-test is a very straightforward test to determine the adhesion properties between fibres and matrix, it appeared that when the material is purely loaded in shear along the fibre-reinforcement directions it is not as discriminative as the UEWS and ATS test for GRE composites as used by FPI. Like the transverse tensile test this may be explained by the effect of imperfections in the laminate production (e.g. voids) that makes the method sensitive to rapid crack propagation from these imperfections that result in scatter in the test outcome.

3.1.3. Transverse-transverse shear strength tests

For this strength property the so-called Iosipescu test has been developed, named after its inventor. The test is performed by loading a strip of UD-reinforced material in pure transverse shear. This is achieved by using special test clamps that ensure that the load line of the shear force goes through the testing area. Moreover, at the location of the test area the specimen is notched. The notch is dimensioned in such a way that practically a uniform transvers shear stress distribution is obtained. Figure 14 shows the testing principle.

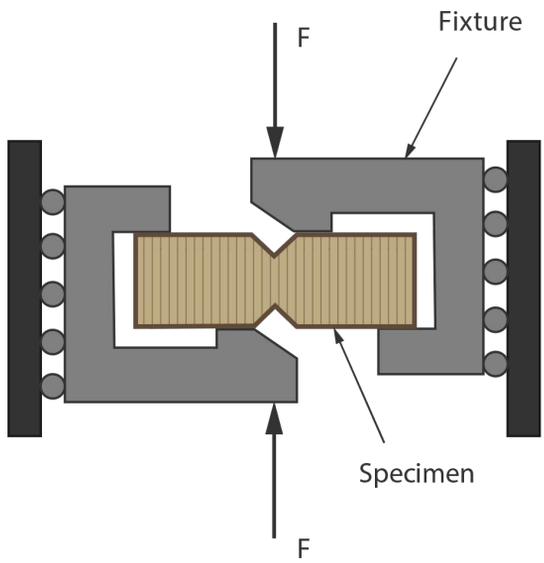

Figure 14. Principle of Iosipescu shear test

Ten Busschen (1996) has performed the Iosipescu test to determine the transverse transverse shear strength for UD-GRP. Figure 15 shows the test setup that was used.

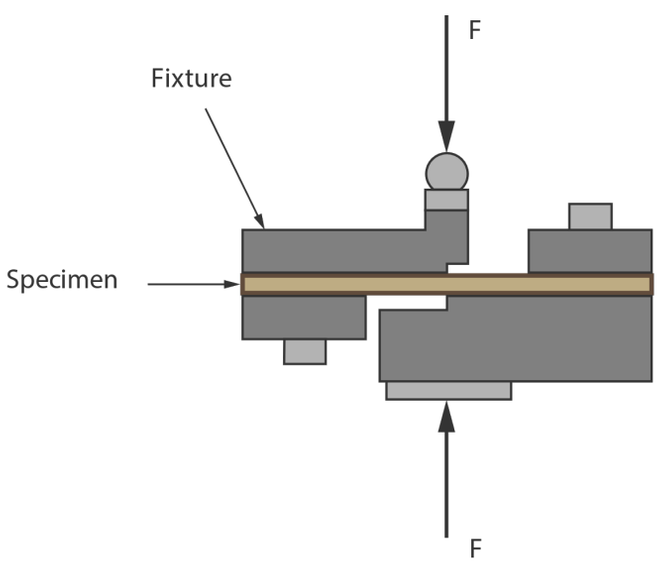

Figure 15. Iosipescu shear test set-up used by Ten Busschen.

The test is also described in many literature references. Although the principle of the test is very suitable for the determination of the transverse-transverse shear strength of the UD-composite, the test is known to be very susceptible to manufacturing variations of the notch and clamping misalignments. Like the tests for the transverse tensile strength and the interlaminar shear strength this method will be very sensitive for imperfections in the laminate manufacturing (e.g. voids) and sample preparation and therefore is not investigated further as a candidate method.

3.2. Development of test method

Because the test methods for the determination of the transverse strengths of UD-GRE that are found are not satisfactory for the use by FPI, a better method must be developed that gives comparable discrimination as with the 'fingerprint-tests'. The transverse tensile strength is thought to be a more discriminative parameter than the longitudinal-transverse shear strength. Therefore, a cross-ply laminate in an ILSS or short beam manner was tested. For this, the following symmetric(s) build up is used to make the test material:

$$[\,0 / 90 / 90 / 90 / 90 / 0\,] = [\,0 / 90 / 90\,]_S$$

The 0 degree layers have a much higher strain at rupture than the 90 degree layers and therefore the crack initiation will start from the inside of the specimen. This will make the test method less sensitive for imperfections in the surface. A short beam test on such laminate specimens is illustrated in Figure 16.

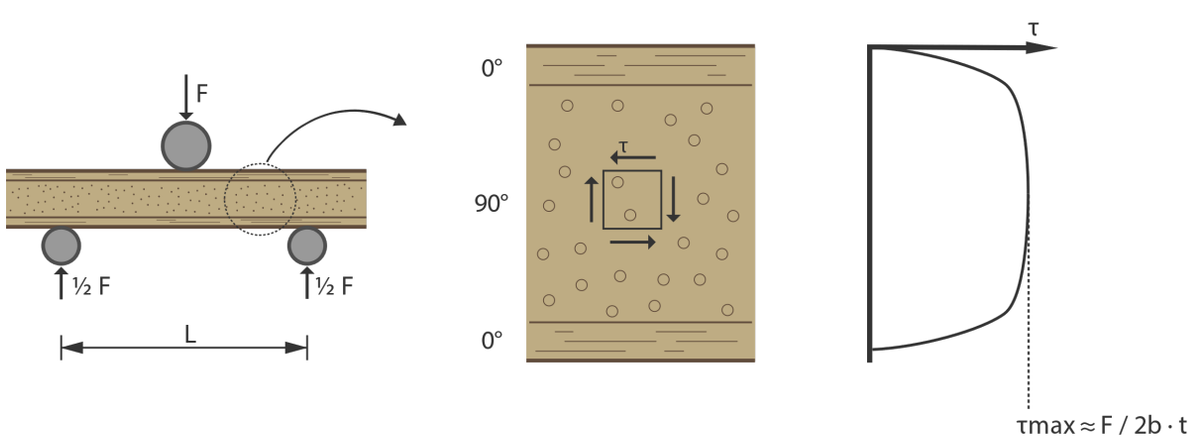

Figure 16. Test setup applied on cross-ply laminate. Applied Force (F) and shear stress (τ) are depicted.

In this manner shear stresses are build up that result in a transverse loading of the 90 degrees inner layer. In directions with an angle of 45 degrees with the horizontal plane normal stresses occur, both in tension and in compression. Cracking is likely to occur perpendicular to the normal tension stress. This is illustrated schematically in Figure 17.

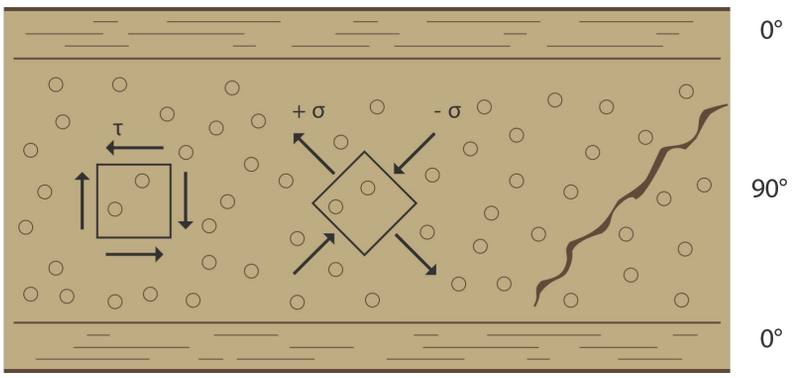

Figure 17. Transverse-transverse shear stress resulting in normal tensile stresses.

The transverse tensile strength is significantly lower than the transverse compressive strength and therefore the 90° inner layer will fail by cracks that are oriented perpendicular to the tension direction in 45° direction. A photograph of this failure is given in Figure 18.

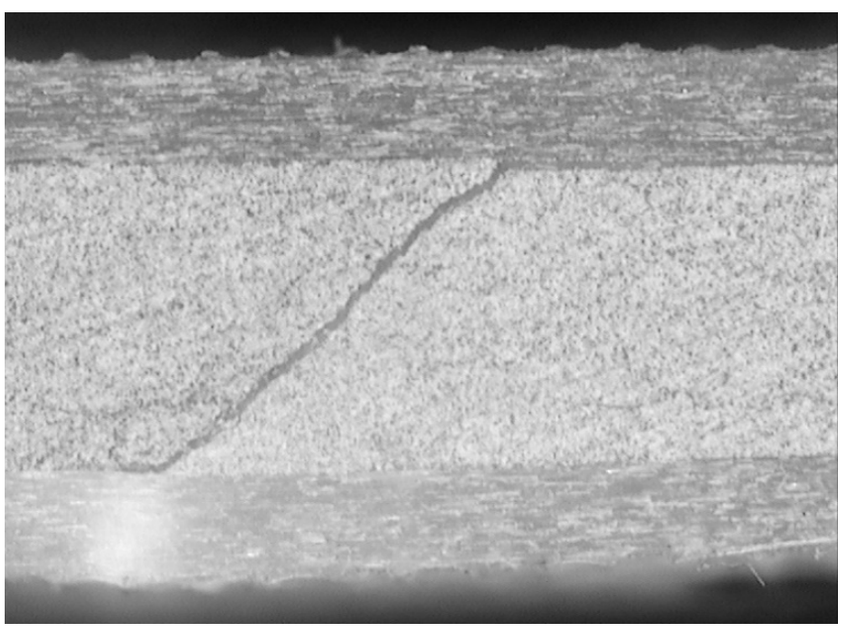

Figure 18. Transverse crack inclined in maximum normal tensile stress direction.

Although in principle this test method is rather insensitive for imperfections in the layer that is transversely loaded, the method did not give the correspondence with the results obtained through UEWS and ATS. There is scatter in the results when the test is repeated. This is an indication that the test does not give sufficiently reproducible results. This may happen if the method is still very sensitive of imperfections that are present in the middle layer, possibly due to the manufacturing process (e.g. voids).

Other 0/90 build-up programmes have been tested. These efforts will not be described in this report. It appeared that the following build up resulted in a series of reproducible and stable results:

[0 / 90 / 0 / 90 / 0 / 90 / 0 / 90 / 0 / 90 / 0]

Possibly the fact that the transverse failure of the 90° layers is distributed over several layers may smoothen the effect of imperfections in these layers.

The new test method of performing an ILSS-like test on the above mentioned 0/90 laminate build up will be indicated by 'Short Beam 0/90 tests' or in short: 'SB 0/90'. The developed procedure for preparation of SB 0/90 samples can be found in Appendix 3.

3.2.1. Carbon test samples

There are some differences in the preparation of the 0/90 test plates for the carbon fibre compared to glass fibre. Since the bobbins are tangentially unwound the winding processing is different as described in Appendix 3 for glass roving. The main difference is the lack of additional tensioners between the mandrel and the carbon reel. Because the 50k carbon tow is much thicker than 1200 tex glass roving only seven 0/90 layers are wound and not eleven as is the case with glass roving. Resulting in the following build-up:

[0 / 90 / 0 / 90 / 0 / 90 / 0]

3.3. Comparison SB 0/90 with ATS on pipe segments.

The following set of glass rovings are tested in fingerprint test (UEWS and ATS) and selected for their characteristics after ageing and exposure to hot-wet (80-100 °C) conditions, see Table 3. The performance of these rovings is indicated as Bad, Medium and OK. The raw data of the fingerprint tests can be found in Appendix 7. These rovings are used for the validation of the macroscopic test. There is not a complete dataset for roving GF1-A and GF1-B. Based on experience from FPI these rovings are expected to perform similar after aging and hot-wet. SUP2 roving GF3-B is an improved version of GF3-A. The fingerprint-samples were made with Epikote 828 resin and MDA hardener. GF3-B is made with BASF 072#23, a MDA replacement.

Name	Manufacturer	Ageing/ storage stability	Hot-wet resistance 80-100°C
GF1-A	SUP3	**Bad**	n/a
GF1-B	SUP3	n/a	**Bad**
GF2	SUP1	**OK**	**Bad**
GF3-A	SUP2	**OK**	n/a
GF3-B	SUP2	n/a	**OK**
GF4	SUP3	**Medium**	**OK**

Table 3. Rovings used in fingerprint tests

Because some of the rovings used in fingerprint test are not available anymore, different rovings have been selected for the current study. Based on the findings with the fingerprint rovings the following rovings are selected for the review of the developed test method, these are called ‘research rovings’ Table 4. SUP2 GF3 is the production roving of prototype GF3-B. SUP1 GF1 was used for comparison with SUP3 GF1-A and GF1-B.

Name	Manufacturer
GF1	SUP1
GF2	SUP1
GF3	SUP2
GF4	SUP3

Table 4. Rovings used in SB 0/90 tests

For storage stability investigations the roving bobbins were aged for 6 weeks at 50 °C in an oven. For hot-wet resistance tests the GRE test samples were exposed to water at 100 °C for 250 hours. Epikote 828 is used as resin, mixed with formulated IPD hardener.

All SB 0/90 results are compared with available results of the ATS-pipe tests. This is done by using the four 'research rovings'. ATS-pipe with MDA-hardener is chosen as representative for the fingerprint tests. Fingerprint test are done extensively both UEWS and ATS on pipe and strip (see Appendix 7).

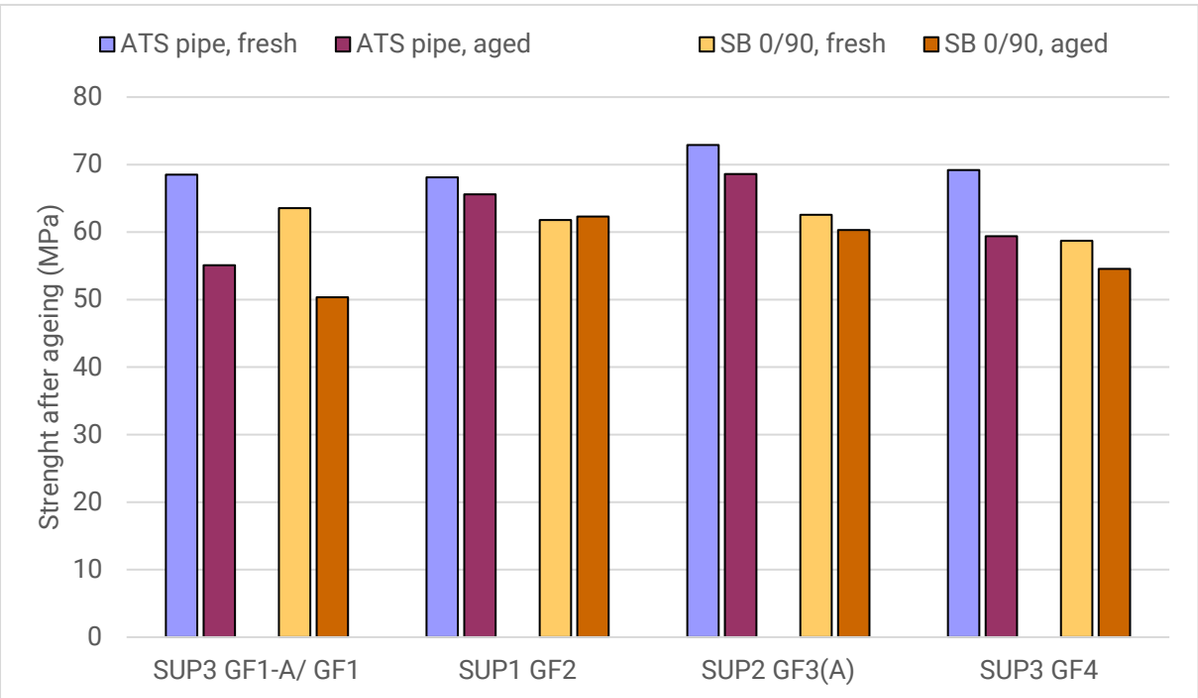

Figure 19. Tensile strength comparison after ageing tested by ATS and by SB 0/90. In this figure the ATS results of roving SUP3 GF1-A are compared with the SB 0/90 results of SUP1 GF1. SUP2 GF3-A ATS results are compared with the SB 0/90 results of roving SUP2 GF3.

First the effect of roving ageing for 5 weeks at 60 °C is investigated by testing specimens made with research rovings in SB 0/90. In Figure 19 the strength of samples made with un-aged ('fresh') and aged roving is given for the research rovings and can be compared with ATS-pipe results. For SB 0/90 results two plates are produced and 5 test specimens are cut and tested from each plate. ATS results are obtained from one pipe per roving type.

There is good correlation between the 'fresh' values and the aged values among the fingerprint and the SB 0/90 test.

In the same manner the effect of hot-wet-treatment was investigated with the research rovings using both ATS as fingerprint test and the SB 0/90. For this the strength is given not-treated ('dry') and after hot-water treatment (1500 hours 80 °C for ATS and 250 hours 100 °C for SB 0/90). The results are presented in Figure 20.

There is good correlation between the fresh and the hot-wet values between the fingerprint and the SB 0/90 test. However, the SB 0/90 tests show a larger drop in properties after hot-wet treatment especially for the roving that are noted as BAD (SUP3 GF1-A, SUP1 GF1 and SUP1 GF2). So, it appears that the SB 0/90 method is more critical for bad rovings.

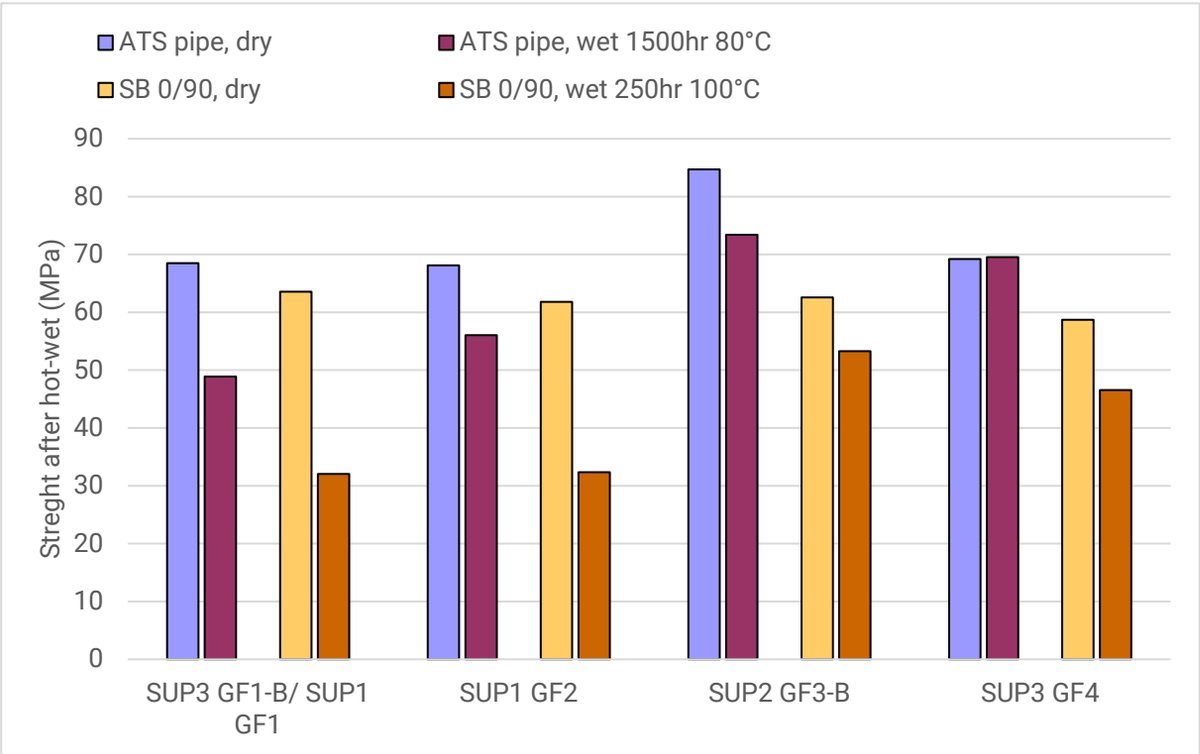

Figure 20. Strength comparison after hot-wet-treatment tested by ATS and SB 0/90. In this figure the ATS results of roving SUP3 GF1-B are compared with the SB 0/90 results of SUP1 GF1. SUP2 GF3-B ATS results are compared with the SB 0/90 results of roving SUP2 GF3.

From the results depicted in Figure 19 and Figure 20 it is clear that there is a good correspondence between the fingerprint ATS-test and the developed method SB 0/90, both for the effect of ageing of the rovings and for the effect of hot-wet treatment of the laminate up to 100 °C.

The same conclusions are found when comparing the SB 0/90 results for ageing and hot-wet-treatment with the UEWS as a fingerprint test. Irrespective the use of MDA or IPD as a hardener.

Test data of the tests with UEWS, ATS and SB 0/90 on which the graphs of Figure 19 and Figure 20 are derived are given in Appendix 7.

4. Nano analysis method

4.1. Literature search

Composite Interphase

A schematic illustration of the composite interphase is shown in Figure 21 including a cross-section of fibre–reinforced composite (left) and a detailed part of the region at the fibre surface (right).

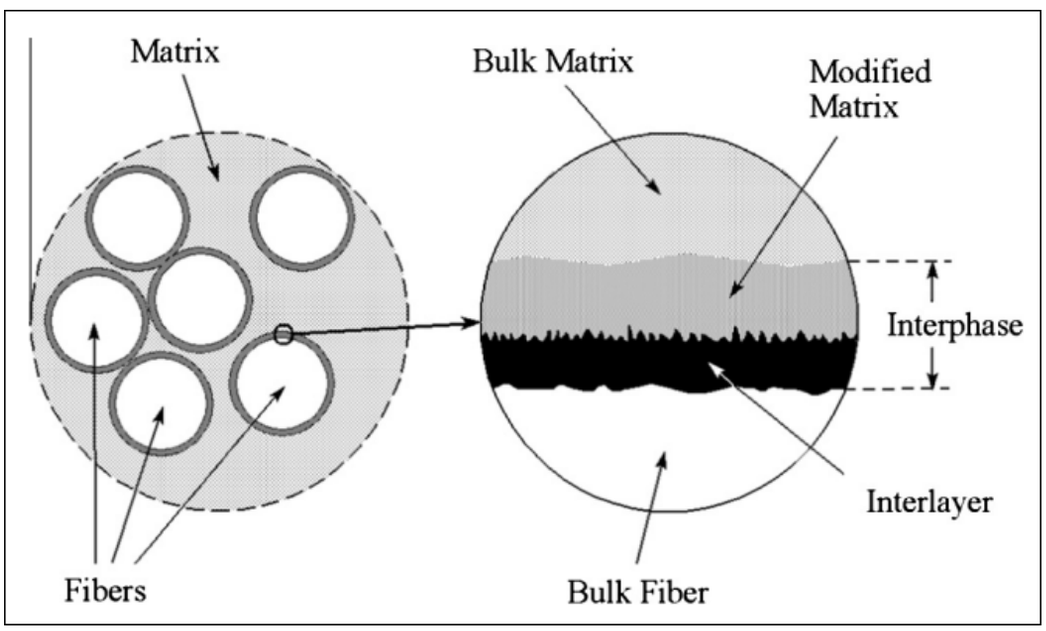

Figure 21. Schematic representation of the composite interphase. (left) Epoxy matrix in which glass fibres are immersed (right) Enlargement of the interphase between the bulk glass and the bulk epoxy matrix, consisting of a glass-to-sizing layer, the sizing itself and a sizing-to-epoxy region,

The interphase between the bulk fibre glass and bulk epoxy consists of three different parts: the glass-to-sizing part, the sizing, and the sizing-to-epoxy part. The function of the sizing (interlayer) is to improve the binding between the glass fibre and the matrix under formation such that a strong and tough link is established between the glass and the epoxy. This composite interphase governs the mechanical properties of a composite. Further details are discussed in reviews by Kim and Mai–Jesson and Watts.

Organosilanes are used as a coupling agent in the sizing, that is applied to the glass rovings. The bifunctional silane molecules act as a link between the glass fibre and resin by forming a chemical bond with the glass surface through a siloxane bridge, and the organofunctional group bonds to the polymeric resin[1]. Interdiffusion and intermixing in the sizing-polymer interface region occurs, due to

[1] Materne, T., et al., “Organosilane Technology in Coating Applications: Review and Perspectives”, Dow Corning Corporation, P.O. Box 994, Midland, MI 48640 USA

penetration of the resin into the chemisorbed silane layer and migration of the physisorbed silane molecules into the resin phase. This leads to an interpenetrated network (IPN) (see Figure 22a)[2]

The reaction of the organosilanes with the hydroxyl-terminated glass surface forms a stable covalent bond, and water is released as a by-product. If the water produced as such is continuously removed by evaporation for instance, the bonding of the silane to glass will continue, until either there is no more silane or no more attachment sites on the glass surface. This reaction however is a reversible reaction. Therefore, it is hypothesized that immersion of this composite in water, such as occurs in a hot-wet treatment, might lead to hydrolysis, a reversal of the coupling reaction, leading to debonding of the silane from the glass. This most probably severely affects the mechanical properties of the composite (Fig 22b). Many microscopic and spectroscopic methods have been applied to reveal the interphase region in specific composite systems and evaluate its thickness. Interestingly apparent interphase thicknesses varied depending on the technique employed for evaluation. In a previous study we have used the tip of an atomic force microscope to scratch off a layer of their surface. By applying a relatively large force during scanning with the AFM leads to the removal of layers, that are not well attached to the underlying hard substrate (which is glass). After removal of this layer a height difference of 40-60 nm was observed, which represents the thickness of the sizing layer.

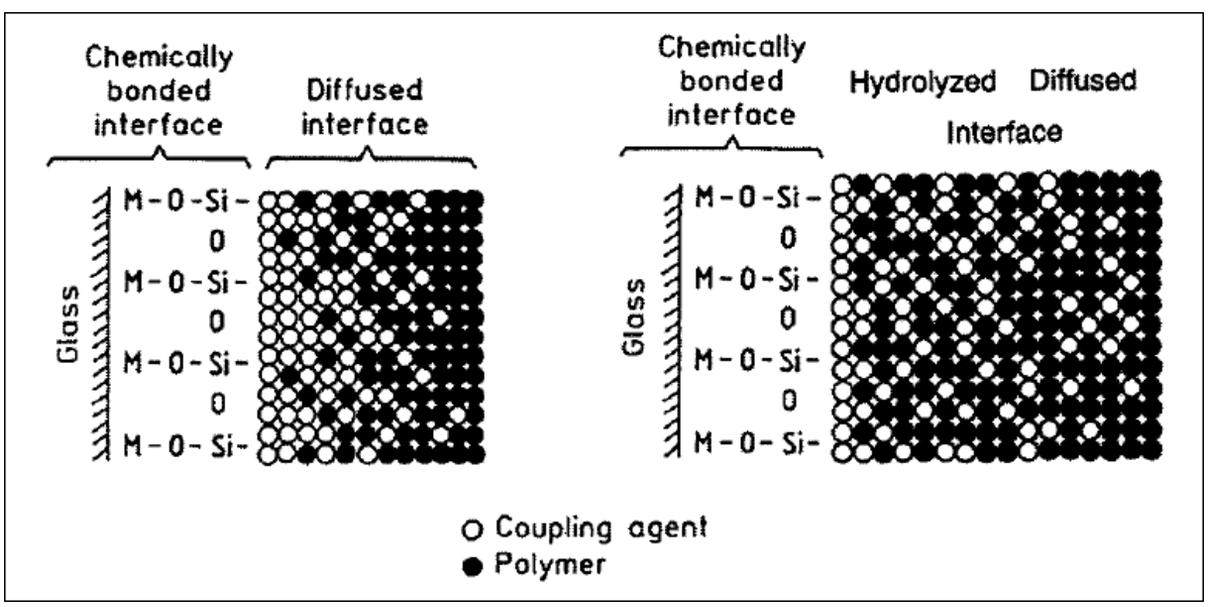

Figure 22. A schematic model for (a) conventional interdiffusion and interpenetrated network (IPN) in a silane-treated glass fibre/polymer matrix composite [ref]; and (b) an model for a hydrolysed diffused interface, after aging in water [ref]. Silanes will debond from the glass surface due to hydrolysis and diffuse further into the epoxy layer, creating a thicker interphase. This debonding from the glass surface will most likely result in a decrease in mechanical strength of the composite material.

Various studies have proven the existence of an interphase region, defined as a distinct phase of different properties to those of the reinforcement and matrix or as a region of gradual change in properties/chemistry across the interface. For instance, AFM based nanoindentation has been used to probe cross sections of fibre-reinforced plastics and to determine the mechanical properties of the interphase which tend to show either a step or a gradient as represented schematically in Figure 23.

---

[2] Plueddemann, E. P., In Proc. ICCI-II, Interfaces in Polymer, Ceramic and Metal Matrix Composites. H. Ishida, Ed. (Elsevier, New York, 1988), pp. 17-33.

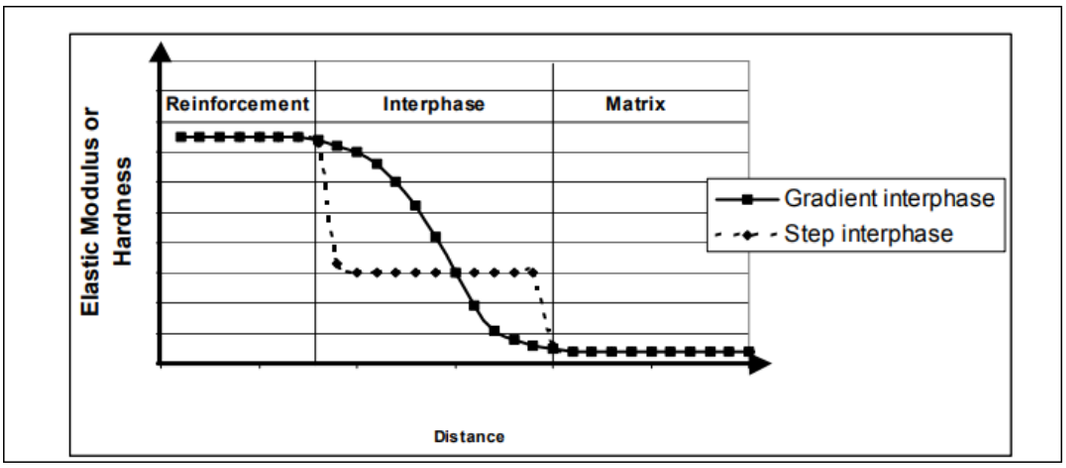

Figure 23. Modulus on composite surface, transition from fibre to matrix

Atomic Force Microscopy

Of particular importance for this study is AFM which has been widely used to study the structure and morphology of polymers and composites at nanoscale resolution. A tip with a point radius of 1 to 10 nm attached to the end of a flexible cantilever (see Figure 24) is used to scan the surface in order to obtain a height image. As the tip is scanned, it is in contact with the surface and as the height changes, the tip will move up and down. This up and down movement is accurately detected by focusing a laser beam on the back of the cantilever beam. As the tip moves up and down, the cantilever bends, and this is detected by looking at the laser beam that is reflected off the back of the cantilever. In many studies tapping mode AFM is used. In this AFM mode, the tip is not constantly in contact with the surface. A small piezo element at the base of the cantilever is applying an oscillatory movement, such that the cantilever moves up and down at its resonance frequency. As a result, the tip moves up and down typically at frequencies of several 10s of kHz. The tip therefore only touches the surfaces very shortly, causing less damage to the sample and the tip itself.

When using tapping-mode you do not only obtain a height image, but also a phase contrast image. This signal is the phase difference between the oscillatory signal applied to the base of the cantilever and the actual oscillatory movement of the tip. Although not in a quantitative manner, this phase signal contains information on the adhesion between the tip and the surface and the mechanical properties of the surface. As mentioned, it does not provide quantitative information, but it does show contrast for example when the surface consists of two different materials (having slightly different adhesion and mechanical properties).

A prerequisite for AFM measurements is that the sample surface is smooth and flat. Therefore, for composites proper polishing is essential.

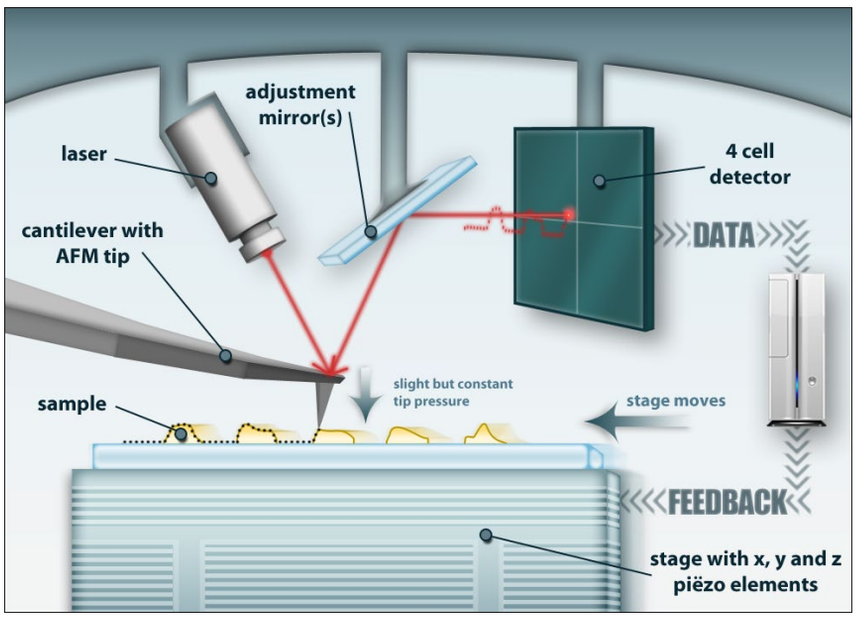

Figure 24. AFM functioning principle

Peak force tapping AFM is yet another mode of AFM, it is able to map mechanical properties of the surface on nanometer scale. In this mode, the tip is moving up and down with respect to the sample, but at a much lower frequency than in tapping-mode AFM. As a result of this, it is possible to record the force as the tip is moving down and up, and obtain a full force extension curve (see Figure 25). This effectively is an indentation experiment, and from the curve various mechanical parameters such as the DMT elastic modulus can be extracted. Other parameters that can be extracted are adhesion and deformation.

In peak-force tapping, this curve is measured and analysed every time the tip moves up and down, and next to a height map, therefore is able to create an elasticity map.

Several mechanical contact models exist that allow the extraction of the elastic modulus from the force distance data. In this case we have applied the Derjaguin-Müller-Toporov (DMT), which was found to be useful for samples with moderate adhesion levels and AFM tips with small radii.
To further ensure that the correct value for the elasticity modulus was calculated, we checked the value with a standard sample, that was supplied by the manufacturer. These are microphase separated polymers of known modulus.

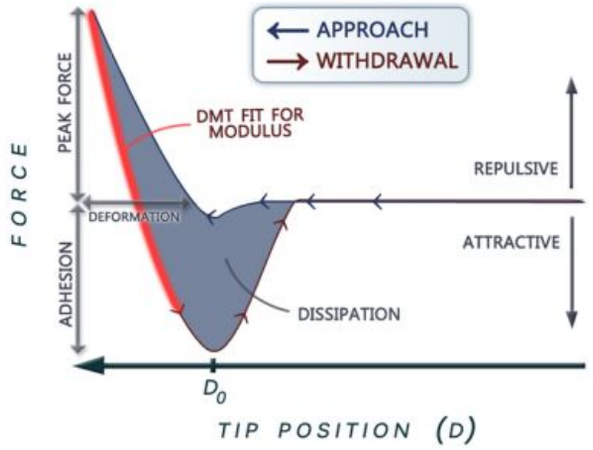

Figure 25. Schematic force distance curve derived during mechanical mapping with peak force tapping AFM. Starting from the position that the tip is furthest away from the surface, the tip is approaching the surface. The tip is not touching the surface yet, so the force is zero (not repulsive, not attractive). When it gets close to the surface, due to adhesion the tip is attracted to the surface, and when going further down, the tip indents the surface, causing it to bend upwards (repulsive force). When a maximum force is reached the cycle is reversed and the tip is retracted. This caused the force to go back towards its zero position and even continue into the attractive regime, as a result of adhesion between the tip and the sample. When further withdrawn the tip dissociates form the surface and the force restores to zero. From this curve different mechanical parameters can be derived.

AFM-IR

Both tapping mode as well as Peak Force are able to construct a topography map of the surface, including its elastic properties with nanometer resolution, but do not provide any information with respect to the chemistry of the surface. Bruker in Karlsruhe, has recently introduced the AFM-IR technique, which combines the high resolution capabilities of AFM with the spectroscopic capabilities of IR absorption spectroscopy.

As schematically shown in Figure 26, a tip is scanning the surface to create a height image, and at the same time infrared radiation is used to illuminate the sample. When the sample is absorbing the IR light, it will slightly increase in size, which can be detected by the AFM tip. This results in a change in the resonance frequency. When the tip is kept at one position on the sample, and the IR wavelength is scanned, a full IR absorption spectrum of the sample below the tip can be obtained. It is also possible to fix the wavelength of the IR radiation (for example at a peak in the spectrum that is known to be related to a specific chemical compound) as you are scanning the surface which gives a 2D image of where a certain compound is located.

This technique is just recently introduced by Bruker and the measurements in this report have been done at Bruker with the help of Hartmut Stadler, PhD, application scientist at Bruker in Karlsruhe. By analysing the interphase between the glass and epoxy using this the AFM-IR imaging technique, we hope to directly visualize the occurrence of hydrolysis at the glass-epoxy interface, when a composite material is exposed to the hot-wet treatment.

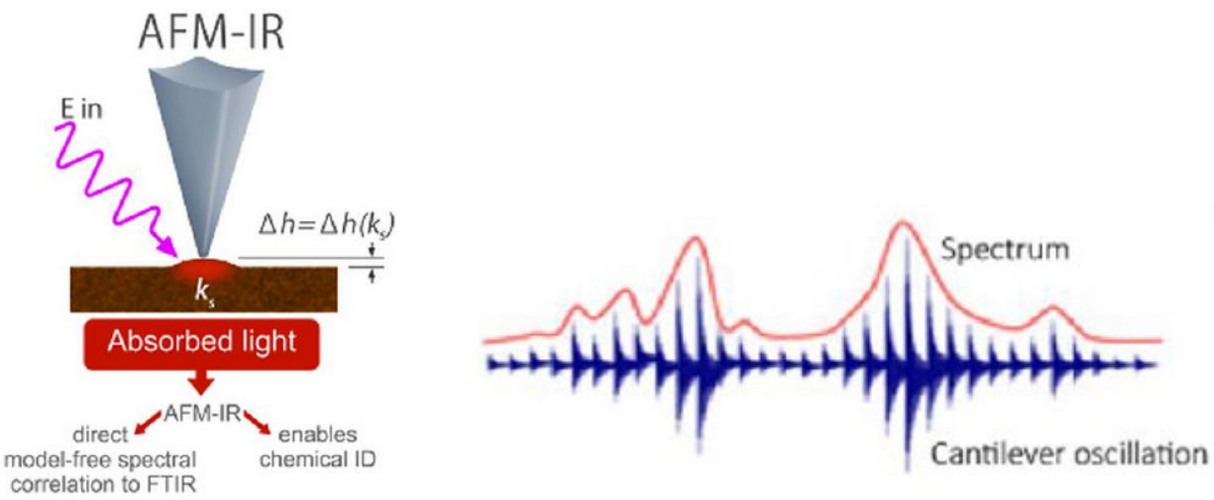

Figure 26. (left) Principle of AFM-IR. As the AFM tip is on the surface, it is illuminated with infrared (IR) radiation. If the IR light is absorbed by the sample below the tip, it will swell slightly and this will influence the cantilever amplitude, which can be measured by the AFM tip.

(right) As the wavelength of the IR light is scanned through a certain part of the IR spectrum, the cantilever oscillation amplitude becomes a direct measure for the amount of absorption. The allows the reconstruction of the IR absorption spectrum of the material below the tip.

4.2. Development of the polishing method

In previous studies we found that glass reinforced epoxy (GRE) samples can be imaged by tapping mode AFM (height) and peak force tapping (DMT modulus).The composite revealed a 40 – 60 nm height difference between the glass fibre cross section and the surrounding matrix (which is found to be higher). Further optical microscopy of GRE samples was conducted using DIC/phase contrast and dark field imaging revealing further heterogeneities over larger areas, such as: different sizes of the fibres (size range), areas with no fibres, densely packed domains, and significant contaminations.

Of particular interest within these studies is the interphase between an individual glass fibre cross section and the surrounding matrix as this interconnects both materials and is most likely a key feature for material performance at the macroscale and might thus deliver an explanation for the significant differences observed between different GRE batches. Atomic force microscopy (AFM) was chosen as the appropriate tool to gain more insight into the characteristics of the interphase between the glass and the epoxy matrix. AFM allows to image the interphase with high lateral resolution, and furthermore allows to map the elastic modulus across the interphase.

Careful polishing of the composite cross-sectional samples in order to flatten the surface is pivotal for the planned AFM measurements. A specific procedure has been developed (described in Appendix 5) in order to decrease the step height between the epoxy and the glass material. The polishing process was carried out using equipment of Struers. The procedure involves rough polishing with subsequently lowering grain size from 68 to 30 to 15 μm (Figure 27: left). This is followed by fine polishing by an automated machine gradually lowering the grain size from 9 to 3 to 1 μm (Figure 27: right). The polishing progress was followed using an optical microscope. Finally, the samples were cleaned with cotton wool and ethanol.

Figure 27. An illustration of a Struers hand polishing system for larger grain sizes. (Right) A photograph of a Struers polishing system for smaller grain sizes using diamond powder as a polishing medium.

In addition to the interphase study using AFM, scanning electron microscopy (SEM) and optical microscopy were used to obtain consistent information from composite samples on larger length scales. The goal was to systematically scan fresh and aged samples in order to yield quantitative information on the occurring damage.

This combination of techniques provides a representative picture of the potential modes of damage and the total amount of damage occurring during ageing.

5. Characterization of glass-matrix systems after ageing and hot-wet exposure

Eight glass rovings (see Table 5) were selected for the investigations in ageing stability (6 weeks at 50 °C in an oven) and hot-wet-performance of GRE samples in boiling water (250 hours at 100, 115 or 125 °C). The first four products ('research rovings') were also used for the validation of the macroscopic test method. The other products are investigated because these are relatively new products or improved products and are indicated by 'test rovings'. All rovings are 1200 tex except for GF6 (2400 tex).

Name	Manufacturer
GF1	SUP1
GF2	SUP1
GF3	SUP2
GF4	SUP3
GF5	SUP3
GF6	SUP3
GF7	SUP4
GF8	SUP5

Table 5. Glass types for investigating ageing and hot-wet performance above 100 °C

5.1. Mechanical test results with research rovings and test rovings

5.1.1. Ageing of roving

For all eight rovings (research rovings and test rovings) the effect of ageing is investigated. Ageing is done by placing the test glass fibre material (roving bobbins) in an oven for 6 weeks at 50 °C. The aged rovings are used to make test samples and the samples are tested with SB 0/90. The results are depicted in Figure 28 (n=10). Numerical data can be found in Appendix 8. As previously stated, roving GF1 and to a lesser degree GF4 performed badly after ageing. The GF7 is the worst performing roving after ageing.

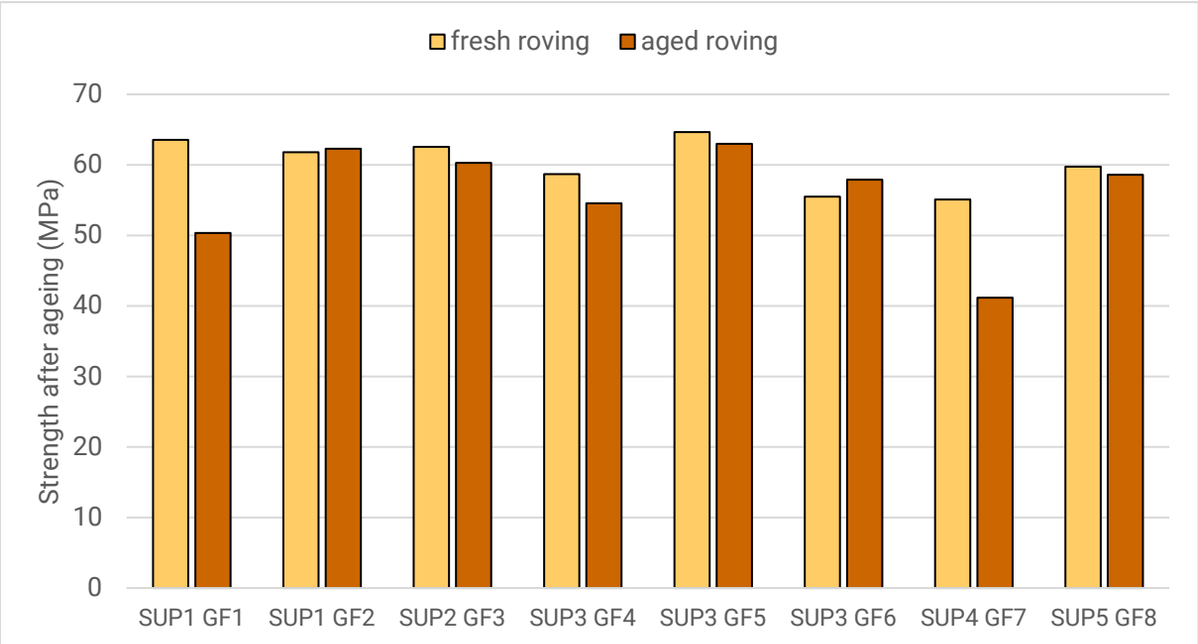

Figure 28. Results of the short beam 0/90 test initially (fresh) and after the roving has been aged in an oven for 6 weeks at 50 °C.

5.1.2. Hot wet exposure of samples

For eight rovings the effect of hot-wet treatment of 0/90 samples is investigated. The test specimen of fresh and aged rovings have been exposed to water at 100 °C, 115 °C and 125 °C for 250 hours. Subsequently SB 0/90 tests were performed. The results of the test with fresh roving are shown in Figure 29.

As already known, rovings GF1 and GF2 perform badly after hot-wet treatment. This is already noticeable after hot-wet treatment at 100 °C. Concerning the test rovings, the reduction in mechanical properties after hot-wet treatment is less pronounced. Overall shows SUP2 GF3 the best retention after hot-wet treatment. Aged rovings performed similar after hot-wet treatment and parallel trends are witnessed (see Appendix 8).

In order to verify whether plastification of the epoxy matrix may influence the results a series of specimen were dried (1 week at 80 °C) after hot-wet treatment and then tested. The results of these dried test show the same difference in performance of the eight rovings as with non-dried specimens. This can be found from the numerical data in Appendix 8.

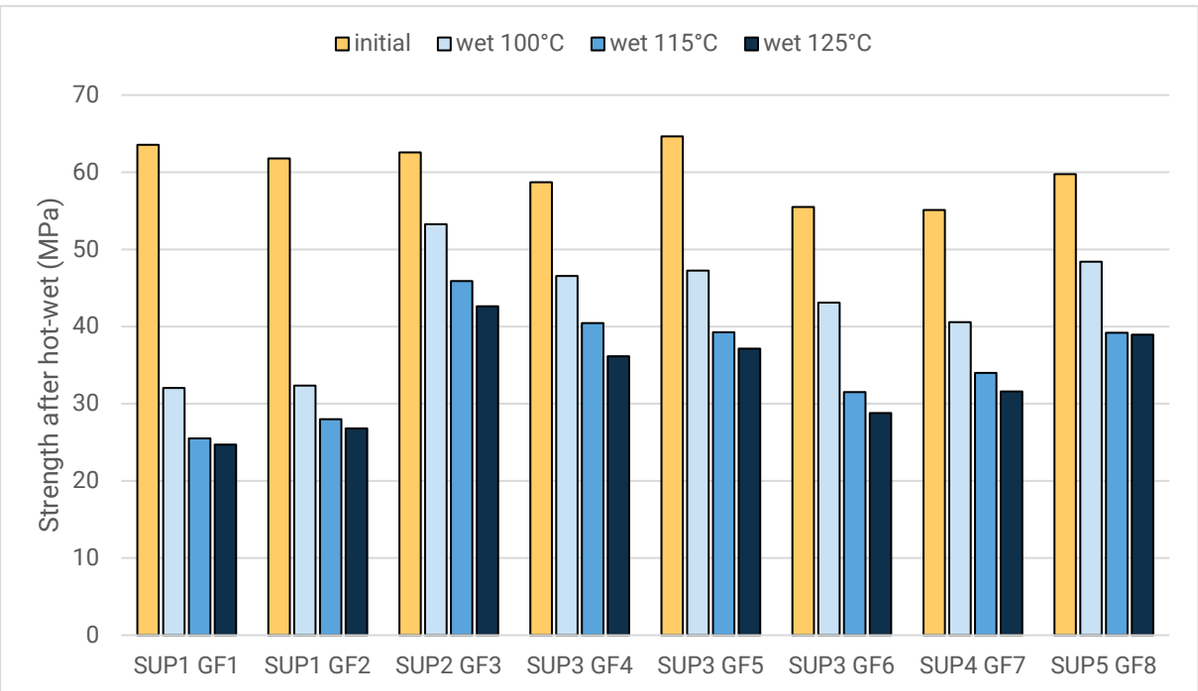

Figure 29. Results of short beam 0/90 test. Samples are prepared with fresh roving and exposed to hot water for 250 hours.

5.2. Evaluation on micro-scale and nano-scale

5.2.1. Polishing

Using the polishing technique described in appendix 5, the height difference between the glass and the epoxy was reduced from about 60-80 nm, down to 5.6 nm in average (Figure 30, left). The height variation within either the glass fibre or the epoxy matrix, is 1.8 nm (Figure 30, right). From this we concluded that it was successful to reduce the height variation by using the improved polishing procedure.

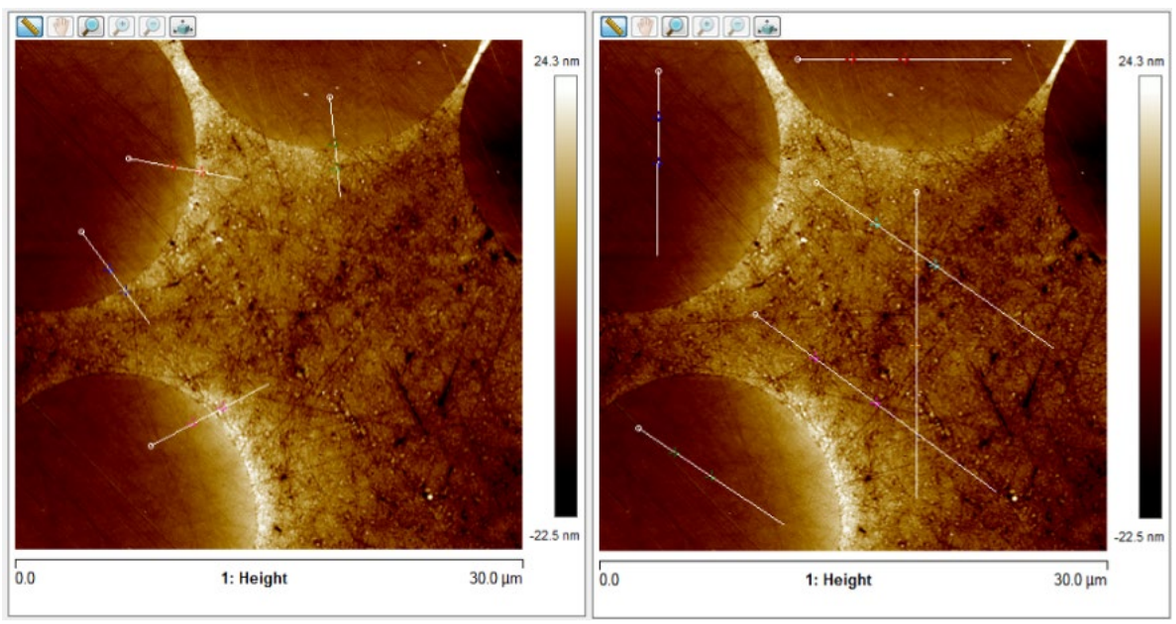

Figure 30. (Left) AFM image of the step height along the interphase. Green line = 0.0 nm, red line = 10.4 nm, blue line = 11.9 nm, pink line = 0.0 nm. Average = 5.6 nm. (Right) AFM image of the height variation within one phase. The average variation was 1.8 nm.

5.2.2. AFM

A large number of measurements using AFM was carried out in order to identify the interphase between glass fibre and epoxy. It appeared that it was difficult to determine the elasticity modulus due to the unavailability of the system for several months due to repairs and a missing calibration standard with properties comparable to the sample.

In conclusion, no significant difference between the modulus of the glass fibre, the epoxy and the interphase was found. As an alternative, an AFM combined with an infrared spectrometer was used to yield new insights on the interphase region. The results are described in the next section.

5.2.3. AFM-IR

AFM-IR is a very novel technology, which Bruker has launched recently. This technique is a combination of atomic force microscopy and IR absorption spectroscopy. In this project we were offered an opportunity to see whether this technique would be able to give us more information, specifically in terms of the materials in and around the interphase of the glass and epoxy.
For this study two specimen made with roving SUP1 GF1 ‘fresh’ have been used. The first one, is as produced (initial), and the second sample is hot-wet treated at 100˚C for 250 hours.

Sample 1 (as produced)

Before starting, contact mode AFM imaging was used to ensure the scanned area (10 x 5 um) contained the interphase between the glass and the epoxy. When positioned, the image area was reduced to roughly 800 x 700 nm, and this was imaged in resonance-enhanced AFM-IR at a IR wave number of 1360 cm^{-1} (Figure 31)

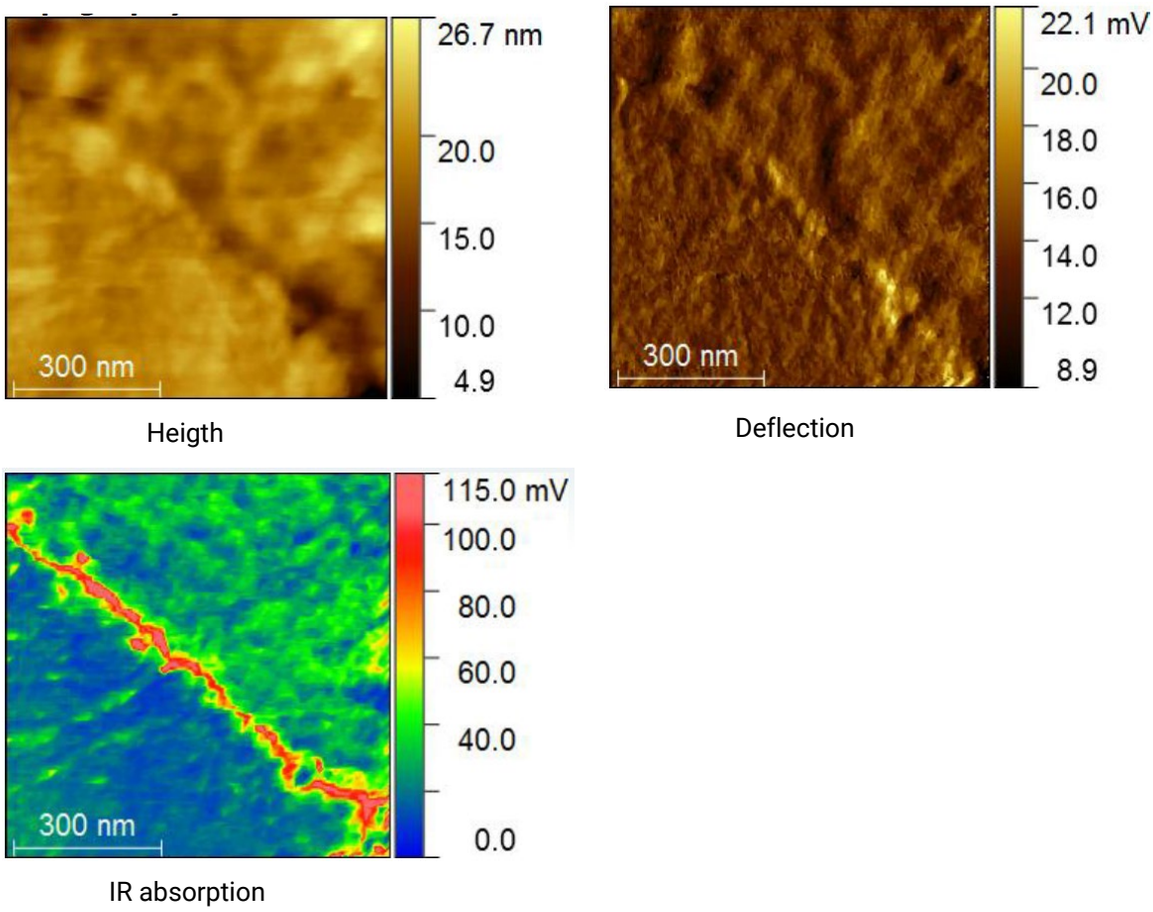

Figure 31. AFM-IR images made of 4017TFF020103 laminate sample, roving type SUP1 GF1. This imaging techniques produces height, deflection and IR absorption images at the same time. All images are 700 x 800 nm, and the interface between the glass (lower left corner) and epoxy (top right corner). The IR absorption image was created at an IR wavelength of 1360 cm^{-1}, that clearly reveals a higher absorption at this wavelength at the glass-epoxy interface.

The technique also allows to take a full spectrum at one position on the sample. Results of these can be seen in Figure 32.

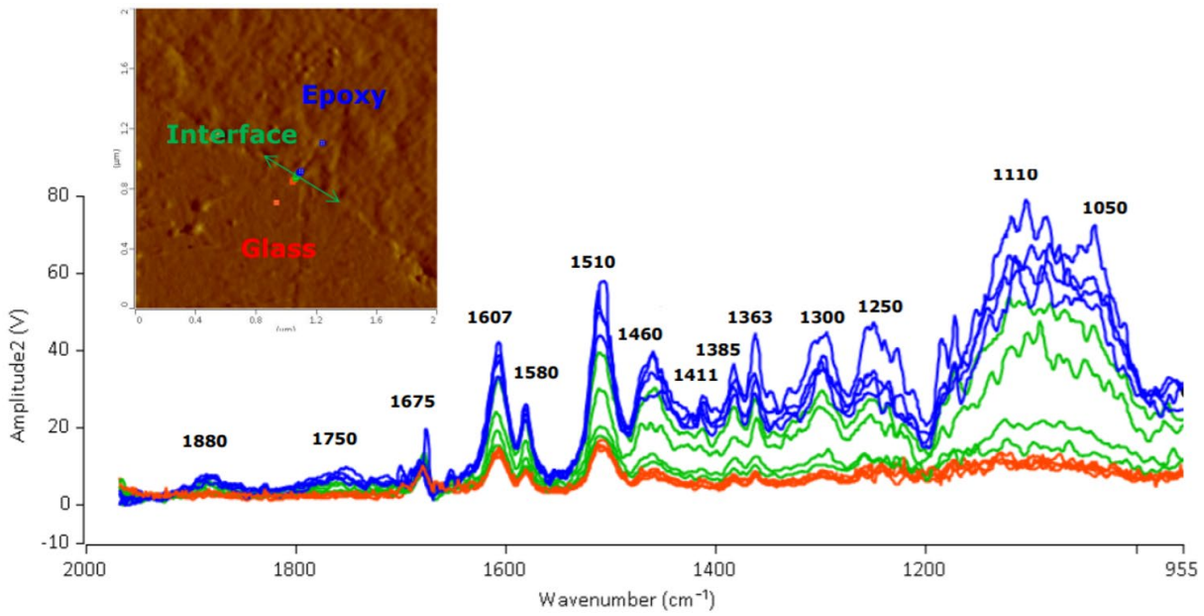

Figure 32. Full IR-absorption spectra recorded at specific locations on the sample on the glass (red), interface (green) and epoxy (blue) phase. Absorption clearly increases as we move from the glass to the epoxy surface.

From the full spectral scans, it is clear that the absorption at specific peaks (1607 cm^{-1} and 1501 cm^{-1}) and a large region from 955 to 1480 cm^{-1} increases when you move from the glass to the epoxy. Although the absorption increase can also be observed at 1360 cm^{-1} in Figure 31, when comparing the glass surface and the bulk epoxy surface, the specific increases of the absorbance at 1360 cm^{-1} at the interface is not reflected in the full spectra in Figure 32. This might be due to the fact that the interface is not positioned correctly within this measurement.

Sample 2 (hot-wet treated at 100˚C for 250 hours).

For the hot-wet treated sample we have followed the same procedure and made a 2 x 2 um AFM-IR scan.

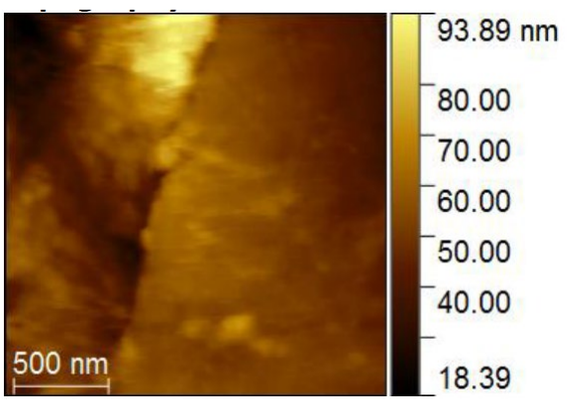

Height

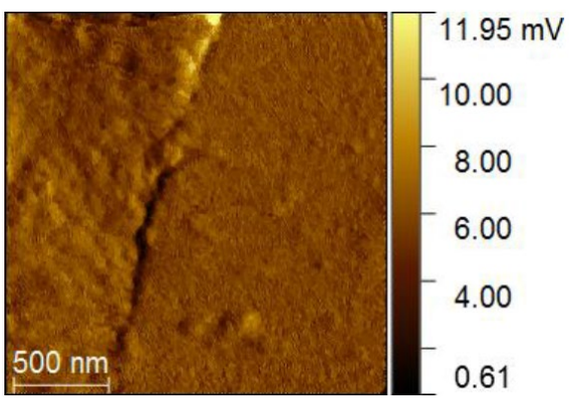

Deflection

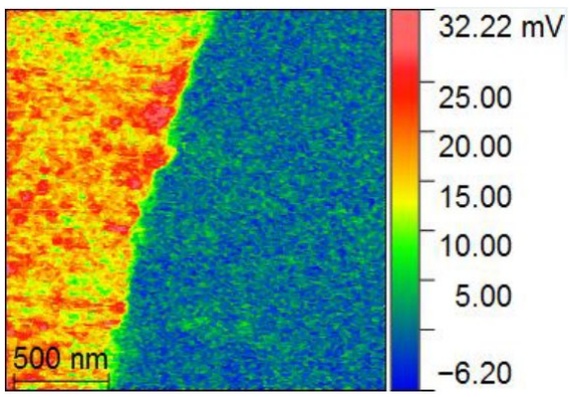

Figure 33. AFM-IR images made of an aged sample. This imaging techniques produces height, deflection and IR absorption images at the same time. All images are 2000 x 2000 nm, and the interface between the glass (right side) and epoxy (left side). The IR absorption image was created at an IR wavelength of 1360 cm^{-1}, that clearly reveals a higher absorption at this wavelength at the glass-epoxy interface.

This AFM-IR image also revealed an increased absorption for 1360 cm^{-1} on the epoxy surface when compared to the glass, but does not show a peak at the interface as for the non-hot-wet treated sample. And for this sample a number of full spectra are recorded at a location on the glass, the epoxy and the interface. The result of these can be seen in Figure 34.

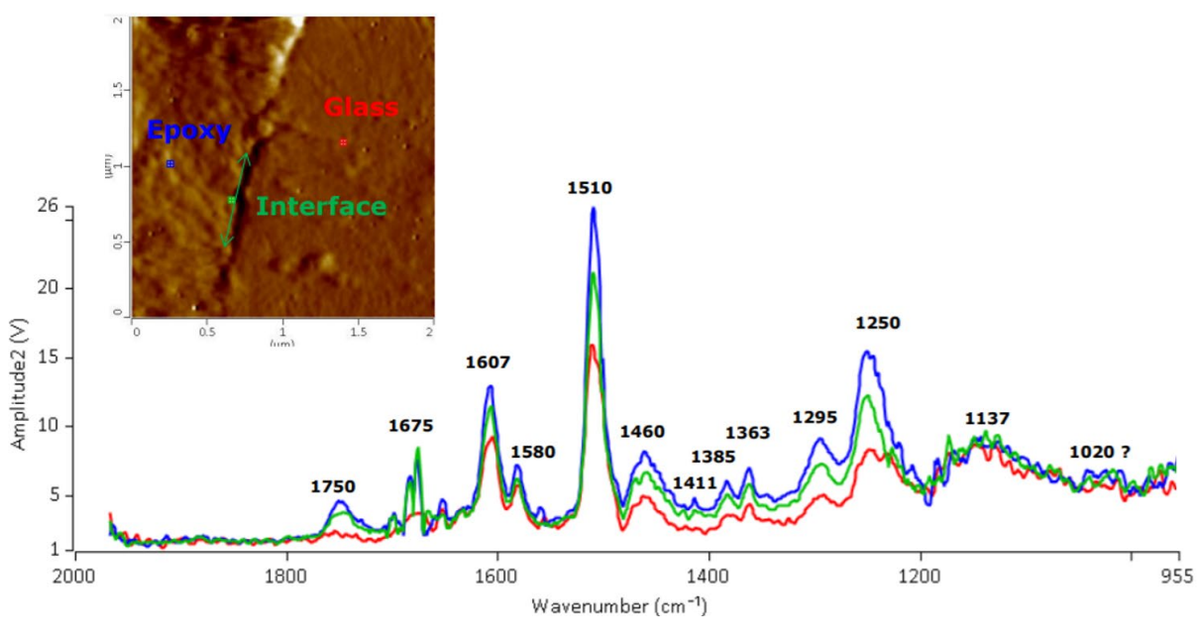

Figure 34. IR wavelength scan ranging scan from 955 to 2000 cm^{-1} of the glass, the epoxy and the interface.

Comparison between the samples.

Here we directly compare the spectra of both samples taken on the glass region and the epoxy region, for the treated (sample 1) and hot-wet treated sample (sample 2) (Figure 35). For the glass region the IR absorption spectrum before and after hot-wet treatment is quite similar indicating that the glass material is not affected by the treatment. Considering the spectra recorded on the epoxy material,

there are some clear differences. The absorption spectrum recorded on the epoxy reveals for the hot-wet treated sample shows fewer and lower peaks in the 1100 to 1400 cm^{-1} region. This is clear evidence that the composition of the epoxy near the glass/epoxy interface is affected by hot-wet treatment. A possible explanation is the hydrolysis of the silanes, caused by the water exposure during the hot-wet treatment. This causes debonding of the sizing from the glass, and diffusion of silanes further into the epoxy matrix.

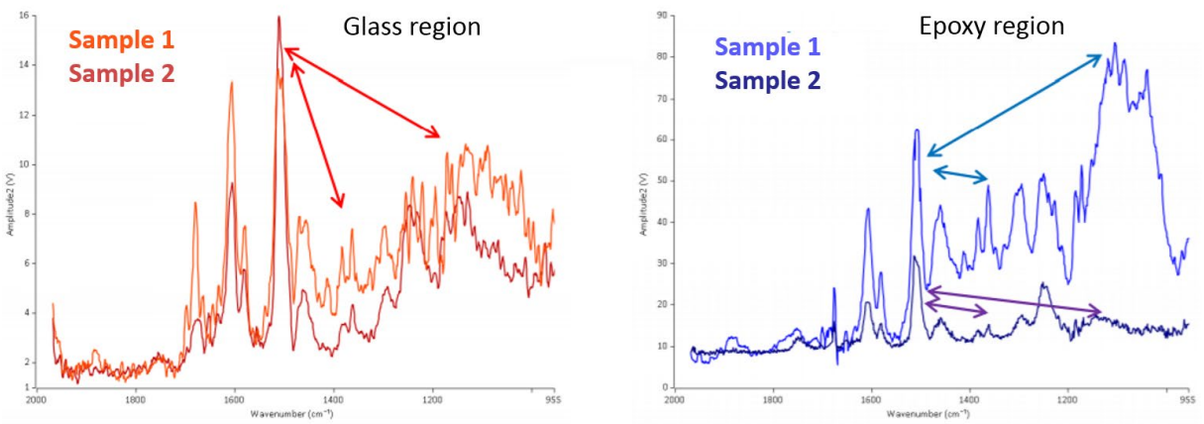

Figure 35. Direct comparison of the IR absorption spectra recorded on the glass region (left) and epoxy region (right) of the sample as produced and the sample after hot-wet treatment (100˚C for 250 hours). On the glass region the IR absorption spectra look similar, suggesting no major changes to the composite material. On the epoxy region however the absorption spectrum looks quite different between the 1100 to 1400 cm^{-1} range, revealing changes in the composite material when the composite before and after the hot-wet treatment is compared.

Conclusion

Please note that the results presented here are a very first proof-of-principle and for statistical significance further experiments need to be done. The results do show that the absorption at 1360 cm^{-1} recorded on glass and epoxy is different. The results also reveal that the IR absorption spectra recorded on the epoxy part are different when a non-treated sample is compared to a hot-wet treated sample. The main difference is in the 1100 to 1400 cm^{-1} range. The hot-wet treated sample reveals more less pronounced peaks and a lower amount of absorption within this range. These peaks hint at bonds containing Si, C, O and H atoms, and hints at a chemical change within the epoxy region close to the interface. In order to conclude with certainty that this is indeed the hydrolysis of the organosilanes, as suggested by others and described in chapter 4, further research is needed.

5.2.4. Scanning electron microscopy (SEM)

In order to study the damage occurred during glass fibre aging in air, samples were visualized using a high-resolution SEM at the MESA+ institute in Enschede (at the University of Twente). The samples were prepared according to the protocol described in appendix 5.

An example of a sample before and after treatment under hot-wet conditions at 100 ˚C for 250 hours is shown below. It shows physical separation of the epoxy and the glass fibres occurs in the aged sample. This is not observed for the non-treated, fresh samples.

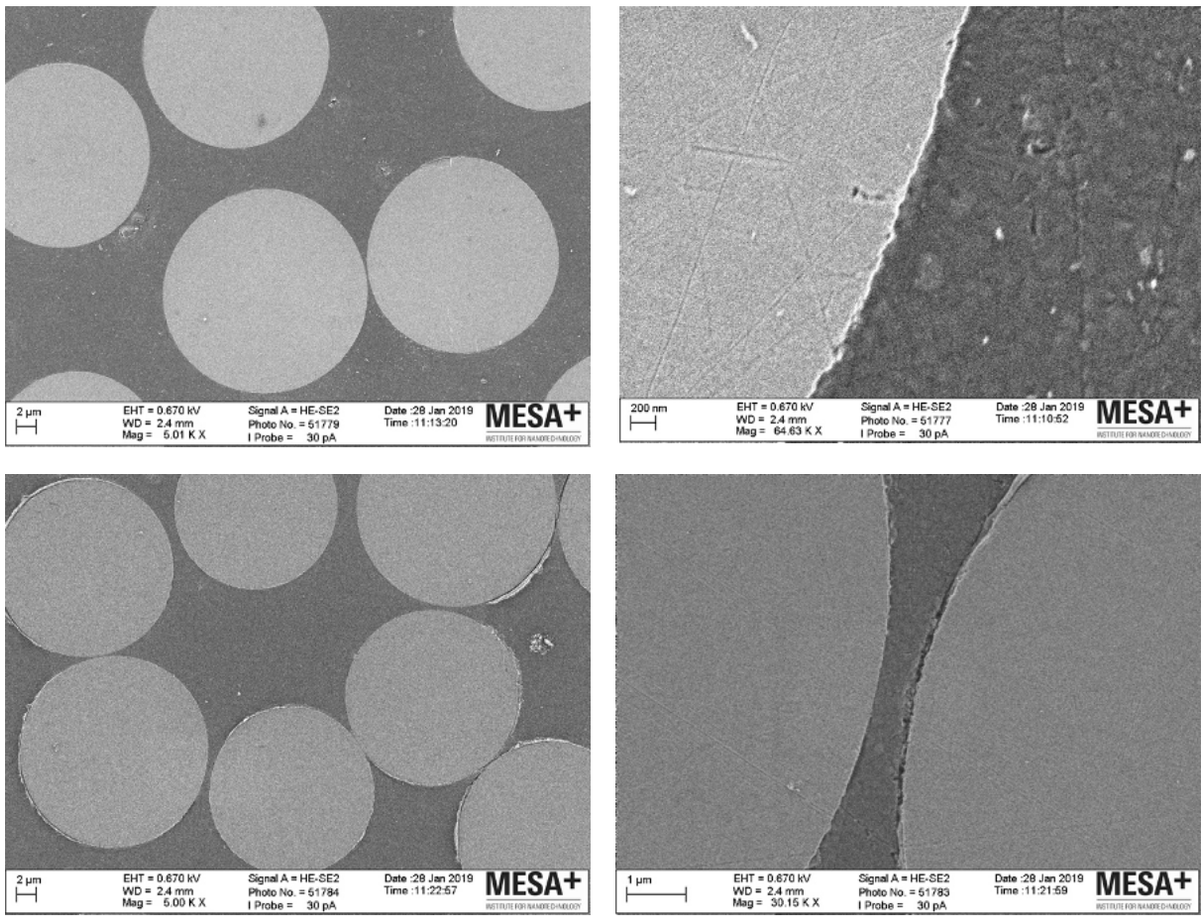

Figure 36. HR-SEM images of a sample before (up) and after hot-wet treatment (below). The epoxy and the glass fibres separate from each other in the hot-wet treated sample.

Furthermore, in Figure 37, it was observed that nearly all glass fibres remain intact during the hot/wet treatment. Cracks occur between fibres and epoxy matrix.

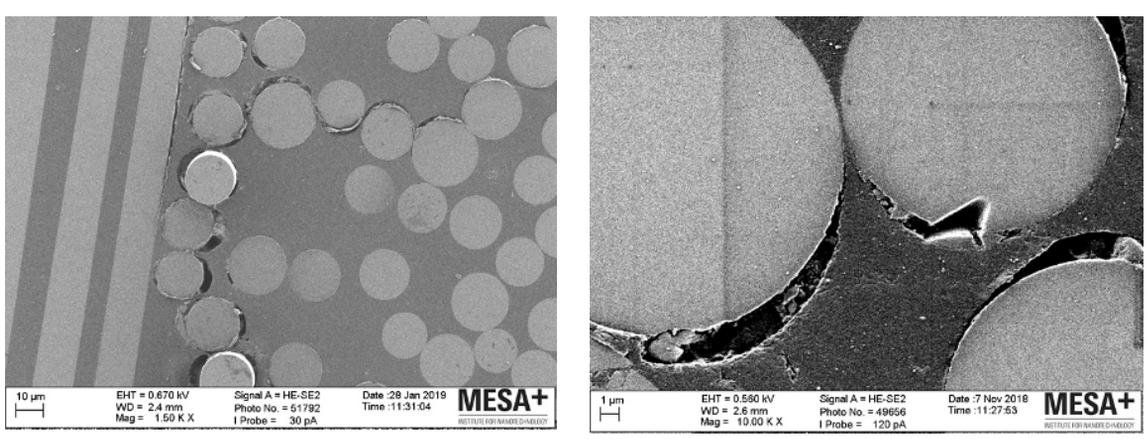

Figure 37. HR-SEM images of an aged sample. Cracks occur at the fibre-matrix-interface. The glass fibres remain intact during delamination.

A possible explanation for the cracks might be the difference in expansion coefficients of the glass and the epoxy matrix. It might also be caused by the debonding of sizing from the glass, resulting from the hydrolysis of the organosilanes. The immersion of water during the hot-wet treatment reverses the bonding reaction and causes the sizing to physically debond from the glass.

5.2.5. Optical microscopy (DIC)

The aim of this research was to obtain an overview of the number of cracks per sample. Both aged and fresh samples were tested which have been exposed to hot-wet conditions beforehand. The results can then be compared with those of the mechanical tests.

For these experiments, samples needed to be prepared. The protocol described in appendix 5 was used. However, for optical microscopy it was not necessary to do a quality check after every sanding step, which is why this step was left out. In short, the composites were sawn into test pieces with a measurement surface area of approximately 75 mm^2. They were embedded in epoxy resin and finally polished. The polishing is necessary in order to make the defects visible with the optical microscope (see Figure 38). A grain size of 1 µm was achieved with the polishing procedure. This procedure causes a mechanical effect on the samples, for example due to vibrations based upon grinding. An influence on the microscopy results cannot be excluded. However, the same procedure was used to the same extent for all samples, so the assumption is that this effect is negligible.

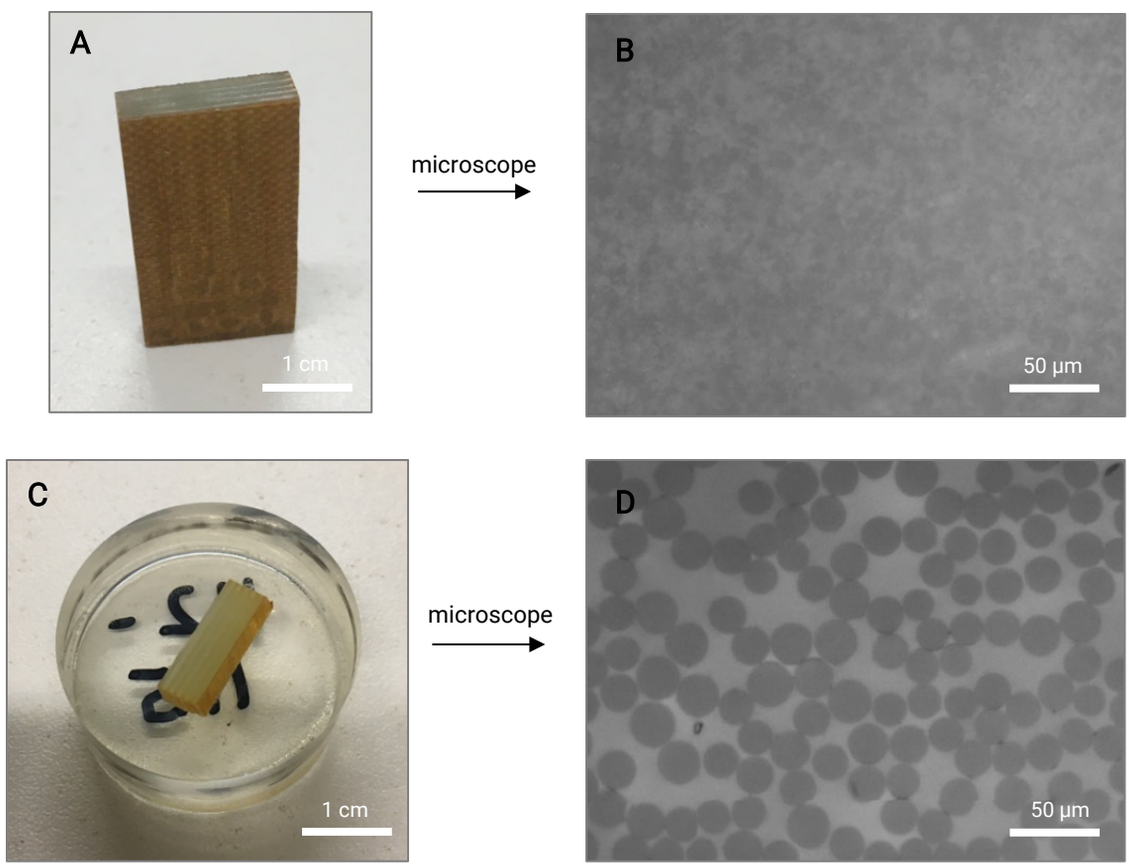

Figure 38. (A) Photograph of a test sample piece before polishing. (B) The microscope image shows that no individual fibres are visible when the sample is not polished. (C) Photograph of a test sample piece embedded in epoxy resin and polished. (D) The microscope image shows that individual fibres and defects are visible.

For imaging the test samples, a 10x phase contrast objective of the EVOS 7000 optical microscope was used. The EVOS is a fully automated microscope offering the possibility of making multiple images in a 2-dimensional grid pattern. The software then stitches the individual images to produce one large image consisting of 60-70 individual images, as the example in the figure below shows. Zooming into the individual cross-ply layers revealed different types of defects. On the one hand there are the already described cracks and on the other hand two types of dark spots were observed. The dark spots will be discussed in more detail first, then the results on the cracks are discussed.

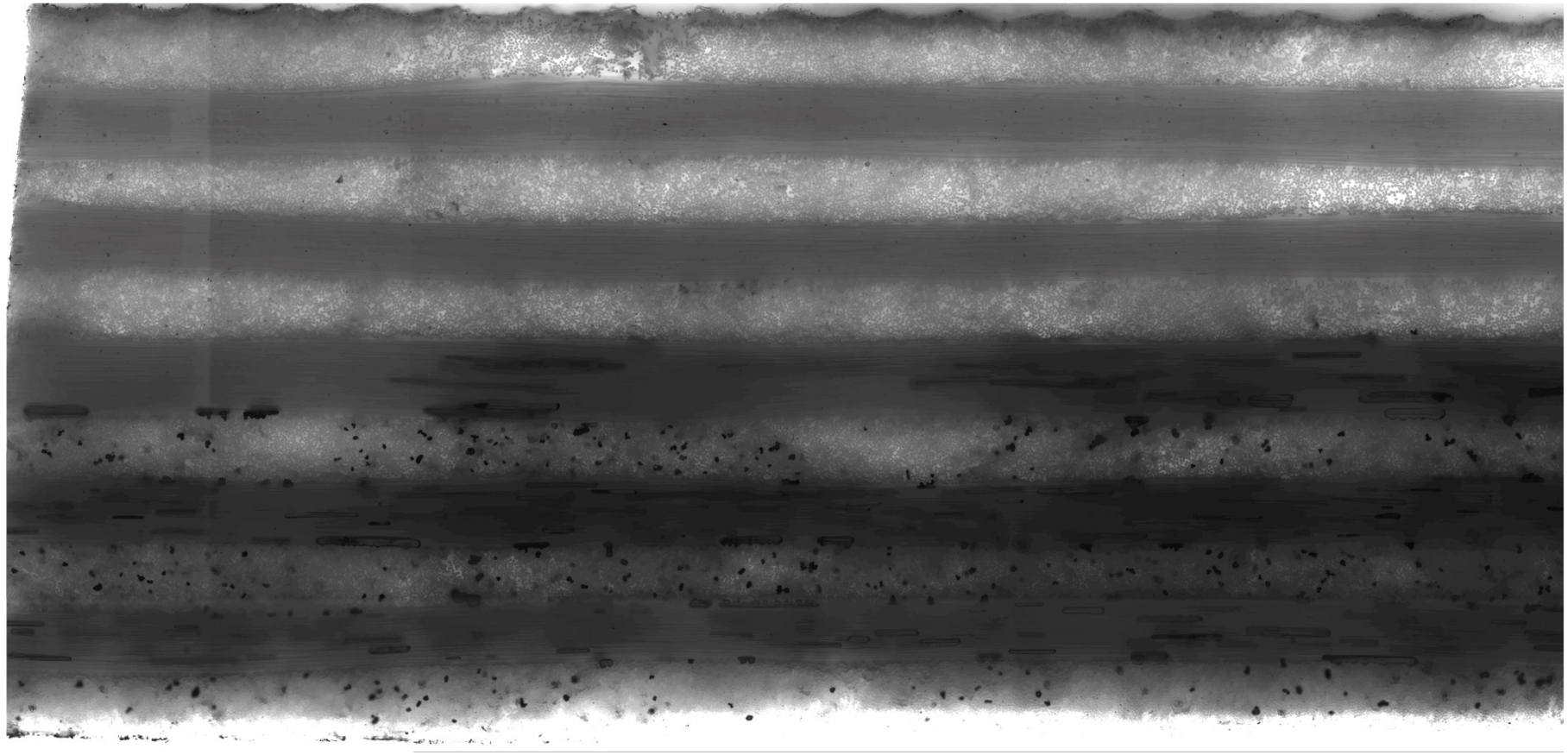

Figure 39. Stitched image of a raster scanned composite sample showing the layered structure. Black spots in the lower part represent voids.

5.2.5.1. Dark spots

The microscopic analysis revealed two types of dark spots in fibreglass laminates. On one hand, non hot/wet treated laminates do show dark spots typically between 3 or more 'close' monofilaments. Enlarged, they appear to be air entrapments. They are called type 1 dark spots. The same type of spots are observed in laminates exposed to 100˚C hot/wet treatment for 250 hours. At temperatures of 115˚C and 125˚C, laminates do show additional dark spots, typically between 2 'close' monofilaments. Enlarged, they appear to be not air entrapments. They are called type 2 dark spots (see Figure 40, right panel).

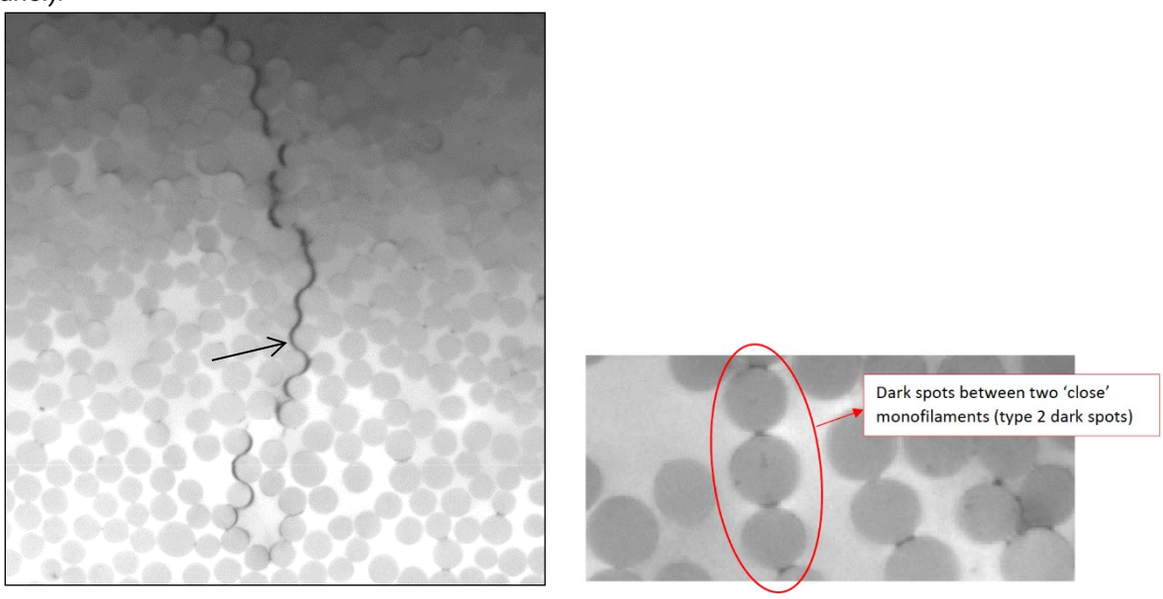

Figure 40. (Left) Cracks in the layers become visible as the image is magnified. An example is indicated with an arrow. (Right) A higher magnification reveals the dark spots type 2.

Dark spots type 2 preferably occur between glass fibres if there is less matrix in between them. For further analysis, the number of these defects was determined for an area of 0.035mm^2 (for all samples). For all types of rovings, it was observed that the number and size of dark spots increased with increasing temperature. The defects become broader at elevated temperatures, forming a line instead of a dot. This development is shown in Figure 41. It suggests that these defects are possibly weak points that can develop into cracks. However, no correlation was found between the number of cracks and the number of dark spots. Further investigation is necessary to test this hypothesis. There were no outliers in the number of dark spots. The number of defects ranged from 0 to 81 for all rovings.

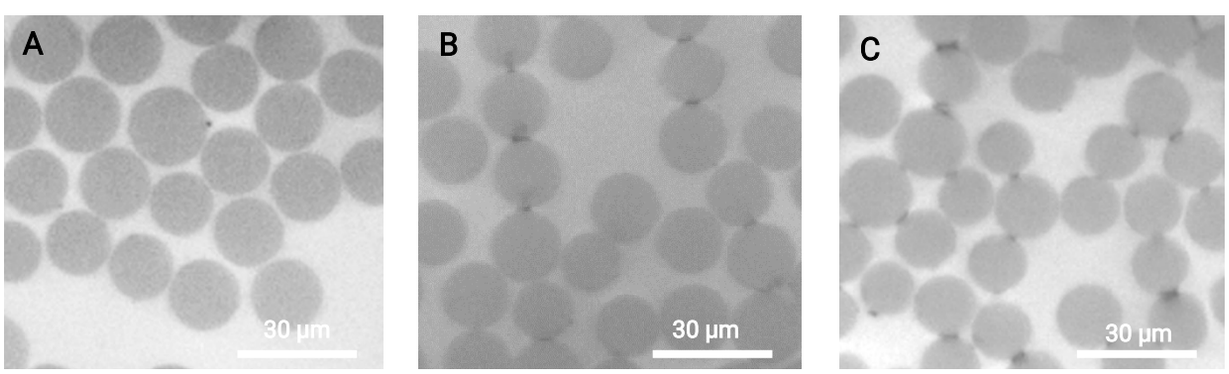

Figure 41. The number and size of dark spots type 2 increased with harsher hot-wet conditions. (A) initial, (B) 115˚C, (C) 125˚C

5.2.5.2. Crack formation

The cracks differ strongly, not just between different samples but also within one sample. On the one hand, they range from fine and short hairline cracks having a length of just 2-3 individual glass fibres, to very thick cracks which run vertically through a complete layer. In all samples it was observed that at lower temperatures of hot/wet-treatment first cracks arise in the outer layers of the sample. With increasing temperature more cracks form in the inner layers as well.
However, when taking a closer look at the results, there was a significant difference for some rovings. For example, hot/wet 121 °C for 3000 hours treated laminates produced from non-aged (fresh) SUP3 GF4 roving show type 2 dark spots, some of them interconnected. This is observed in the external cross-ply layer particularly. Interconnected type 2 dark spots seem to have formed some cracks here. Hot/wet 121 °C for 3000 hours treated laminates produced from aged GF4 roving show a significantly increased number of these interconnected type 2 dark spots, both at internal- and external cross-ply layers. They are more pronounced at external layers, where the interconnected type 2 black spots seem to have developed in cracks. This behaviour correlates with earlier TFF1 findings, where GF4 showed to be relatively sensitive for ageing in air.

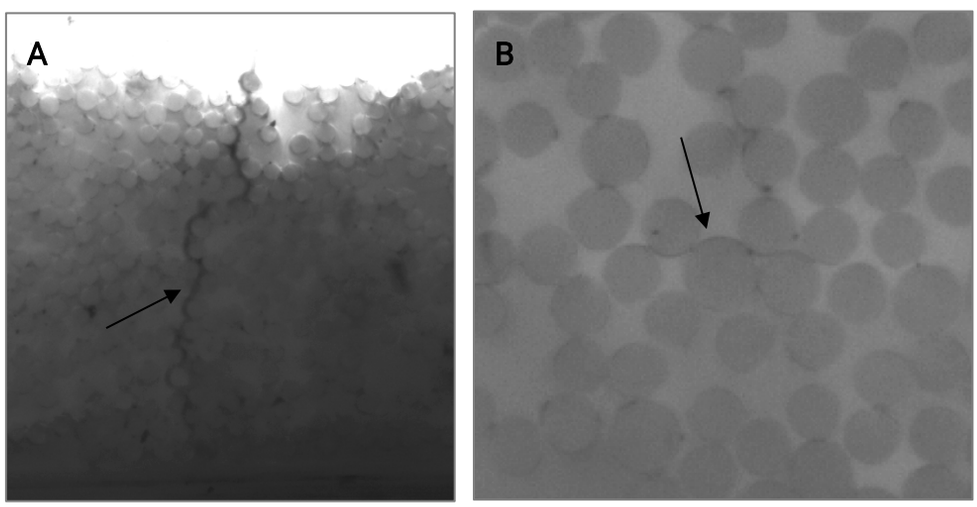

Figure 42. (A) A large cracks passes through a composite layer. (B) A thin crack is indicated by the arrow.

The number of cracks did increase with increasing temperature of the hot/wet treatment in all samples. The extent of this increase varied depending on the type of roving. Furthermore, it was noticed that the hot-wet conditions of 100 ˚C had little or even no effect on 6 out of 8 samples. However, if the temperature is increased to 115 or 125 ˚C, the increase in cracks becomes more apparent. Two examples of this behaviour are shown in Figure 44. During the experiments it was observed that cracks tend to branch and thus increase the extent of damage even more. Often, cracks did also start at voids. An example is shown in Figure 43.

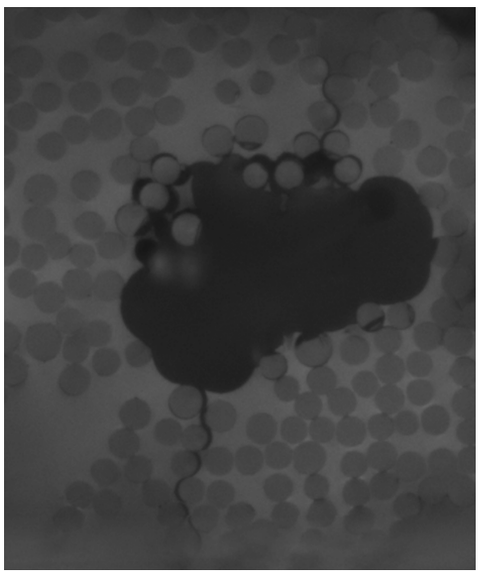

Figure 43. Cracks often appear at large voids in the composite.

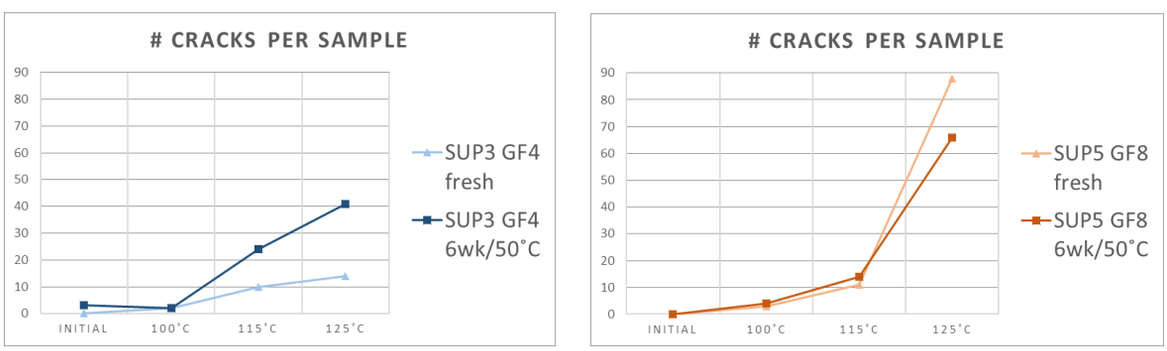

Figure 44. The number of cracks per sample plotted against the applied hot-wet conditions for fresh and aged roving. Whereas the step from initial to 100 ˚C shows has minor influence, the effect of hot-wet conditions at 115 ˚C and 125 ˚C is significant.

The number of cracks per sample generally ranged from 0 to 90, depending on the applied temperature of the hot/wet conditions. In appendix 6, the procedure of defect determination is described. Three of the eight samples will be discussed in more detail because of their noticeable results. It was observed that roving SUP2 GF3 out of all samples was by far the least susceptible to develop cracks. Even after the hot-wet treatment at 115 ˚C and 125 ˚C, the number of cracks in this sample increased only slightly to not at all. The situation was very different for roving SUP4 GF7. The temperature of 115 ˚C resulted in more than 90 cracks (aged sample) and after treatment at 125 ˚C in 240 (fresh) or even 344 cracks (aged) fractions. The results of these two rovings, which are the extremes in this experiment, are shown in the figure below. Roving SUP1 GF2 was an outlier. Both the fresh and the aged sample initially showed an increase in cracks, but the number decreased again at higher temperature. The analysis was repeated and the samples were checked for correct labelling to rule out errors. The observed phenomenon cannot be fully explained. It is assumed that this is the result of the small measuring area of 75 mm^2 and that the sample could be heterogeneous.

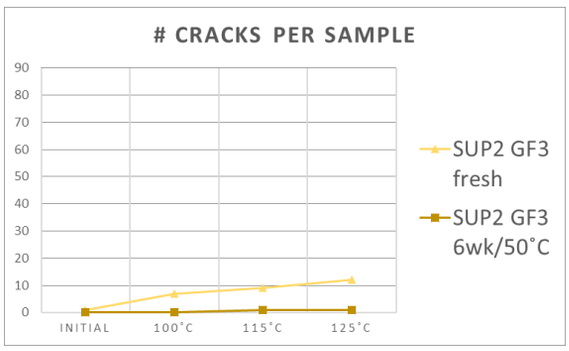

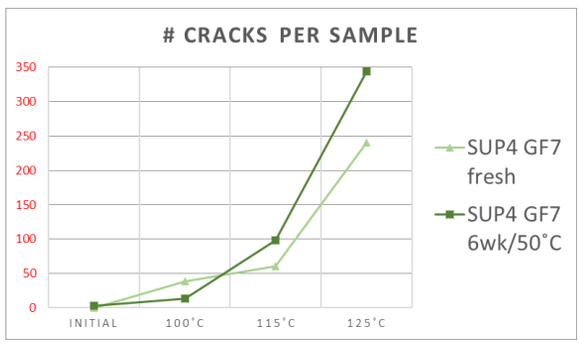

Figure 45. The number of cracks was the lowest for SUP2 GF3 (left), whereas SUP4 GF7 (right) showed the most fractions.

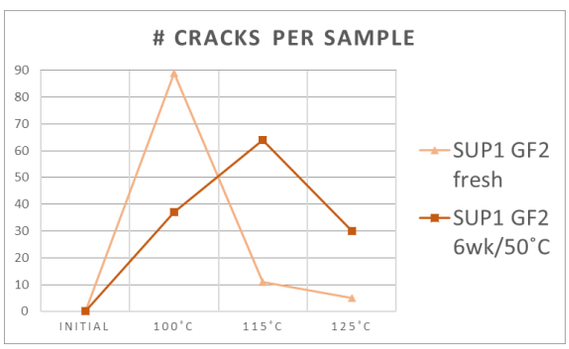

Figure 46. Sample SUP1 GF2 showed unexpected results. The number of cracks shows an increase first but decreases again, probably due to heterogeneity of the sample.

6. Long-term hot-wet exposure tests of 121 °C with selected rovings.

6.1. Mechanical test results with selected rovings.

To investigate the effect of a longer exposure time to hot-wet treatment a selection of rovings is tested with SB 0/90 after hot-wet exposure at 121 °C (250 °F). Samples were exposed to water for 500, 1000, 3000 and 5000 hours. Rovings GF1 up until GF8 were tested although not all samples were available as fresh and aged. The results of the tested fresh rovings are depicted below. The numerical results can be found in Appendix 9.

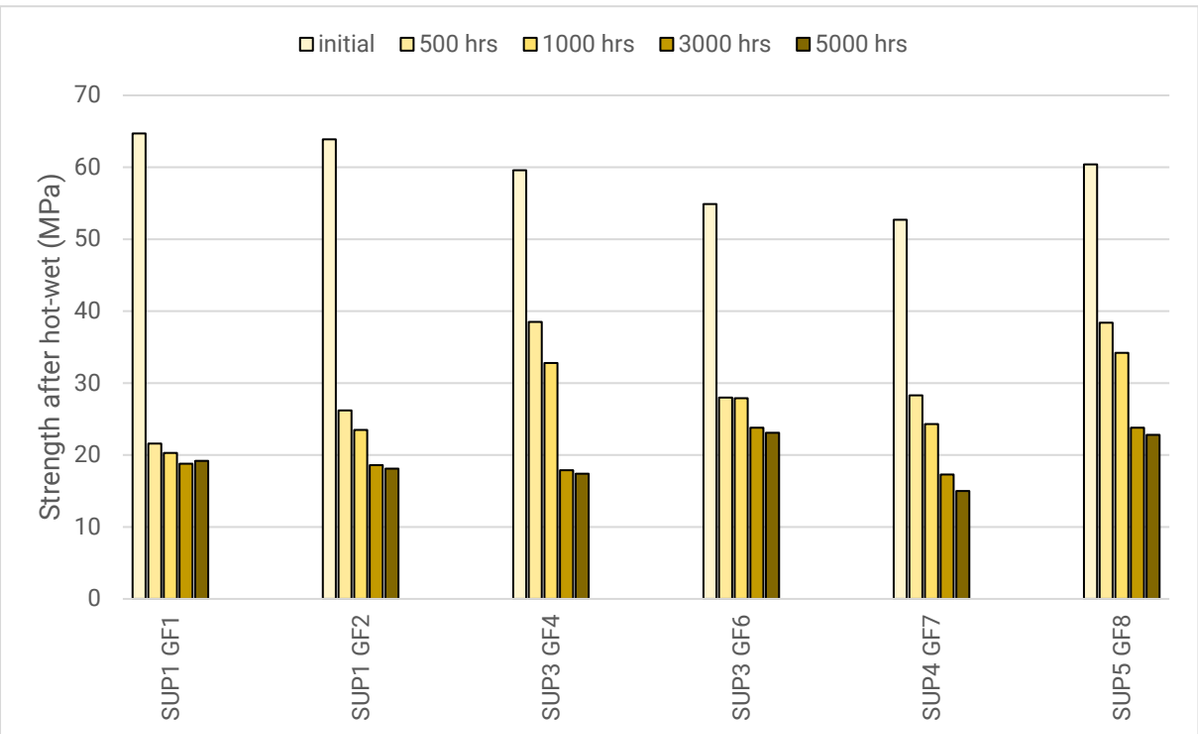

Figure 47. Results of the short beam 0/90 test of samples made with fresh roving and exposed to water at 121°C, for 500, 1000, 3000 and 5000 hours in comparison with the initial sample.

The results of the tested aged rovings are depicted in Figure 48. Again, roving GF1 and GF2 show a very large drop in properties directly after 500 hour exposure. For roving GF6 and GF7 the drop is less pronounced but clearly visible after 500 hour exposure. Rovings GF3 and GF8 show the best retention after 500 and 1000 hour. However, after 3000 hours exposure the retention has dropped to circa 25-30%.

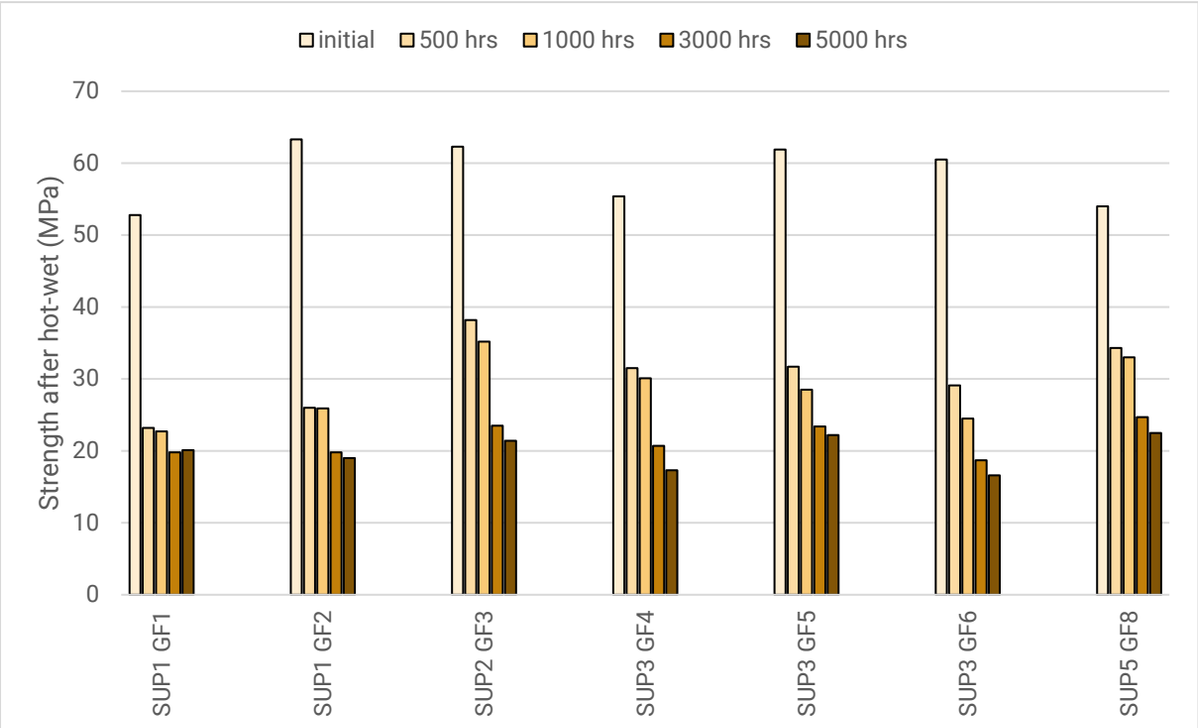

Figure 48. Results of the short beam 0/90 test of samples made with aged roving and exposed to water at 121 °C, for 500, 1000, 3000 and 5000 hours in comparison with the initial sample.

6.2. Evaluation on micro-scale and nano-scale

6.2.1. Optical microscopy (DIC)

For this analysis, the samples were prepared as described in section 5.2.5. The imaging with the EVOS microscope and the subsequent analysis was identical as well (see Appendix 6).

The number of cracks and dark spots type 2 was analysed for these samples. Rovings SUP2 GF3 and SUP3 GF5 showed the least amount of cracks (maximum of 20). In addition, no increasing trend with increasing duration of hot/wet conditions was detected. Rovings SUP3 GF4 and SUP5 GF8 did show more cracks with increasing duration of the hot/wet conditions. Furthermore, the total number of cracks was much higher.

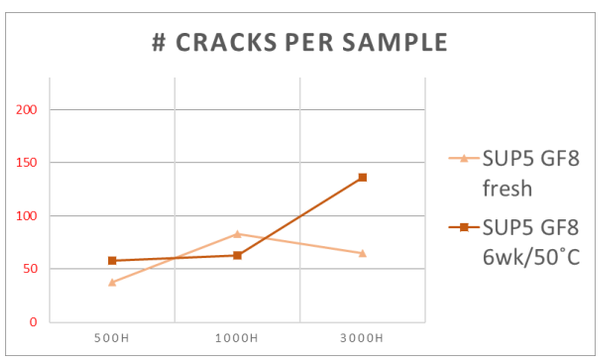

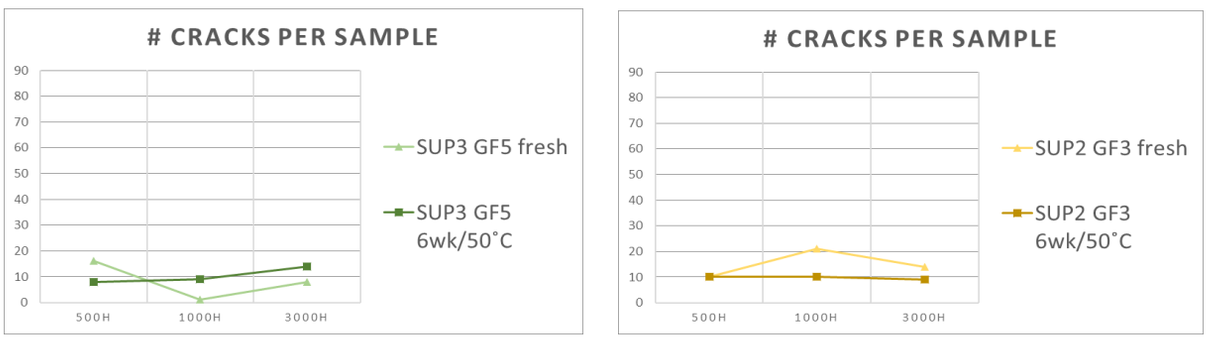

Figure 49. The number of cracks per sample plotted against the applied hot-wet conditions for fresh and aged rovings. The bottom graphs show rovings that do not respond to a longer duration and have nearly no cracks, whereas the top graph shows a roving that shows a higher number of cracks on the sample.

Considering the dark spots type 2, in all samples an increased number was observed with increasing duration of hot-wet conditions, see appendix 13. There was no difference in dark spot count between fresh and aged samples and the different types also showed no significant differences in the number of dark spots. The number ranged from 21 to 82 for all rovings.

7. Comparison with carbon fibre reinforced systems at 150 °C.

SUP6 CF1 carbon tow (manufactured in 2015, 2017 and 2018) has been selected for investigation with the SB 0/90 test and was compared with glass roving GF3 regarding ageing stability and hot-wet resistance at 100 °C and 150 °C (Table 6). This glass roving is selected for comparison because it performed best of all glass fibre rovings in hot-wet conditions. The matrix used in these tests consists of a high Tg amine cured epoxy.

Name	Manufacturer
CF1	SUP6
GF3	SUP2

Table 6. Tow and roving used in SB 0/90 tests

7.1. Mechanical tests

As described in section 2.5, CF1 carbon tow was tested with SB 0/90. 0/90 test plates were manufactured and the effect of ageing of the carbon tow is investigated. The results are given in Figure 50. Two test plates have been made from carbon tow manufactured in 2017.

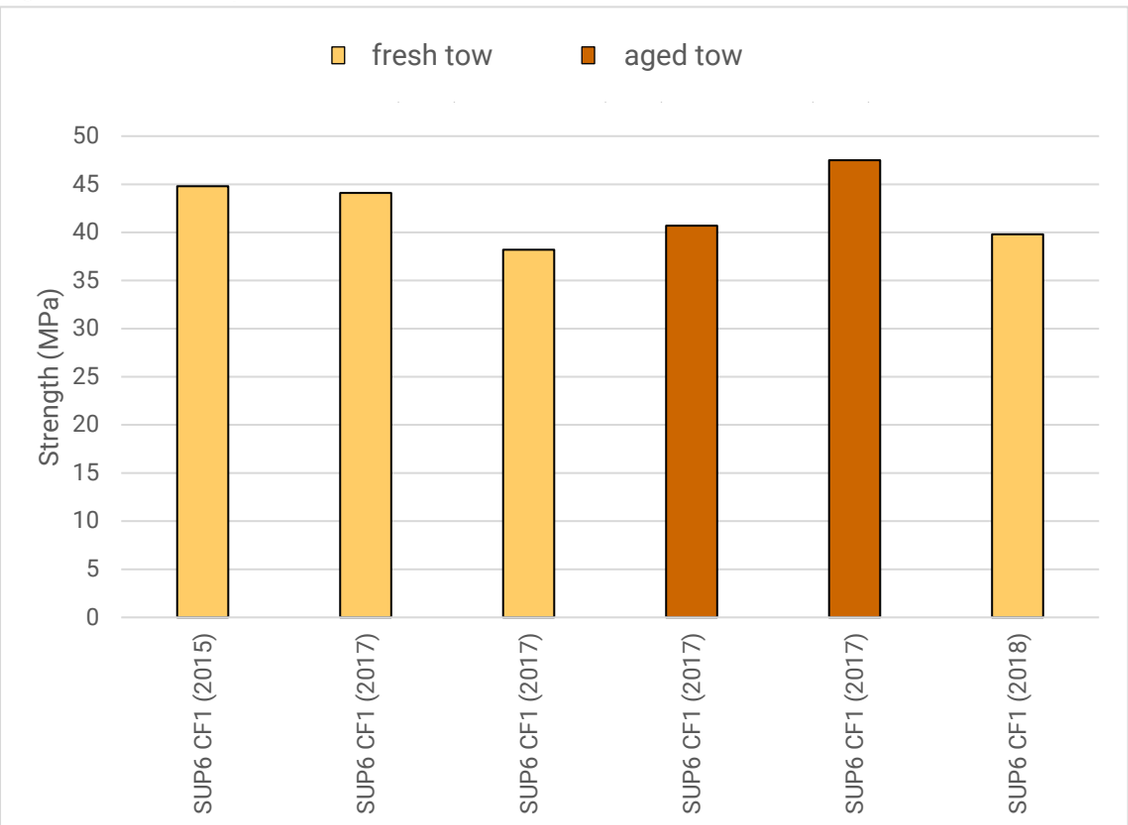

Figure 50. Results of the short beam 0/90 test initially (fresh) and after the carbon tow has been aged in an oven for 6 weeks at 50 °C. Years indicate the manufacturing date of the carbon tow.

The hot-wet behaviour of fresh carbon reinforced epoxy samples has been investigated and is presented in Figure 51. Besides the carbon fibre also the best performing glass roving at hot-wet conditions (SUP2 GF3) has been tested. The samples were exposed to water at 100 °C and 150 °C for 250 hours.

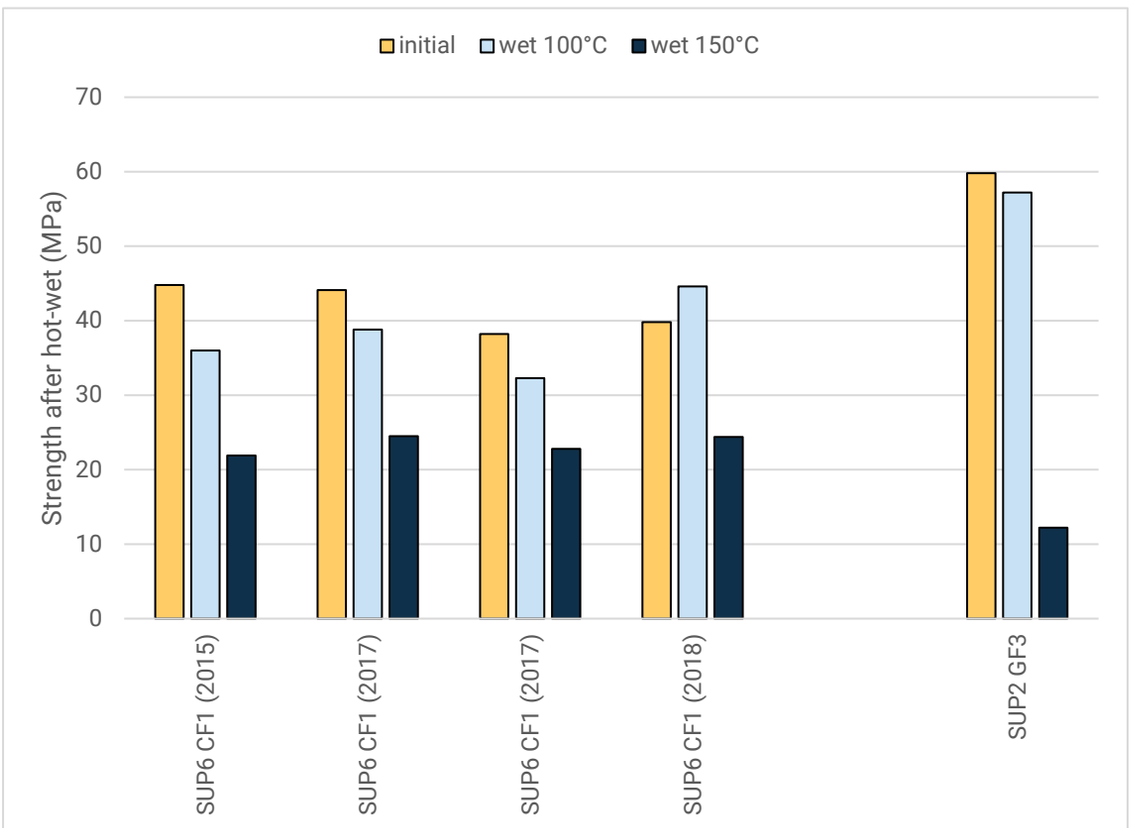

Figure 51. Results of short beam 0/90 test samples made with fresh SUP6 carbon tow and fresh SUP2 glass roving after exposure to hot water. Years indicate the manufacturing date of the carbon tow.

Both glass fibre and carbon fibre samples showed good retention after 250 hrs at 100 °C. The retention in strength of GF3 after 100 °C hot-wet treatment can probably be explained by the resin recipe that is used in this experiment. The addition of Epikote 496 raises the Tg of the resulting resin. From the results it is clear that the glass fibre roving does not perform well after exposure at 150 °C. The carbon fibre samples show good retention after 250 hours at 100 °C and a reasonable retention after 250 hours at 150 °C.

7.2. Optical microscopy (DIC)

During this experiment, the crack formation in carbon fibre composites was studied. The use of carbon is a promising alternative to glass in case the product will be exposed to high temperatures. Figure 52 shows a comparison of glass and carbon fibre composites made with the same carbon tow and fibreglass roving as in paragraph 7.1. They are both produced from the same high Tg epoxy matrix, treated for 500 hours at 150 ˚C in wet conditions. The glass fibre product (left image) does not withstand such extreme conditions, whereas the carbon product (right image) shows neither cracks nor dark spots. Ageing the carbon fibres for 6 weeks at 50 ˚C did not have an influence on the results. These results show that carbon fibre reinforced systems are well suited for applications in high temperature conditions.

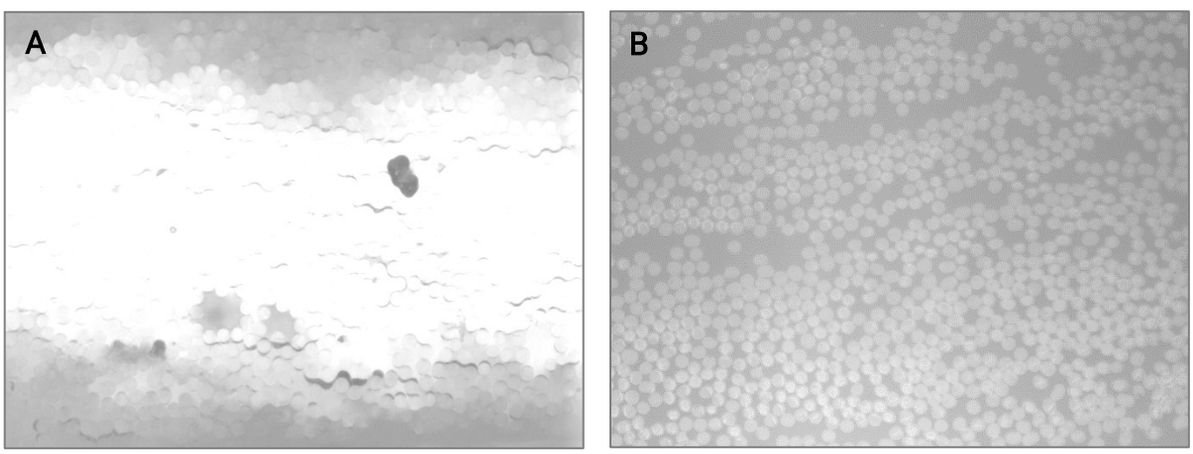

Figure 52. (A) The glass fibre composite treated with a temperature of 150˚C shows more than 1000 cracks on an area of 75 mm^2. (B) The carbon composites did not show any defects after treatment under identical conditions.

7.3. Scanning electron microscopy

Carbon composites were also visualized using HR-SEM. The fibres show a rough edge and a smaller diameter. Whereas a glass fibre is approximately 15 µm, a carbon fibre has a diameter of only 7 µm. Both factors lead to an increased surface to volume ratio and therefore a higher contact surface to the epoxy. That could lead to a better connection to the matrix material. Some cracks and de-lamination can be detected using the HR-SEM after 500 hours of ageing. However, the extent is much less compared to glass fibre composites.

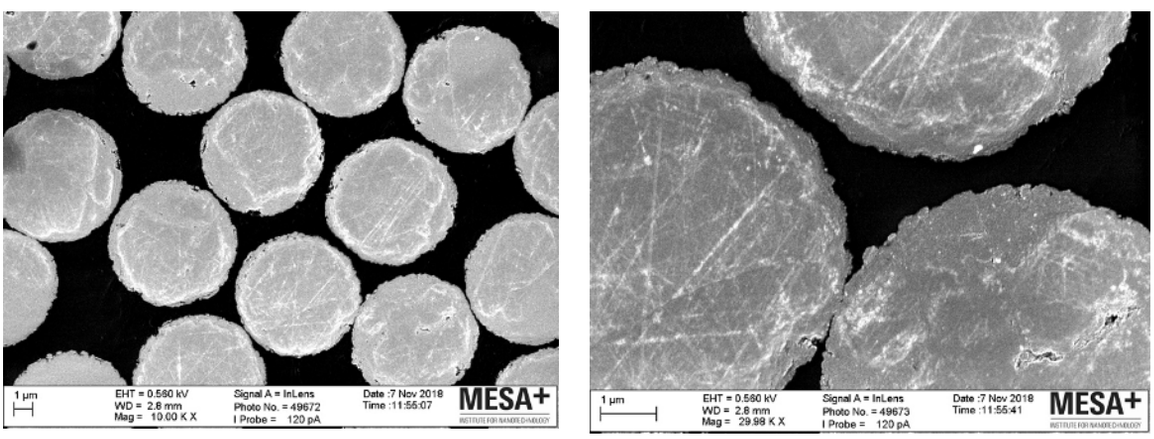

Figure 53. HR-SEM of unaged carbon composite. The fibres show a rougher edge and a smaller diameter compared to the glass composites.

8. Discussion

In the previous chapters several glass fibre products have been evaluated on their performance in GRE after ageing and after long-term hot/wet exposure at different temperature levels. Evaluations have been made both with the macroscopic test (SB 0/90 test) and with the microscopic quantification of cracks. However, the ranking of performance of the different products as was found with the macroscopic test does not seem to correlate with the ranking as was found with the microscopic quantification of cracks. In this chapter, the observations by the two methods are given a closer look. Moreover, it is tried to get a better understanding of the performance of GRE after hot/wet exposure by a more detailed investigation of the microscopic development of damage in the composite. All observations and analysis of these observations lead to a more refined understanding of the performance of the different glass fibre products.

8.1. Microscopical evaluation of development of damage in GRE in hot/wet-exposure

Several typical defects were observed during microscopic evaluation, which will be discussed in more detail below.

Two types of dark spots were present in nearly all samples. On one hand, air inclusions between 3 or more ‘close’ fibres could be observed. These are referred to as type 1 dark spots. Such air inclusions can be caused by either (i) air bubbles that are present in the mixed resin and hardener just prior to impregnation of the glass fibres or (ii) by locally decreased glass fibre impregnation, for instance resulting from sporadic excessive sizing of glass fibres as discussed in chapter 1.3 and figure 8. An increase in temperature or duration of hot-wet exposure did not lead to an increasing number of type 1 dark spots. Type 2 dark spots, on the other hand, showed a different behaviour. These dot-shaped defects between 2 ‘close’ fibres sparsely appeared in initial laminates. However, their number increased significantly with increasing hot/wet exposure temperatures & times. In addition, they start to interconnect to each other, finally resulting in cracks. This type of defect seems to have an effect on the mechanical properties of the composites. Several observations support this hypothesis. For example, hot/wet 121 °C for 3000 hours treated laminates produced from aged SUP3 GF4 roving showed a significantly increased number of interconnected type 2 dark spots compared to the non-aged roving. In the external cross-ply layers, type 2 black spots were interconnected and seem to have developed in cracks. This behaviour correlates with results from the previous TFF1 project, where GF4 showed to be relatively sensitive for ageing in air. Furthermore from this study, the aged SUP3 GF5 roving showed to be less sensitive for ageing in air. This again correlates to the results presented here, because only some isolated type 2 dark spots and occasionally a crack in the external layers were observed. A third example is the SUP2 GF3 roving, which showed a low sensitivity for roving ageing. Our findings here support this observation, since GF3 showed a very low number of dark spots type 2. In conclusion, the appearance of dark spots type 2 between ‘close’ fibres is an interesting behaviour. The interphase between glass and epoxy plays a crucial role in adhesion of both components. The interphase extends into the epoxy matrix. If the glass fibres get too close, there is effectively no bulk epoxy, which might result in the breaking of the material just there. This might also mean that adjusting the distribution of the glass fibres in the composite could lead to an improved resistance against higher temperatures.

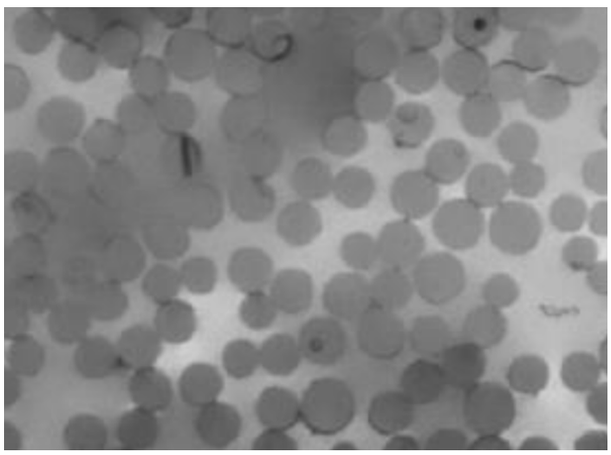

Figure 54. SUP3 GF4 aged & hot/wet 121 °C @ 3000 hr – Many connected type 2 dark spots at 'close' monofilaments forming cracks at the inner layers of polished cross-section.

Another observation were the dark areas near the next cross-ply layer, not between 'close' monofilaments. These areas close to the next cross-ply layer are sometimes difficult to analyse. Sometimes they look like cracks but when zooming in they appear not interconnected and different to type 2 dark spots. They do not appear between 'close' monofilaments. This could be an effect of polishing. However, that could not be verified in this project.

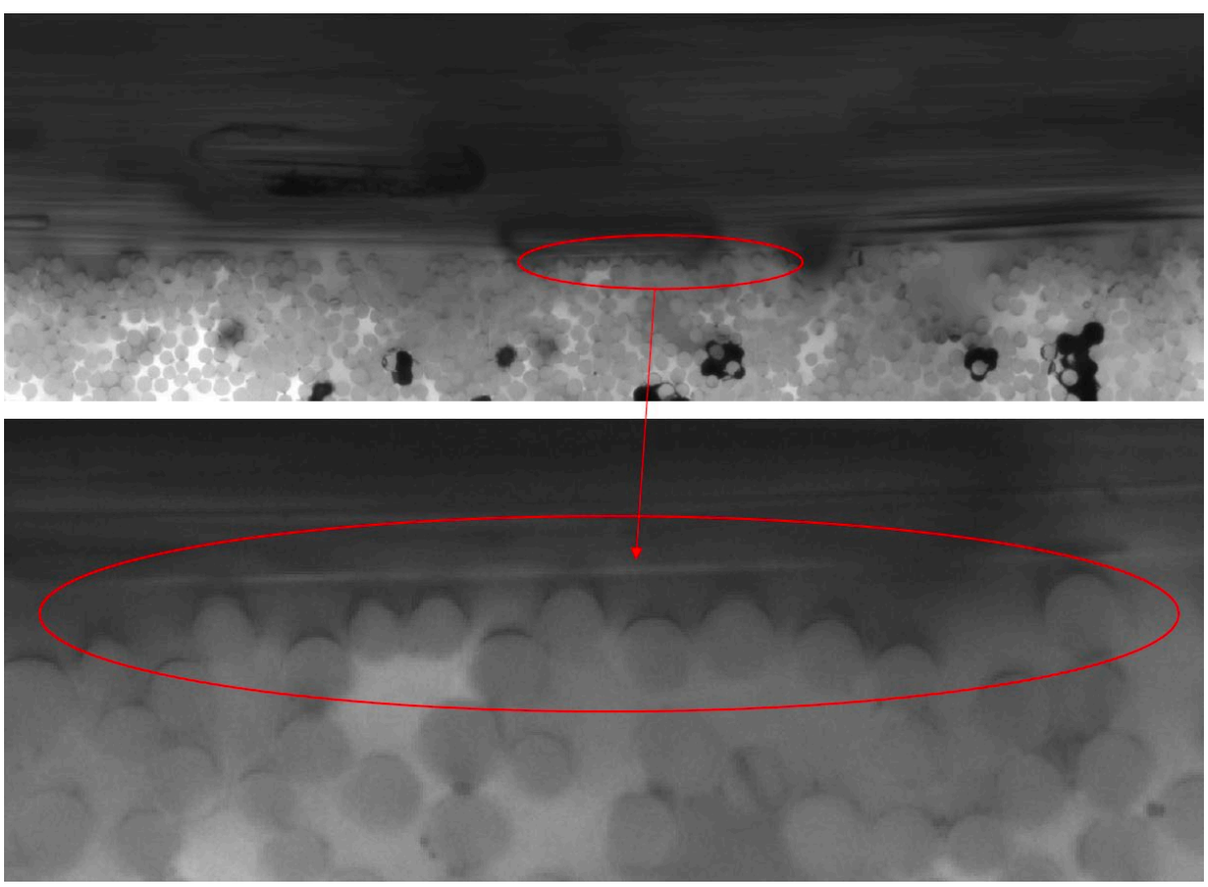

Figure 55. Dark spots at monofilaments near the next cross-wound layer. They do not appear between 'close' filaments, what distinguishes them from type 2 dark spots.

Voids, with or without loose monofilaments, were also observed during microscopic analysis. Cracks often arise at voids. We propose a mechanism for this behaviour. During hot/wet treatment, voids are

filled with water. Due to that, monofilaments at the edges of these voids experience a higher stress than filaments with a longer distance to voids. This mechanism could lead to a) released monofilaments which we then observe as single fibres in the void or b) cracks developing from one monofilament to another deeper; that seems to happen especially if the density of filaments at the edge of the void is high.

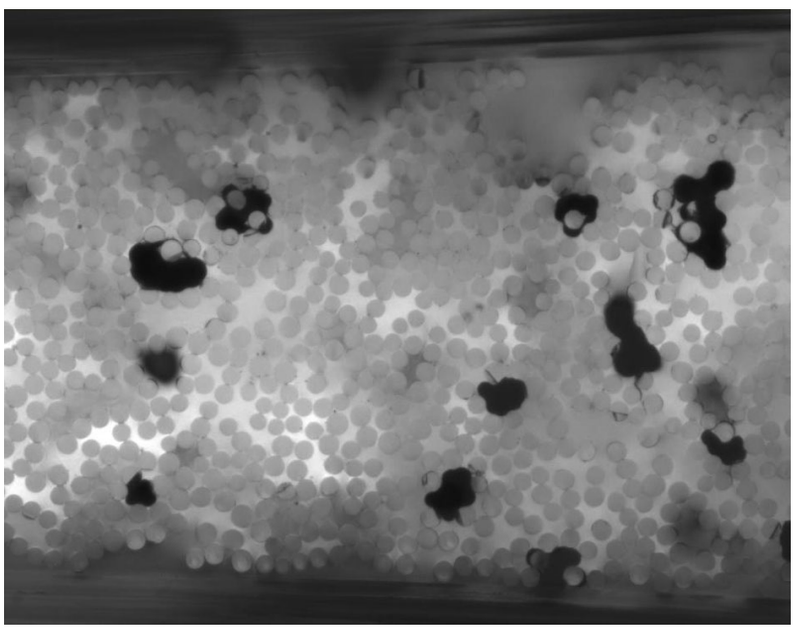

Figure 56. SUP2 GF3 non-aged (fresh) and hot/wet 121 ˚C for 3000 hours treated composite. Cracks at voids are observed as well as monofilaments in the voids.

The scope of the microscopic evaluation was a 'damage rating' based on the number of cracks on the obtained photographs. It has to be mentioned that the variance in the number of observed defects is large between different samples, but also within the same sample. In addition, the area compared is quite small. All this is hampering a reliable damage-rating determination. Examples are shown in Figure 57. The two images seem to be comparable. However, the number of cracks observed in the whole sample differs distinctly, which can be observed in Figure 45 as well. This non-homogeneous character of the samples shows that conclusions cannot be drawn based on single images. Nevertheless, we can conclude that the microscopic photos contain valuable and new information. However, a scientific 'damage rating' based on these photographs was not possible within the scope of this project.

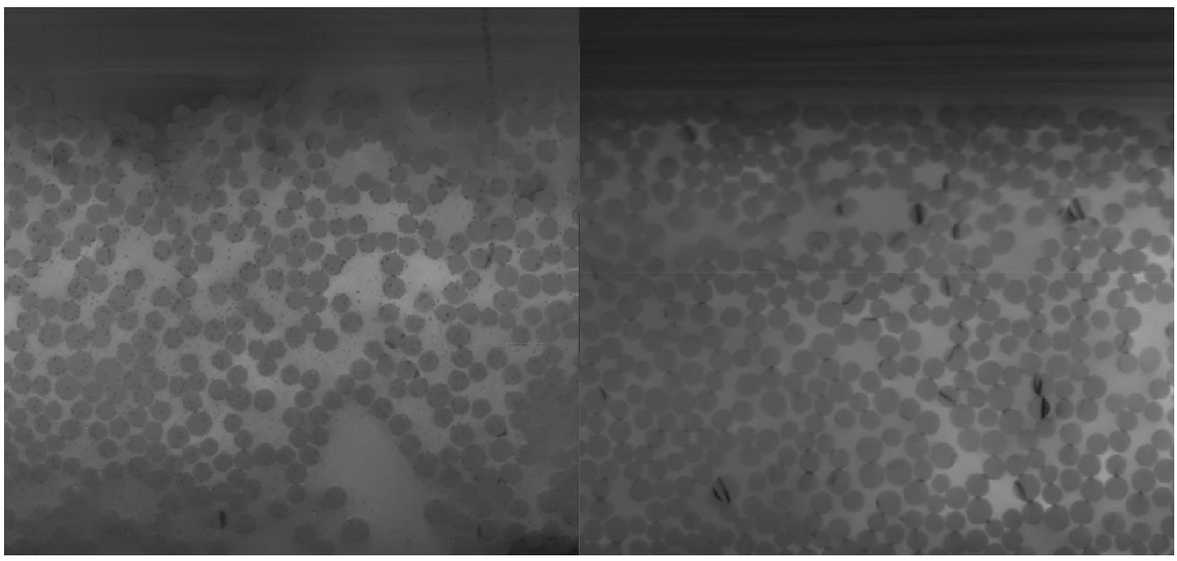

Figure 57. (Left) fresh SUP5 GF8, 250hr@125 ˚C number of cracks ~14. (Right) fresh SUP3 GF4, 250hr@125 ˚C, number of cracks ~89

8.2. Correlation between macroscopic and microscopic test results

In the previous chapters results are presented in bar charts. This gave a good insight in the differences in performance of glass fibres after ageing (hot storage) and long-term hot/wet exposures at different temperatures. However, by presenting the macroscopic test results as a function of hot/wet-exposure temperature more information can be obtained as shown in the graphs in Figure 58 up to Figure 60. Figure 58 shows the initial SB 0/90 as well as the SB 0/90 after hot/wet exposure over 250 hours at 100 °C, 115 °C and 125 °C. Apart from both SUP1 rovings, all rovings show more or less parallel lines between initial SB 0/90 and SB 0/90 after 250 hours of exposure at 100 °C. This may indicate that we are looking at the temperature effect of the only material that is identical in these laminates - being the resin matrix. Apparently, until 100 °C, the various matrix-to-glass bonding strengths of these roving types do not play a critical role yet. Only at 115 °C and 125 °C we start to see differences. This correlates with the findings of the microscopic analysis (see section 5.2.5.1, Figure 41), where type 2 dark spots are typically absent in initial and at 100 °C for 250 hours exposed laminates, while they start to appear at 115 °C and more so at 125 °C. The macroscopic SB 0/90 cross-ply tests seem to correlate with the microscopic observations here. In addition, the hot/wet 125 °C for 250 hours exposed laminates do show a significantly increased amount of type 2 dark spots. This behaviour was seen in all fibreglass laminates. This may also relate to the SB 0/90 results shown in Figure 58.

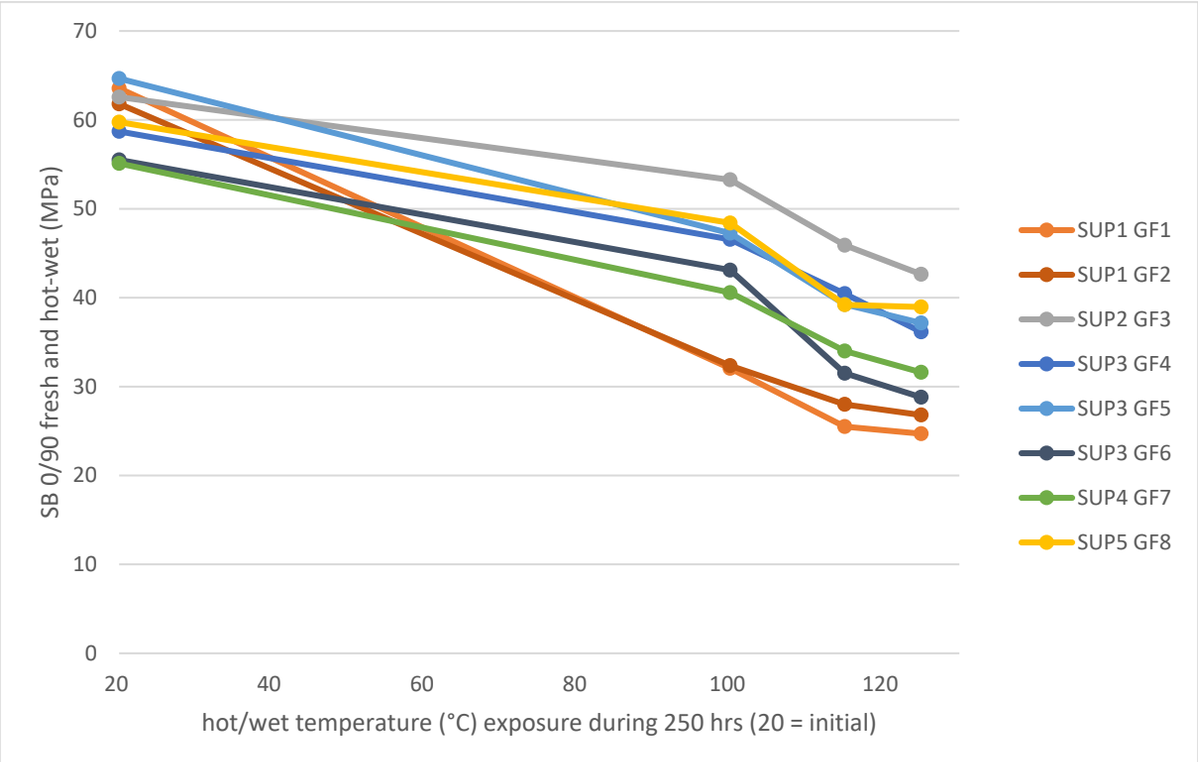

Figure 58. Hot/wet tests on cross-ply laminates produced from non-aged roving, 250 hours exposure time at 100 ˚C, 115 ˚C and 125 ˚C.

The general trend in Figure 59 and Figure 60 correlates well with the microscopic data as well as the known FPI fingerprint qualifications where SUP2 GF3, SUP3 GF5 and SUP5 GF8 are seen as good quality rovings showing proper storage stability, while aged SUP3 GF4 showing low SB 0/90 strength after 5000 hours. The non-aged GF4 shows a bit low result, but that might be the result of ageing effects of the GF4 prior to receiving this roving as 'fresh' for this project. The 5000 hour results do not differ much from 3000 hours, this might have to do with a logarithmic effect of hot/wet exposure, as it is the case for known fibreglass pipe regression tests. Further, it must be noted that the low performance of aged GF4 at 121 °C hot/wet is not picked-up yet by the 250 hours exposure test. The long-term performance of this roving was mainly demonstrated by the 3000 hours and 5000 hours data points at 121 °C. This is line with the observations made during microscopic analysis, where 1000 hours exposed aged GF4 showed non-connected type 2 dark spots in internal cross-ply layers and some connected at the external monofilaments, whereas 3000 hours exposed aged GF4 shows clear connected type 2 dark spots in all layers.

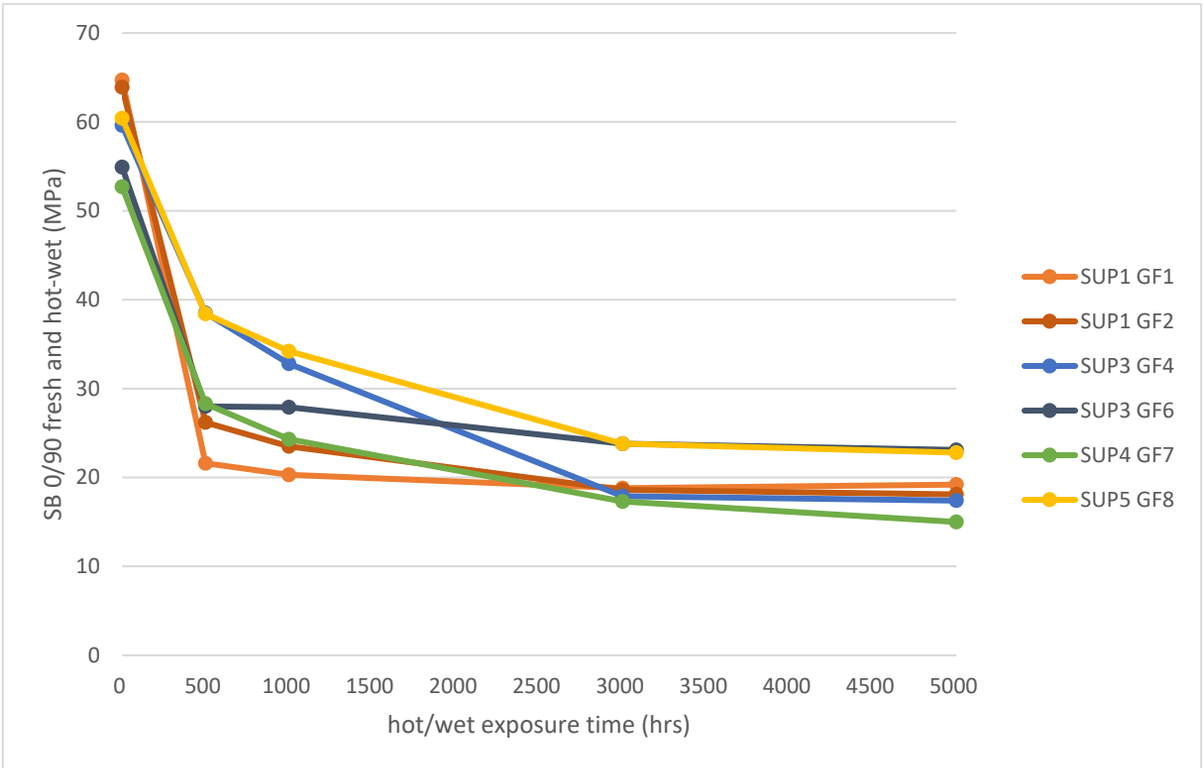

Figure 59. Hot/wet tests on cross-ply laminates produced from non-aged roving, at 121 °C for 500, 1000, 3000 and 5000 hours exposure time.

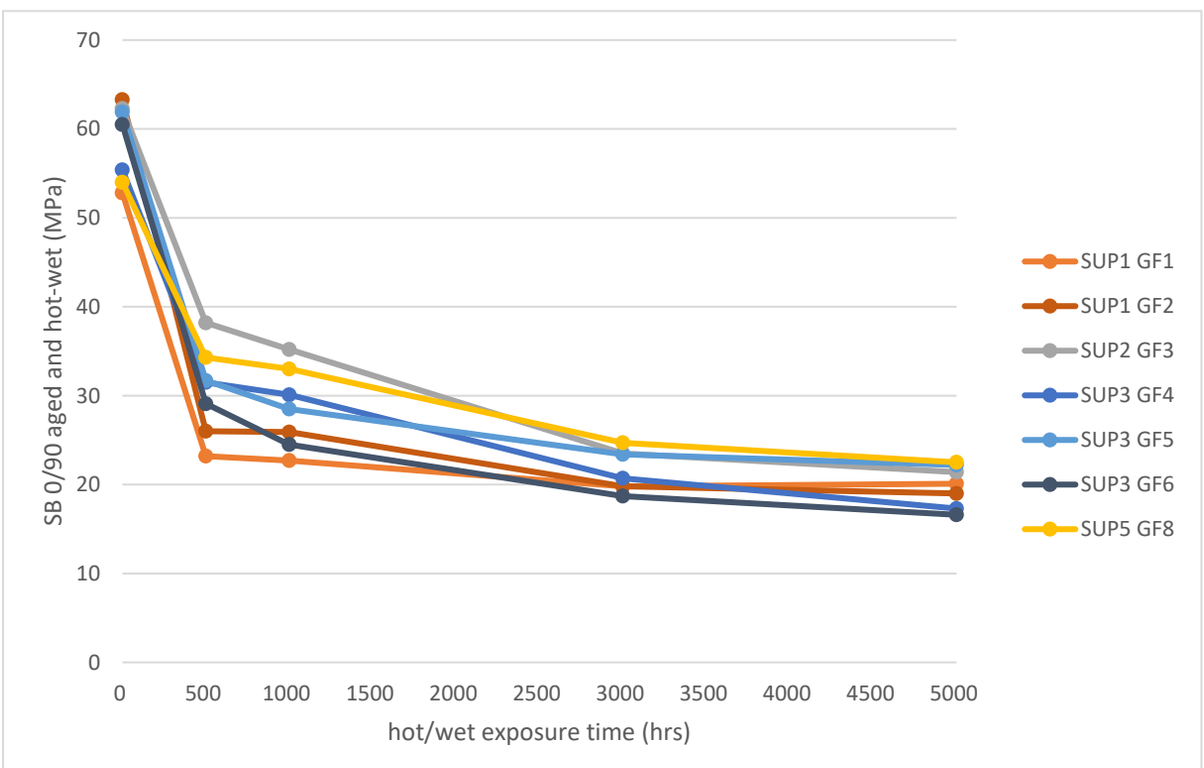

Figure 60. Hot/wet tests on cross-ply laminates produced from aged roving, at 121 °C for 500, 1000, 3000 and 5000 hours exposure time.

We have also obtained some results from the microscopic and macroscopic evaluation that cannot be related to each other. However, in general two trends were observed: (1) The development of type 2 dark spots seem to correlate with SB 0/90 strength and (2) The development of cracks seem to correlate with SB 0/90 results. An example for this second trend is the aged SUP3 GF4, exposed at 121 ˚C for 1000 hours, which does show a considerable amount of type 2 dark spots in the internal cross-ply layers, but not interconnected. Figure 60 still shows a reasonable SB 0/90 strength of 30MPa at 121 ˚C/1000 hours, placing GF4 among the three best performing rovings here. After 3000 hours exposure the isolated type 2 dark spots have developed into connected type 2 dark spots and cracks. The SB 0/90 strength dropped to 21 MPa placing GF4 amongst the worst three, while the 5000 hours SB 0/90 dropped to 17 MPa, close to the worst performing roving. This also correlates with the findings of the previous TFF report, where this roving type showed to be relatively sensitive for storage conditions.

9. Conclusions

A new macroscopic test method has been developed for the determination of the performance of GRE in filament wound applications. This method complies with the requirements that were formulated in the research assignment:

- Discriminative for the performance in filament-wound GRE pipes like UEWS and ATS tests ('fingerprint tests').
- Can be performed when only one roving bobbin is available
- Can be performed with basic specimen preparation and standard testing equipment

The method is based on the winding of dry glass fibre roving on a flat plate in such a way that a specific cross-ply (0/90) build up is realized. After winding of the dry glass package the epoxy resin is infused with vacuum under foil and the composite is cured. The resulting plates are cut to strips and are tested in a three-point short beam set-up and is therefore called the SB 0/90 test.

Tests with four roving types that have been extensively tested within FPI with the fingerprint tests showed that there is a good correlation between the SB 0/90 test and the fingerprint test with respect to the effect of glass ageing and with respect to hot/wet performance up to 100 °C.

Nanoscale characterization tools such as atomic force microscopy and scanning electron microscopy have been applied on cross-sections of the laminates. Specific interest was on the structure and properties of the interphase layer between the glass of the fibres and the bulk epoxy surrounding it. To enable these nanoscale measurements, the samples needed to be polished extensively. A protocol for polishing was developed resulting in a height different of only 5.6 nm between the glass and the epoxy, and height variations of only 1.8 nm in either phase.

Unexpectedly, applying peak-force tapping mode AFM on the interphase region did not show a region with a significant difference in elasticity modulus when compared to the glass fibre and the epoxy region. Therefore, the novel AFM-IR technique was applied that allowed the recording of IR absorption spectra on a very local scale. Although this is only a very first proof-of-principle experiment with only 2 samples, it clearly shows that the composition of the epoxy close to the glass/epoxy interface is affected by the hot-wet treatment (reveals a different absorption spectrum). A possible explanation is the hydrolysis of the silanes, which is caused by the water exposure during the hot-wet treatment. This results in the debonding of the sizing from the glass and diffusion of the silanes further into the epoxy matrix.

High resolution scanning electron micrographs of samples after a hot-wet treatment, showed a physical separation of the epoxy glass from the glass surface (which was not observed in non-treated samples). Possible explanation for this might be the different thermal expansion coefficients of the different materials but might also be assisted or caused by the debonding of the sizing from the glass, resulting from the hydrolysis of the organosilanes in the sizing. The immersion in water during the hot-wet treatment is thought to reverse the bonding reaction, causing the sizing to physically debond from the glass.

In order to quantify the defects in composite samples made of different rovings, an optical microscope was used to scan them in a 2D-grid pattern. Using this technique, crack formation was

observed in the outer layers of the sample in first instance, whereas the number of cracks in inner layers increased at higher temperatures of hot/wet treatment. In addition, cracks were observed to start at defects, e.g. dark spots or voids. We assume that this occurs due to a higher stress on monofilaments close to a defect. However, additional research would be necessary to prove or disprove this hypothesis. Out of all rovings, SUP2 GF3 was the least susceptible to develop cracks.

Another phenomenon that was observed during optical microscopy were dark spots. They were either air entrapments (dark spots type 1) or they preferably occur between close filaments with barely any matrix material in between (dark spots type 2). The number of dark spots type 2 increased with higher hot-wet treatment temperature. Generally, very few have been observed at 100 °C while they were increased in number at 115 °C and 125 °C. This effect correlates with the SB 0/90 findings. Additionally, these spots tend to interconnect and develop into cracks. The increasing number of these spots correlates with a decrease in mechanical properties found during the previous and this TFF project, which leads to the conclusion that dark spots type 2 have a negative effect on the composite strength.

The sample area, analysed using optical microscopy, was small and a high variance was observed. Although this was hampering a reliable damage rating, the general trend of the mechanical properties correlated well with the microscopic data.

With the developed tests (SB 0/90 and microscopic crack quantification) glass ageing and the hot/wet performance of 8 roving types has been evaluated. The hot/wet performance has been evaluated for exposures of 250 hours in water of 100 °C, 115 °C and 125 °C respectively.

For the performance of the 8 different glass fibre products that have been tested it can be concluded that:

- The GF1 of SUP1 performs the worst of all roving types with respect to ageing.
- With respect to hot/wet performance the rovings GF1 and GF2 (both of SUP1) perform relatively bad. The best performance is found for the GF3 of SUP2.

From the 8 rovings mentioned a series of 6 rovings have been selected to evaluate the hot/wet-performance at a temperature of 121 °C (250 °F) for exposure times of 500 hours, 1000 hours, 3000 hours and 5000 hours, respectively. It can be concluded from these tests that:

- The major drop in properties as compared to the non-exposed results occurs after 500 hours of exposure.
- Similar as the other hot/wet-exposure tests the GF1 and GF2 (SUP1) perform the worst in the series.
- The best performance in this series is found for SUP2 GF3 and GF8 of SUP5.

Carbon reinforced epoxy (CFRE) has been evaluated as well in hot/wet-performance based on the CF1 carbon fibre roving of SUP6. Samples of 4 different sample preparation runs have been tested fresh (non-exposed) and after exposures of 250 hours at 100 °C and 150 °C respectively. As a reference glass fibre, the GF3 of SUP2 is exposed and tested as well in this series. From the results it can be concluded that:

- The retention of properties of CFRE after 250 hours exposure to water of 150 °C is 50% or more. The retention found for the glass fibre roving GF3 after this exposure is 20%.

- SEM-evaluations of the interphase between carbon fibre and epoxy matrix show a tight connection of the phases. Delamination was observed sporadically, but to a lesser extent compared to glass fibre composites.
- Glass fibre reinforcement seems not to be suitable for composites that are exposed for longer times in hot/wet-conditions at a temperature level of 150 °C.

Appendix 1 Micromechanics of UD-GRE composites

UD-GRE

Fibre reinforced plastics (composites) can be built up in various ways. In most cases a layered structure is formed by reinforced layers (plies) that are stacked to form a laminate. An individual layer (ply) is built up from reinforcing fibres that are oriented in the plane of the layer and that are embedded in resin (matrix).

In case the reinforcing fibres in a ply are all oriented in one direction this ply is called unidirectionally (UD) reinforced. In case a laminate is formed by unidirectionally reinforced plies and the reinforcement directions of all plies are the same, the laminate is called a unidirectionally reinforced laminate or UD-laminate.

In case a UD-laminate is built up with glass fibres as reinforcing fibres and epoxy resin as a matrix material this laminate is called a UD-GRE laminate. In the following this type of laminate is further considered.

Macroscopic composite behaviour

On a macroscopic scale a UD-GRE behaves as a homogeneous, anisotropic material. Individual fibres can't be seen and the introduction of forces on a product of such a material is on a significantly larger scale than the diameter of the fibres, which is in the order of 20 μm. However, the material behaves anisotropically: the macroscopic behaviour is strongly dependent on the direction of consideration. For the macroscopic characterization of UD-GRE the longitudinal and transverse directions are introduced.

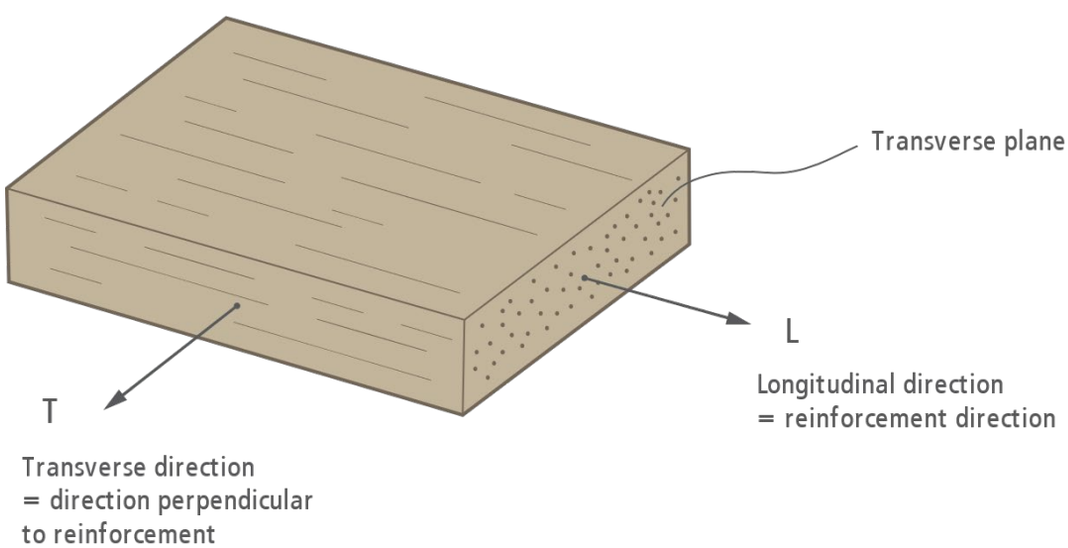

Figure 61. Fibre directions in unidirectional glass reinforced epoxy.

In Figure 61 only one transverse direction is given in the plane of the laminate. Perpendicular to the longitudinal direction is always a transverse direction, this means that there are many transverse directions but they are not depicted in the figure. This transverse direction may differ slightly in behaviour from the other transverse direction as a result of e.g. the shape of the reinforcement bundles of which the individual plies are composed.

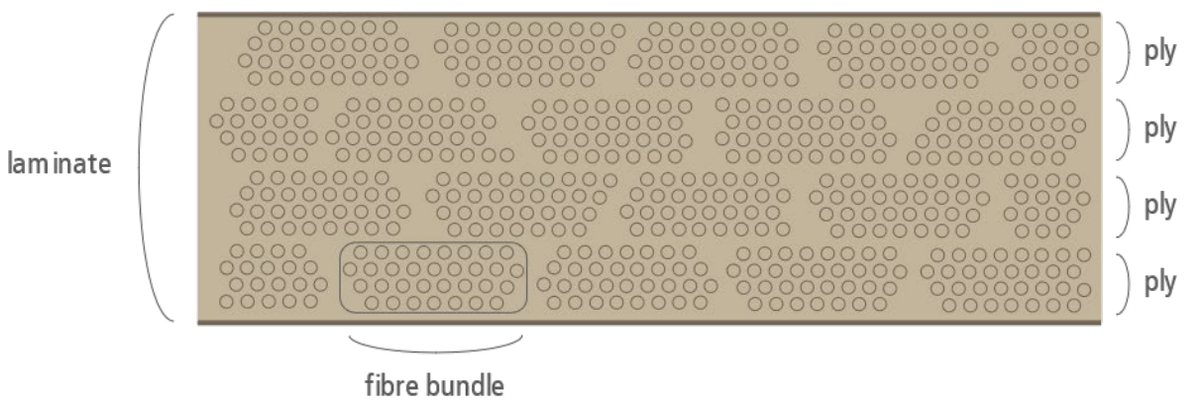

Figure 62. Schematic of fibre bundles in the plies in the transverse plane

In many situations the stresses in the plane of the laminate are dominant and the macroscopic stress state is a plane stress state. Although also an in-plane shear stress is possible in first instance the macroscopic normal stresses in L- and T-direction are considered: σ_L and σ_T . For a representative UD-GRE[3] the following values for stiffness and strength are found see Table 7 (indicative values).

Parameter	Symbol	Unit	L-direction	T-direction
Modulus of elasticity	E	GPa	40	10
Tensile strength	σ_t	MPa	1200	50
Compression strength	σ_c	MPa	600	150

Table 7. Indicative mechanical properties of GRE.

Considering the fact that a cured epoxy resin can have a tensile strength of 80 MPa it is clear that in the L-direction the fibres result in a reinforcement (composite tensile strength of 1200 MPa) but in the T-direction the fibres result rather in a weakening (composite tensile strength of 50 MPa).

Effects on micro scale on the transverse strength

The transverse tensile strength $\sigma_{T,t}$ of 50 MPa for a typical UD-GRE can be effected by several effects on micro scale. This has been extensively investigated in the PhD-thesis of Ten Busschen. To illustrate that there are more effects on the transverse tensile strength than the strength of the resin, he

[3] fibre mass fraction: m_f = 0.75 = 75 % (fibre volume fraction = v_f = 0.60 = 60 %)

selected a polyester resin with the same resin properties as the epoxy (same E-modulus, same tensile strength and same strain at rupture) and then a transverse tensile strength is found in the order of 15 to 20 MPa. In the following micro scale effects are described that influence the transverse tensile strength of a unidirectional reinforced ply.

In order to quantify effects and make them comprehensible, often a regular fibre distribution is selected as a model. This approach is allowed for understanding the effects but it must kept in mind that in reality the non-regularity of the fibre distribution has also effects on the transverse tensile strength as will be explained later on. It is started to consider the simplest fibre distribution: a square fibre arrangement (Figure 63).

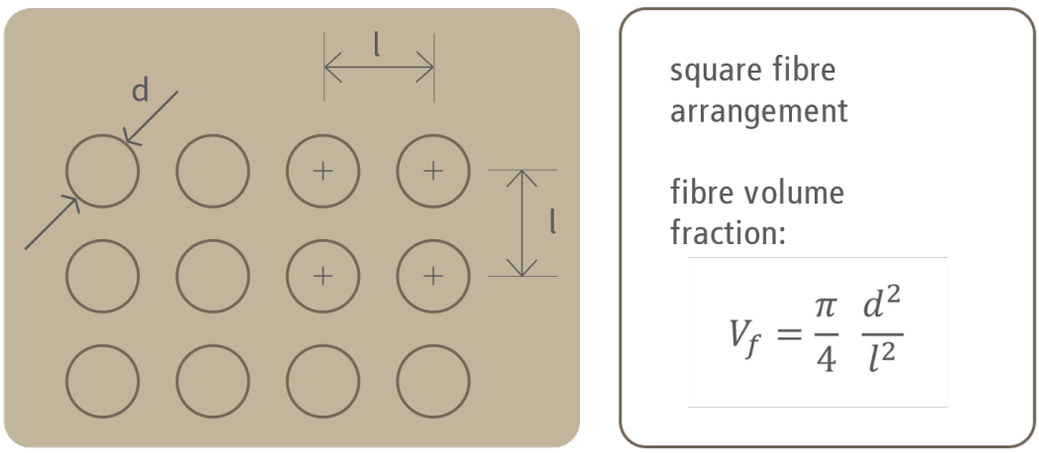

Figure 63. Square fibre arrangement, distribution model.

Because the E-modulus of the glass fibre (70 GPa) is typically 20 times the E-modulus of the matrix, during transverse tensile loading the composite strain ε_c is the result of the straining of the matrix between two fibres ε_m . When two adjacent fibres are considered, the macroscopic composite strain results in a displacement of these fibres of ΔL . Because the length of the resin part (L – d) is much smaller than the total part considered (L) this results in the so-called strain magnification effect (Figure 64).

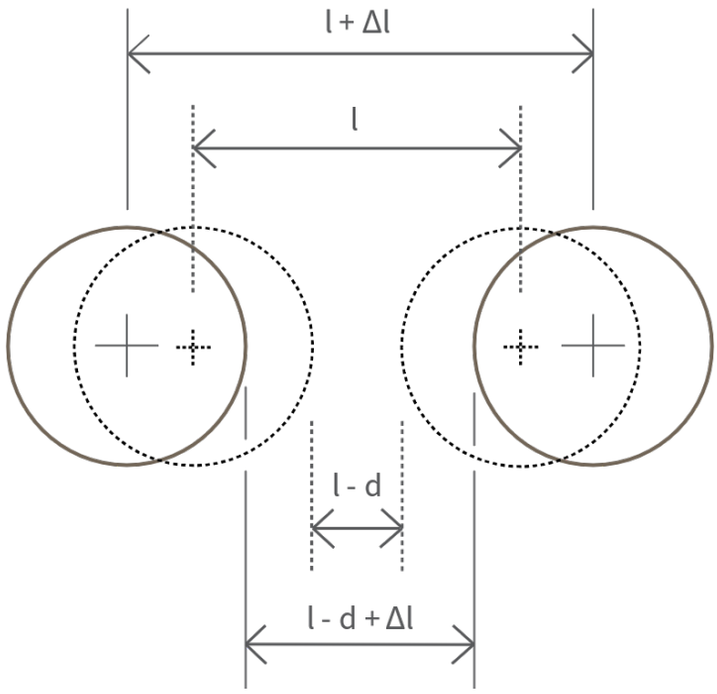

Figure 64, Strain magnification

Combining the formulas for composite strain (ε_c) , matrix strain between the fibres (ε_m) and fibre volume fraction (v_f) it follows:

$$\varepsilon_c = \frac{\Delta L}{L}$$

$$\varepsilon_m = \frac{\Delta L}{(L - d)}$$

$$V_f = \frac{(\frac{1}{4}\pi \cdot d^2)}{L^2}$$

$$\varepsilon_m = \frac{\varepsilon_c}{1 - \left(\frac{4V_f}{\pi}\right)^{\frac{1}{2}}}$$

Of the latter formula the strain magnification factor is plotted as a function of the fibre volume fraction in the graphs below:

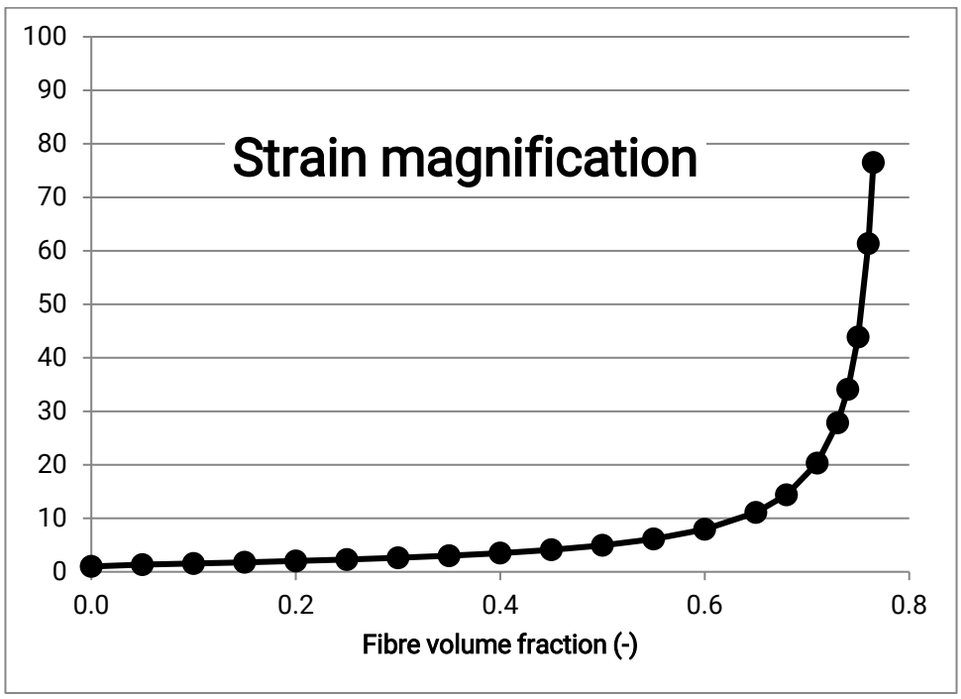

For instance, for a UD-GRE with a fibre volume fraction of 0.6 (60 %) a strain magnification factor of 7.9 is calculated for a square array of fibres. When a uniaxial loading would be assumed this would imply that when the resin has a strain at rupture of 0.04 (4 %), the composite would already fail in transverse direction at a composite strain of 0.04 / 7.9 = 0.005 (0.5 %). This corresponds good with the composite transverse strength when calculated from the strain:

$$\sigma_{Tt} = E_T \cdot \varepsilon_c = 10000 \cdot 0.005 = 50\ MPa$$

Also, from the graph it follows that the strain magnification tends to infinity when the fibre volume fraction approached the value $v_f = \pi/4 = 0.785 = 78.5$ % when the fibres are touching each other.

However, there are other effects to be considered. For instance, when the bonding between resin and fibres is poor. A simple approach is to assume again a square arrangement of fibres and assume that there is no fibre/matrix adhesion at all. Though not completely correct it may be assumed that the composite consists of a square arrangement of holes instead of fibres. In this case the surface over which the transverse stresses are to be transmitted is significantly smaller than the total surface of the composite. It can be calculated that the same strain magnification factor applies for the increase of matrix stress as compared to the composite stress.

For example, for a UD-GRE with a fibre volume fraction of 0.6 = 60 % and a tensile strength of the epoxy matrix of 80 MPa a composite transverse strength can be calculated with this model to be:

$$\sigma_{Tt} = \frac{\sigma_m}{7.9} = \frac{80}{7.9} = 10\ MPa$$

Although this model for debonding is a strong simplification of reality it shows that a large effect of debonding can be expected. This has also been found by Ten Busschen in his PhD-thesis.

Another effect is the non-linear stress-strain behaviour of the matrix, which has a positive effect on the transverse strength (more strain is possible at the same stress level). However, this effect is not as pronounced as strain magnification and poor bonding.

Finally, on microscale there is the effect of resin shrinkage. This effect is very large for polyester resins because these resins show a significant shrinkage in the solid state that can build up micro stresses. Generally polyester resins show a volumetric shrinkage as compared to the initial liquid state of typically 8 %. However, for epoxy resins this effect is much smaller: volumetric shrinkage is of the order of 1 to 2 % and occurs mostly when the epoxy is still liquid and is not capable to build up micro stresses.

Meso scale effects

It is clear that the irregular fibre distribution is very complex to model. However, qualitatively some considerations are possible. For instance, a group of fibres that are very close to each other form a relatively stiff part in a less stiff surroundings. This reacts as a stiff inclusion that will not be strained to the same level as the surrounding material does. This effect will reduce the effect of strain magnification and debonding because this area is not fully loaded.

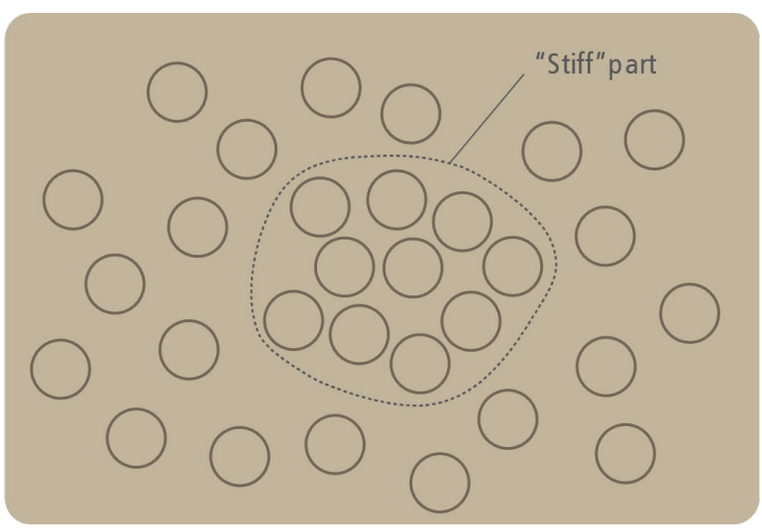

Figure 65. Schematic of irregular fibre distribution

On the other hand, it can be expected that a certain magnitude of the fibre volume fraction many neighbouring fibres will touch and will result in extreme strain magnification. Then there are no isolated stiff parts but the composite is throughout too densely packed. Although a theoretical maximum fibre volume fraction is possible of 0.907 = 90.7 % in case of a hexagonal fibre arrangement, in practice the fibre volume fraction never becomes higher than about 0.75 = 75 %, which corresponds to a fibre mass fraction of about 0.87 = 87 % .

Appendix 2 Mechanical testing of composites

Mechanical testing of long-fibre reinforced composites

Mechanical testing of fibre reinforced plastics (composites) involves the use of specific tests. Specially in the case of long-fibre reinforced plastics the effect of the accompanying anisotropic behaviour requires dedicated test methods. In this project our attention is focused on long-fibre reinforced plastic composites.

In the standardized test method for tensile testing of plastics already a clear division is made between non-reinforced and reinforced plastics:

ISO 527 *Plastics – Determination of tensile properties*

Part 1 General Principles
Part 2 Test conditions for mouldings and extrusion parts
Part 3 Test conditions for films and sheets
Part 4 Test conditions for isotropic and orthotropic fibre-reinforced plastic composites
Part 5 Test conditions for unidirectional fibre-reinforced plastic composites

Also, for flexural testing of plastics for fibre-reinforced plastics a dedicated test is standardized that differs from the method for non-reinforced (isotropic) plastics:

ISO 178 *Plastics – Determination of flexural properties*

ISO 14125 *Fibre-reinforced Plastics – Determination of flexural properties*

Moreover, the phenomenon of interlaminar shear failure will only be observed in the case of long-fibre reinforced plastics. To characterize the so-called Interlaminar Shear Strength (ILSS) test methods are standardized:

ISO 14130 *Fibre-reinforced Plastics – Determination of the apparent shear strength by short-beam method*

ASTM D2344 *Standard Test Method for Short-Beam Strength of Polymer Matrix Composite Materials and Their Laminates*

Besides these test methods there exist many test methods that are dedicated for the testing of long-fibre reinforced composites. Many of these methods originate from the aerospace industry where the use of highly-oriented fibre-reinforced plastic composites already started in the 1960's. (A comprehensive summary is found in *Experimental Mechanics of Fiber Reinforced Composite materials,* J.M. Whitney, I.M. Daniel, R.B. Pipes, 1984)

Generally, when performing mechanical tests on long-fibre reinforced plastics it can be discriminated between behaviour that is dominated by the fibre properties and behaviour that is dominated by the properties of the interaction between fibre and plastic (matrix). As opposed to fibre-dominated properties (tensile stiffness and strength in reinforcement direction) the properties that are dominated

by the fibre-matrix-interaction generally are difficult to determine by testing. Besides, the test results generally show much scatter and are very sensitive for test set-up and test procedure.

Tests on UD-rods

An effective way to test the interaction between (glass) fibres and a thermoset resin is to test unidirectionally reinforced rods, so-called UD-rods. Based on one roving bobbin a manifold of UD-rods can be made that can be tested in different tests (flexural test, compressive test, ILSS) and in different conditions (as moulded, after different exposures to hot-wet environments, etc.). The test is described in the following standard.

ISO 3597 ***Textile-glass-reinforced plastics – Determination of mechanical properties on rods made or roving-reinforced resin.***

Part 1 General considerations and preparation of rods
Part 2 Determination of flexural strength
Part 3 Determination of compressive strength
Part 4 Determination of apparent interlaminar shear strength

Testing of UD-rods is a test method that is widely used by glass fibre producers for purposes of quality control, development of new products and competitive evaluations.

Characterization of filament-wound composites

Filament-wound composites are applied in pipes and tanks, especially when corrosion resistance or a low weight are required. As a result of the production process these composites are long-fibre reinforced composites and therefore the mechanical testing must be dedicated for these materials. In view of the TFF-project in the following it is concentrated on filament-wound glass-fibre reinforced epoxy (GRE) pipes as produced by Future Pipes Industries (FPI). (In the project the use of carbon fibres is left open as an alternative for glass fibre.)

In a previous TFF-project (2014-2016) the different mechanical test methods for filament-wound GRE pipes have been evaluated. Some of these tests are:

UEWS: Ultimate Elastic Wall Stress (limit of elastic stress-strain response, FPI-test)
ATS: Axial Tensile Strength (axial test on complete pipe, ASTM-test)
TEL: Tensile Elastic Limit (axial test on pipe segment, FPI-test)
ILSS: ILSS on 1) pipe laminate, 2) NOL-ring segment or 3) woven roving laminate

Of the latter test, the ILSS, it is known from previous research that the predictive quality of this test is insufficient when a UD-rod is tested made of the glass-fibre roving in consideration (ISO 3597 Textile – glass-reinforced plastics Determination of mechanical properties on rods made of roving reinforced resin). However, when ILSS is tested with a laminate based on a woven roving made with glass-fibre roving in consideration the test appears to be discriminative. Moreover, it has been found that testing of the material after exposure to water of 80 till 100°C gives extra information of the quality of the glass fibre – epoxy combination for long-term behaviour.

A standardized procedure for the characterization of GRE pipes is described in:

ISO 14692 ***Petroleum and natural gas industries – Glass-reinforced plastics (GRP) piping***

Part 1: Vocabulary, symbols, application and materials
Part 2: Qualification and manufacturing
Part 3: System design
Part 4: Fabrication, installation and operation

Effect of elevated temperatures

An elevated temperature may result in several effects (as compared to a lower temperature):

A Thermal expansion of the resin (α = 80 ppm/°C) and the glass fibres (α = 4 ppm/°C)
Anisotropic composite expansion behaviour resulting in interlaminar stresses
(These effects may be investigated by FEM-analyses)

B Reduction of interlaminar strength
(This can be investigated by testing of strength with non-closed specimens.)

C Change of elastic resin properties (lower E-modulus)
Increase of viscoelastic behaviour of the resin (specially around or above Tg)
(These effects may be investigated by DMTA-analysis)

D Higher mobility of water molecules (quicker diffusion through the resin)
Higher level of water uptake by the resin (swelling)
More aggressive effect of water molecules on resin, glass/resin-interface and glass
(These effects may be investigated by nano-analysis)

A method to extrapolate short-term data to long-term data for fibre reinforced pipes and fittings by using regression lines is described in the following standard.

ASTM D2992 – 18 ***Standard Practice for Obtaining Hydrostatic or Pressure Design Basis for 'Fiberglas' (Glass-Fiber-Reinforced Thermosetting Resin) Pipe and Fittings'***

Glass fibre characterization

Clearly a simple and discriminative test for the characterization of the suitability of a glass fibre product (roving) for application in GRE pipes is not yet present. Up till now it is necessary to make filament wound tubes or a woven roving fabric laminate for testing a candidate glass fibre roving.

Besides elementary glass fibre properties that are required (minimum glass strength, low filamentation, good impregnation behaviour) the interaction with the epoxy resin must be characterized. Based on the fact that the strain level at which microcracking starts to occur appears to be a measure for the quality of this interaction the current project focusses on the use of a cross-ply type of specimen. In this manner controlled transverse cracking can be investigated, as is described in chapter 3 of this report.

The choice to use a cross-ply specimen for testing is not arbitrary. From the experience of Ten Busschen in his PhD-work (1996) it is difficult to obtain specimens with sufficiently constant quality to be discriminative when making the specimens also by filament winding. The so-called ring-test that

has been studied in this PhD-work has even been tested by Future Pipes Industries in close cooperation with PPG Fiber Glass Industries where Ten Busschen worked at that time. This test showed too much variation in results when repeated and therefore could not be used. As already reported, an ILSS-test performed on unidirectionally (UD) reinforced rods proved also to be not sufficiently discriminative.

Appendix 3 Procedure of manufacturing SB 0/90 test samples

1. Scope

This procedure describes the production process of a [0/90°] cross ply, by dry winding and vacuum infusion. This test is referred to as the SB 0/90 test, which stands for short beam bending testing of 0/90 laminates.

The description for vacuum infusion is applicable for the following recipe:

- Bisphenol A based epoxy resin
- DETDA+IPD curing agent.

When different resins and/or curing agents are used this procedure may not be useful.

2. Dry winding

2.1 Material and equipment

- Two roving bobbins.
- Mould, consisting of a (GRE) plate of approximately 30 x 30 x 2 cm covered by PET foil capable to resist 135 °C. Two threaded ends are applied at two sides of the plate to be connected to the mould frame. See figure 2.2.1.
- Mould frame, to clamp the mould in the chuck of the lathe.
- Lathe to rotate the mould and to travel the carriage in axial direction at a speed of 4 mm per rotation.
- Roving arrangement to guide the roving.
- Mould release agent.
- Guiding frame capable to achieve winding tension and to break the roving.
    - See figure 2.5.2 and figure 2.5.3.
- Peel-ply and Teflon tape.

2.2 Mould preparation

The preparation starts by cleaning the mould and the threaded ends. All tape residues need to be removed and the thread at the ends needs to be re-cut if necessary. To release the cross ply the preparation is being continued as described below

Apply Teflon tape to cover the edges of the mould. See figure 2.2.1

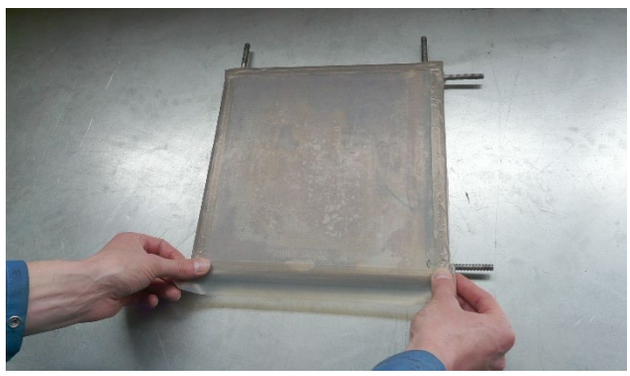

Figure 2.2.1, Teflon at corners and edges of the mould.

Apply release agent on the mould. Polish the release agent until a thin uniform film is formed. See figure 2.2.2.

Figure2.2.2, Polish the applied release agent.

Apply a pre-cut peel-ply around the mould. Connect both ends of the peel ply using Teflon tape. The width of the peel ply is a bit smaller than the space between the threaded ends. The taped side is marked as bottom by writing a B at the corners. The non-taped side is marked as top by writing a T at the corners. See figure 2.2.3.

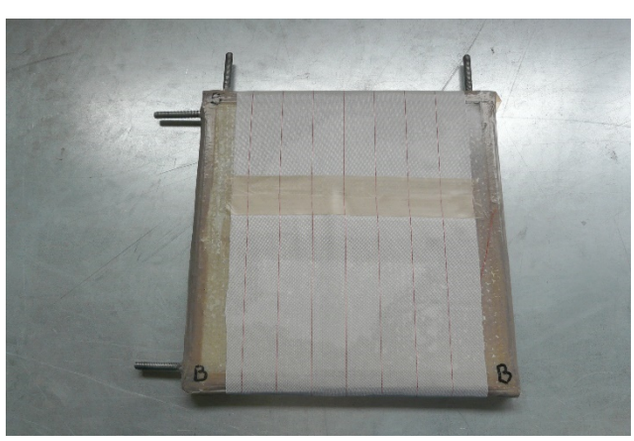

Figure 2.2.3, Applied and taped peel ply. Taped side marked with

2.3 Dry winding set up

A lathe is used for dry winding of the cross ply. The guiding frame is fixed at the tool post of the cross slide. The mould frame is clamped in the chuck. Rovings from two bobbins are guided by a set of bars and a spreader through the guiding frame to the mould. See figure 2.3.1 and 2.3.2.
When the roving is fixed to the mould the lathe is winding the cross ply by rotation of the chuck and the travel of the carriage. At the end of the mould, one layer has been produced. The mould is being rotated and turned over 90°. By traveling the carriage to its start position while the chuck rotates a second layer is applied, 90° rotated compared to the first layer. This process is repeated until the required number of layers are applied.
Figure 2.3.1 shows the practical set up and figure 2.3.2 gives a schematic overview of the set up.
The setup is divided in two parts:

- Roving arrangement
- Lathe set up

Figure 2.3.1, overview dry winding setup.

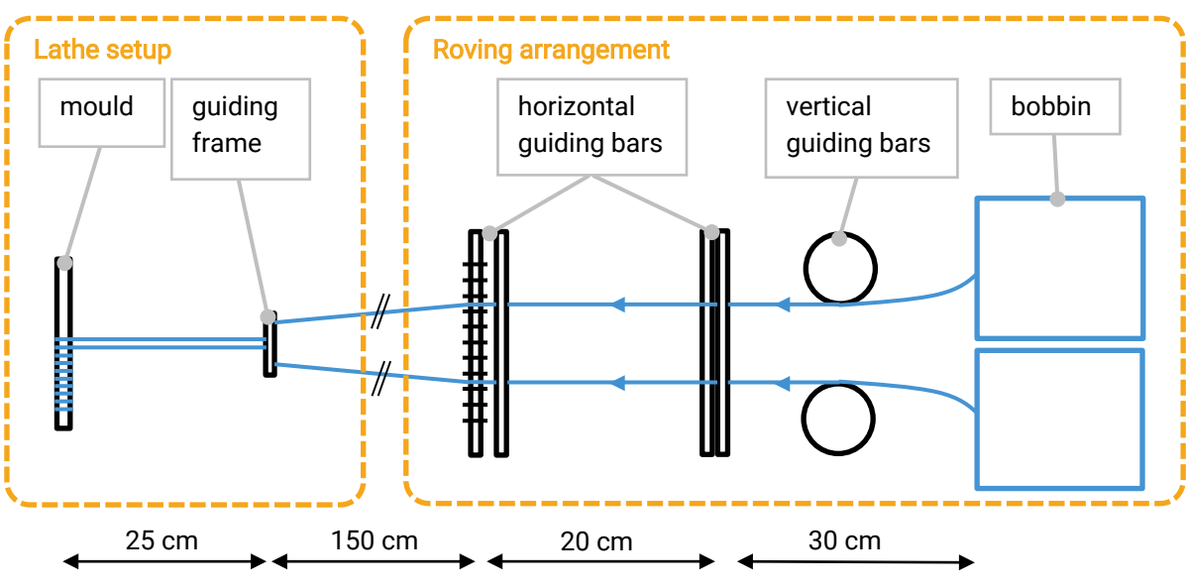

Figure 2.3.2. Schematic the top view of the dry winding setup with blue marked roving. At the right the roving arrangement to guide the rovings from the bobbins to the guiding frame in the cross slide of the lathe. At the left the mould is connected to the chuck of the lathe and the guiding frame is connected to the cross slide of the lathe.

2.4 Roving arrangement

The roving arrangement, as stated in figure 2.4.1, consists of:

- Table
- Two bobbins
- Four horizontal guiding bars including roving spreader
- Two vertical guiding bars

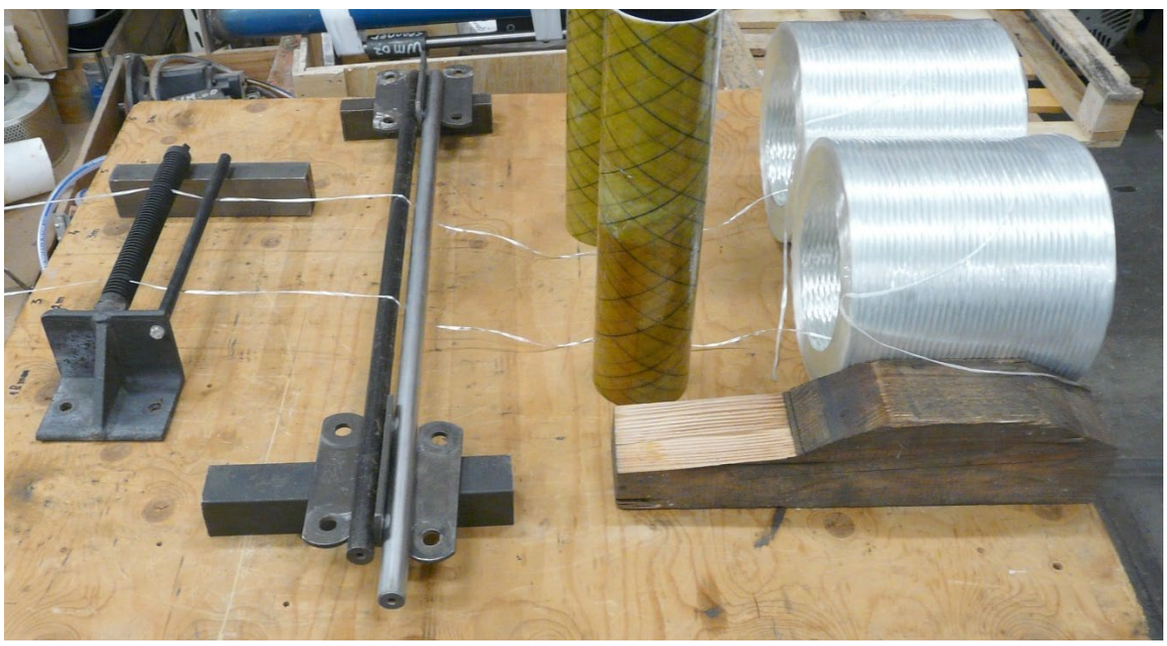

Figure 2.4.1. roving arrangement.

The roving is guided by two vertical bars to four horizontal guiding bars. In the set-up of figure 2.4.1 the roving is pulled out of the bobbins and crosses the bars to break the roving. To reduce twisting, the rovings are separated in the spreader (the last bar). The roving arrangement is positioned at least at 1.5 meters from the lathe.

2.5 Lathe set up

The lathe setup contains (see figure 2.5.1 and 2.5.2.):

- Lathe
- Mould frame with prepared mould
- Guiding frame

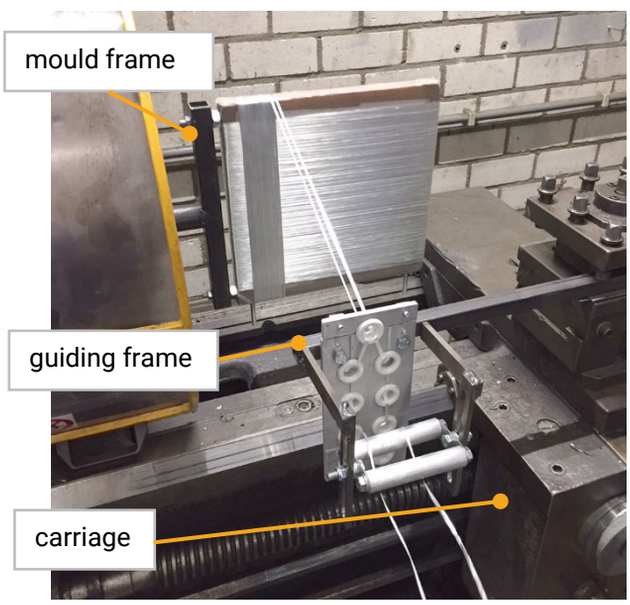

Figure 2.5.1. lathe setup.

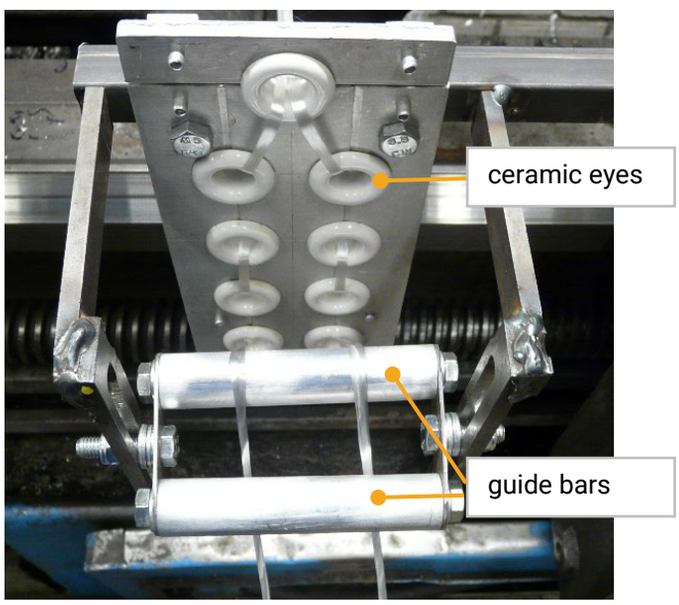

Figure 2.5.2, Roving through guiding frame.

The mould is clamped in the chuck of the lathe by the mould frame. After leaving the arrangement both rovings pass the guide bars and the ceramic eyes as indicated in figure 2.5.1 and 2.5.2. Distance and position of the ceramic eyes and guide bars as in figure 2.5.3.

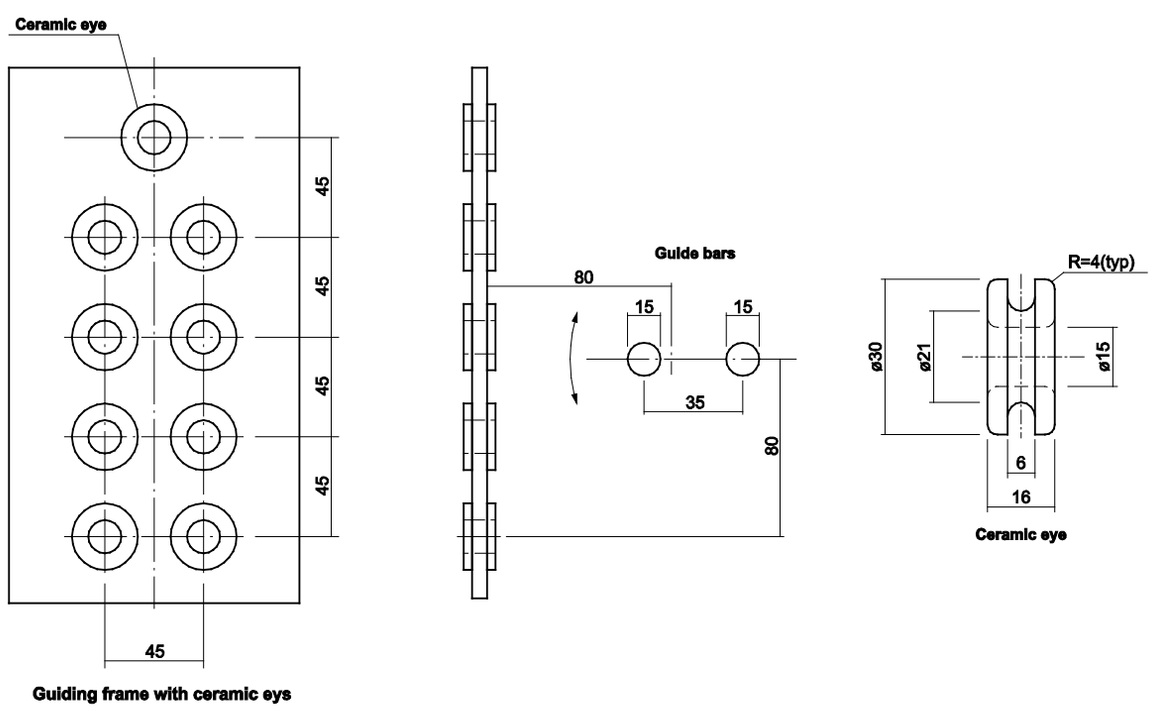

Figure 2.5.3. dimensions and position of ceramic eyes and guide bars.

2.6 Winding

The roving is applied on the mould at a speed of 32 rpm. The travel in axial direction of the roving is 4 mm per rotation for a 30 cm wide mould. This amounts to 0.0625 mm axial travel per cm of mould circumference.
The winding tension is achieved by the guiding frame. The winding tension is measured by touching the roving by hand behind the guiding frame during the start of the winding process. The roving may bend slightly when little pressure is applied. When the winding tension is to high 3 ceramic eyes per roving shall be used instead of 5. The applied roving shall be removed and the winding shall be restarted.
The total overall width of both rovings, including spacing, shall be 8-10 mm at the first contact with the mould.

Enter the correct settings in the lathe and test the rotation speed of the chuck and the travel of the carriage.
Connect the mould to the mould frame and clamp the mould frame in the chuck of the lathe.
Subsequently tie the rovings to the threaded end at the left side or tape the roving at the left side of the mould using Teflon tape. See figure 2.6.1.

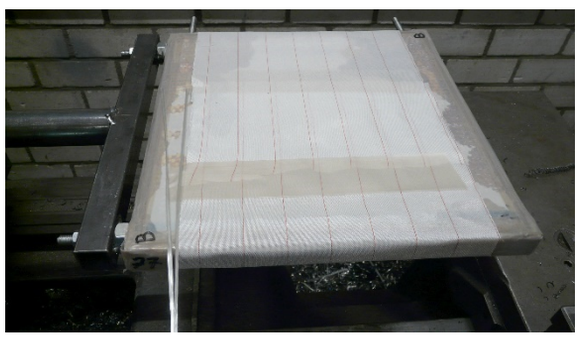

Figure 2.6.1. taping the roving on the mould.

Start the lathe. The carriage travels to the right, winding the roving. Stop the carriage just before the thread end at the right side of the mould.
The first layer in 0° direction has been produced.
See figure 2.6.2

Figure 2.6.2. first layer in 0° direction.

Release the mould from the frame.
Rotate and turn the mould over 90° as indicated in figure 2.6.3. Connect the mould to the frame.
The threaded ends can be used to guide the rovings during rotating and turning.
The carriage is traveling to the start position to apply a layer in 90° direction.

Figure 2.6.3. rotated and turned mould.

When the second layer is completed the mould is released from the frame and is being rotated and turned in to its start position as indicated in figure 2.6.4.

Figure 2.6.4. rotated and turned mould after second layer.

The winding process is completed when 11 layers have been applied. 6 layers in 0° direction, 5 layers in 90° direction. See figure 2.6.5.

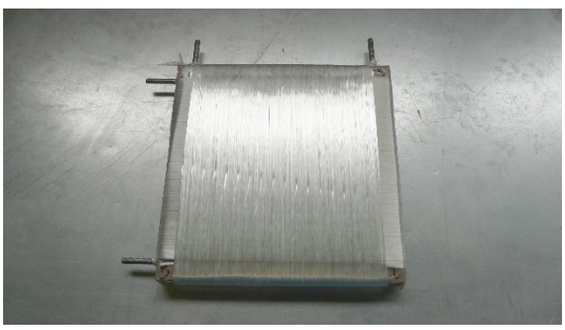

Figure 2.6.5. completed cross ply.

3. Vacuum infusion

3.1 Materials and equipment

- Resin and curing agent

Resin:	Un-modified bisphenol-A epoxy resin		
Curing agent:	DETDA +IPD		
	Mixing ratio:	DETDA	70 (by weight)
		IPD	30 (by weight)
Infusion recipe:	Mixing ratio:	Resin	100 (by weight)
		Curing agent	25 (by weight)

- Infusion equipment (tubes, spiral band, foil, peel-ply, flow-mesh and tacky tape)
- Teflon tape
- Thermometer
- Vacuum pump
- Table
- Hot air blower
- Box
- Oven (temperature range up to 150 °C)

3.2 Preparing, infusion and curing

Heat the cross ply in the oven for 75 minutes at 70 °C.

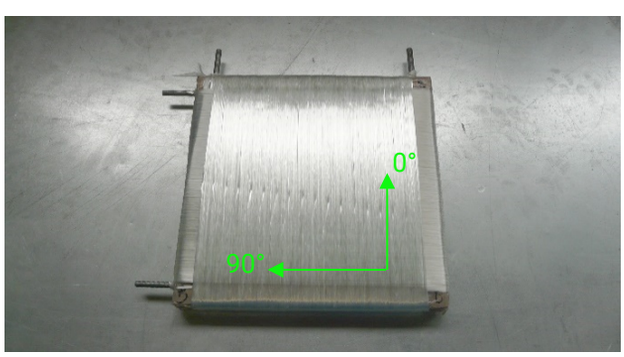

Figure 3.2.1. cross ply, including roving direction.

Apply peel-ply in 90° direction of the cross ply. This is perpendicular to the last roving direction. See figure 3.2.1.
Connect both ends of the peel ply at the bottom side (marked with B) of the cross ply using Teflon tape Cover the threaded ends using Teflon tape.
See figure 3.2.2.

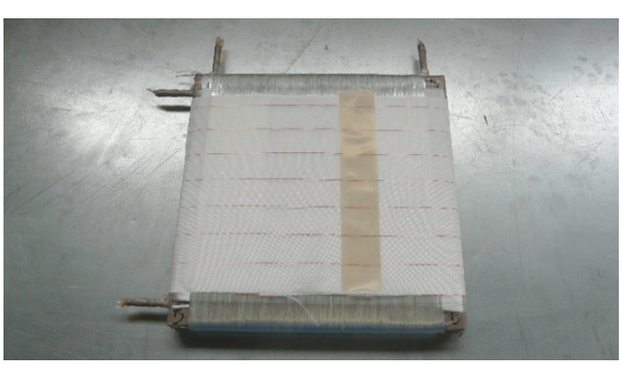

Figure 3.2.2. peel ply taped at the bottom side and covered threaded ends.

Tape two small strokes of peel ply (appr. 25 x 5 cm)
to the edges of the cross ply using Teflon tape.
See figure 3.2.3.

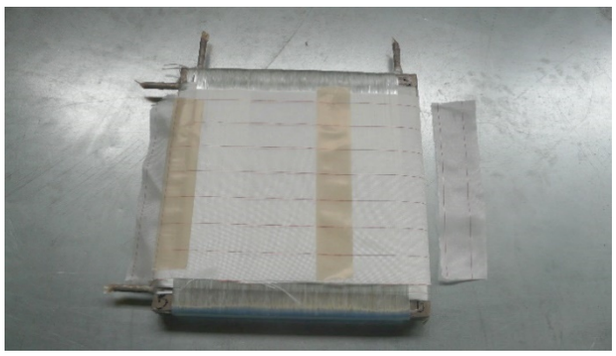

Figure 3.2.3. two strokes of peel ply applied to the edges.

Apply two spiral band tubes to the edges as recipe tube and vacuum tube during the infusion.
See figure 3.2.4.

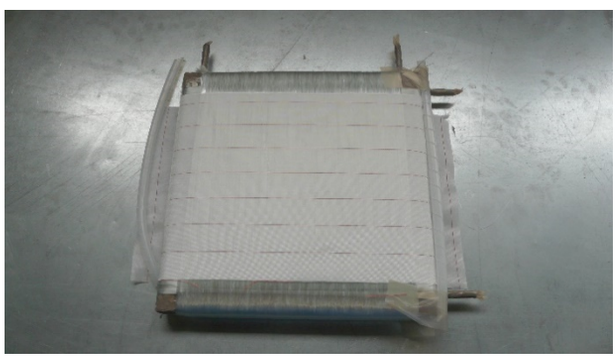

Figure 3.2.4. two spiral band tubes applied.

The spiral band tube is a bit stretched and fixed to the cross ply using Teflon tape. Stretching the spiral band tube allows the recipe to pass through during infusion.
See figure 3.2.5.

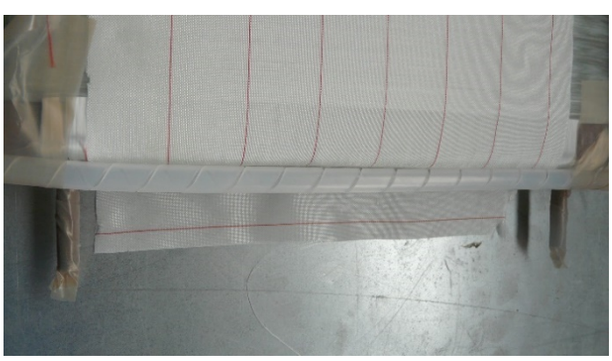

Figure 3.2.5. Stretched spiral band tubes.

The peel-ply strokes are wrapped around the spiral bands and are fixed at the peel-ply using Teflon tape.
See figure 3.2.6.

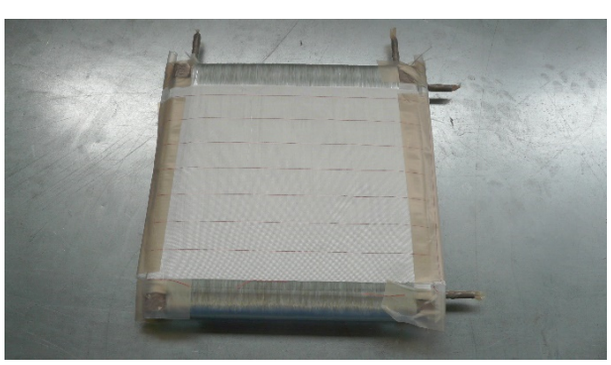

Figure 3.2.6. fixed spiral band tubes.

Apply flow-mesh on top, bottom and one edge of the peel-ply. At the open side the flow mesh ends approximately 4 cm before the edge of the peel-ply.
See figure 3.2.7.

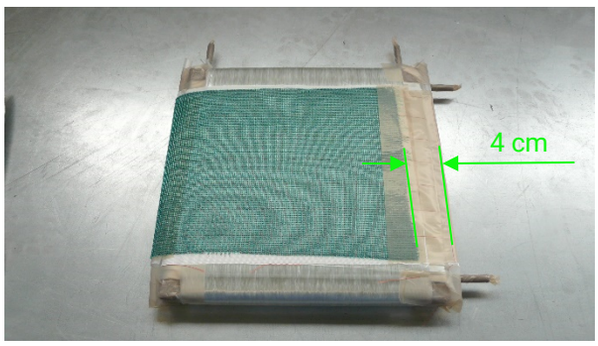

Figure 3.2.7. flow mesh applied.

Put the top side (T) up. Place the cross ply on top of the vacuum foil (approx..70 x 70 cm). See figure 3.2.8.

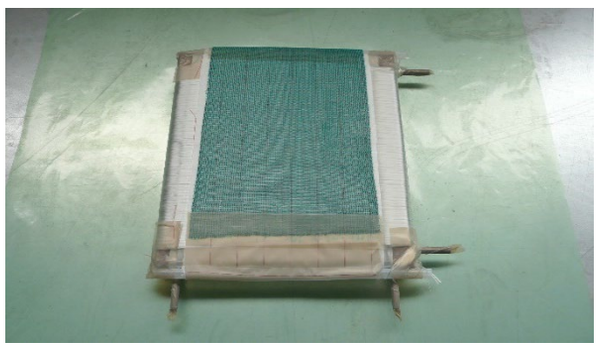

Figure 3.2.8. cross ply on vacuum foil.

Tacky tape is applied as a square around the cross ply.
Stretch the foil when the tape is being applied.
Tape loops (8x) are applied at the corners of the square.
Cover the tacky tape with a protection layer.
See figure 3.2.9. and figure 3.2.10.

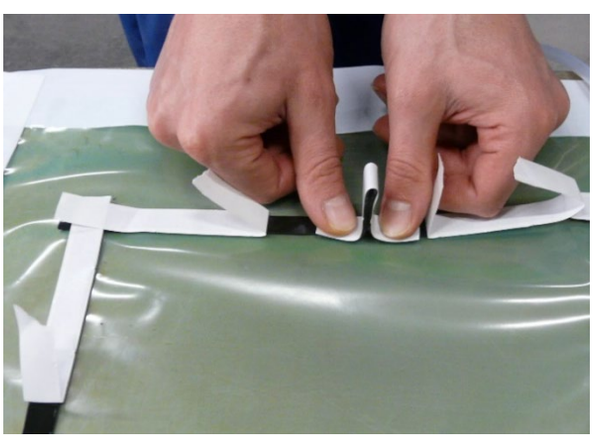

Figure 3.2.9. tape loops at the corner of the square.

Connect two tubes to the spiral bands. One recipe tube (inlet) and one vacuum tube (outlet). Fix the tubes to tacky tape at the corners of the square.
Apply a tape loop on top of the tubes.
Cover and smoothen the open ends of the spiral tubes using clay or Teflon tape, to avoid leakages during the vacuum infusion. See figure 3.2.10.

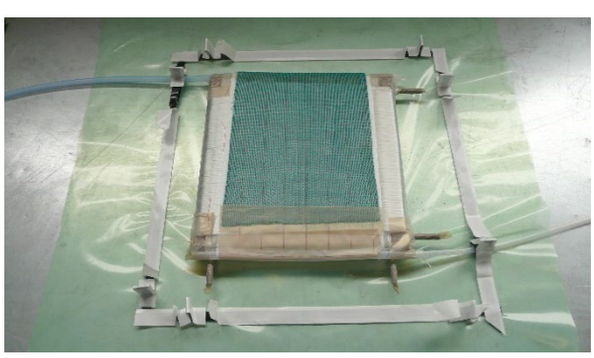

Figure 3.2.10. inlet and outlet tubes at the corner of the square.

Apply vacuum foil to the tacky tape to create a vacuum bag. Start at a corner and go around. The vacuum foil at the top needs to follow the loops
to be able to set during vacuuming.
See figure 3.2.11.

Figure 3.2.11. applied vacuum foil at the top, following the tape loops.

Put a (tape) clamp on the injection tube (inlet). See figure 3.2.12.

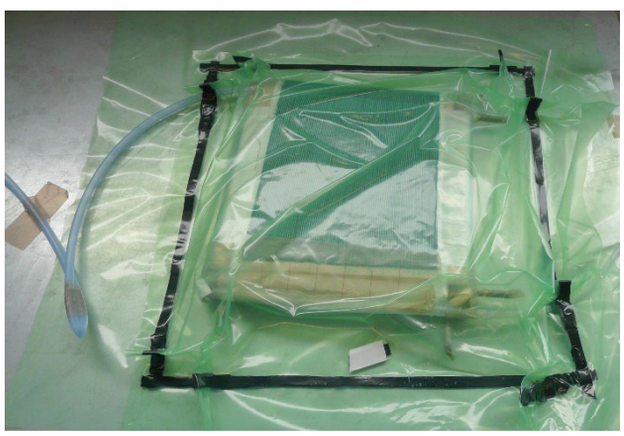

Figure 3.2.12. tape clamp at the injection tube (inlet).

The vacuum tube (outlet) is connected to the cask of the vacuum pump. See figure 3.2.13.

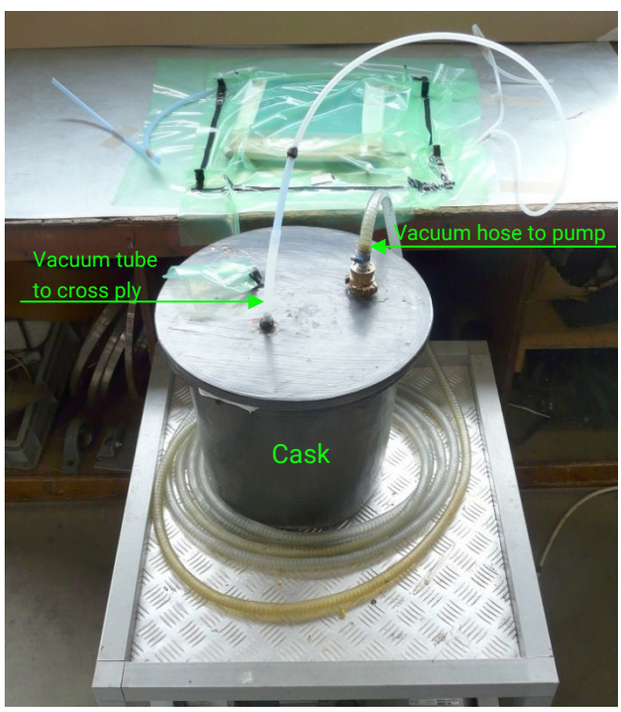

Figure 3.2.13. vacuum tube (inlet) connected to the cask of the vacuum pump.

Connect the cask to the tap of the vacuum pump via the vacuum hose. See figure 3.2.14.

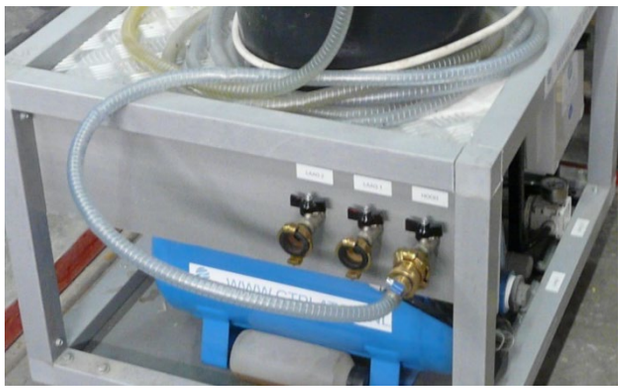

Figure 3.2.14. vacuum hose connected to the tap of the vacuum pump.

A maximum and minimum vacuum level needs to be set for the vacuum pump. The maximum achievable vacuum level is influenced by the atmospheric pressure.
The vacuum pump needs to be set between -0.960 bar and -0.940 bar as indicated in figure 3.2.15.

Figure 3.2.15. setting for vacuum pump.

Check the vacuum bag for leaks by applying the vacuum gradually. Smoothen the top foil of the bag during vacuuming. See figure 3.2.16.
In case of leaking the tacky tape, the foil, the hoses and the sealing of the cask need to be checked for incomplete sealing.

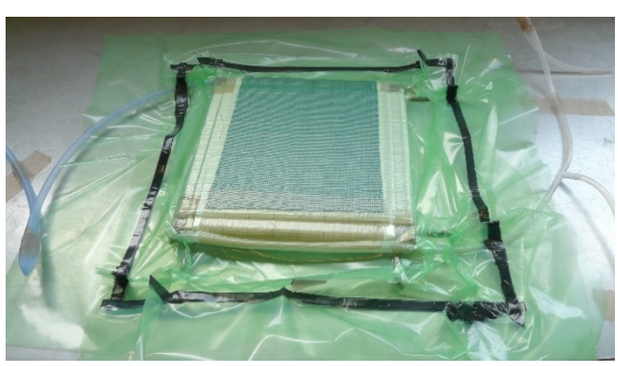

Figure 3.2.16. check the vacuum bag for leaks.

Place four spacers below the sample to elevate it approx. 1 cm above the table. See figure 3.2.17.

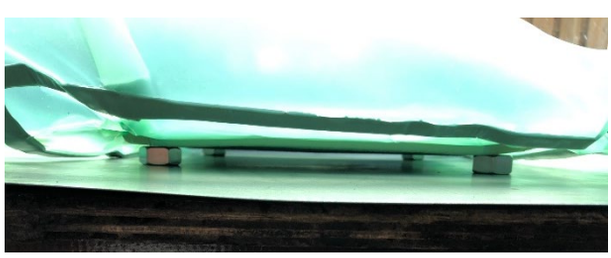

Figure 3.2.17. Lift the sample from the table.

Put the box over the vacuum bag and place the hot air blower inside. Switch on and set the hot air blower to achieve a temperature of 45 – 50 °C.
See figure 3.2.18.

Figure 3.2.18. Hot air blower in the box.

Close the box using a lid and check the temperature in the box regularly. See figure 3.2.19.

Figure 3.2.19. closed box.

Prepare 1000 g infusion recipe by weighing resin and curing agent in the right mixing ratio. Heat the recipe in an oven to a temperature of 35 – 40 °C. See figure 3.2.20.
(for mixing ratio of recipe see section 3.1)

Figure 3.2.20. resin and curing agent.

Mix resin and curing agent.
The temperature of the recipe after mixing needs to be 35 – 40 °C. See figure 3.2.21.

Figure 3.2.21. resin and curing agent.

Check the temperature at the top side of the vacuum bag. The temperature needs to be 45 – 50 °C before the start of the infusion. See figure 3.2.22.

Start the infusion by putting the recipe tube (inlet) in the infusion recipe.
Open the clamp in the recipe tube.
The recipe tube needs to stay in the recipe during infusion and first curing. See figure 3.2.23.
No air shall enter the recipe tube. Secure the recipe hose to the recipe container.

Figure 3.2.22. check the temperature at the top of the vacuum bag.

The recipe is running over the flow mesh and starts infusing the cross ply. Close the lid of the box.
When the infusion is completed, cure the cross ply for approx. 10 hours at a temperature of 50 – 60 °C in the box. The vacuum shall be maintained during the curing.

Figure 3.2.23. Infusion of the cross ply.

After the first curing the foil, the tubes and the flow mesh are removed and the layer direction is written on the cross ply. See figure 3.2.24.

A second curing follows in two steps:
Step 1: Curing at 80 °C for 2 hours.
Step 2: Post-curing at 135 °C for 3 hours.

After the curing process the degree of cure is determined by DSC (Different Scanning Calorimeter)
The curing is accepted when Tg(1) is 135 – 150 °C.
When Tg(1) is too low the cross ply needs to be cured again. When Tg (1) is too high the cross ply needs to be rejected.

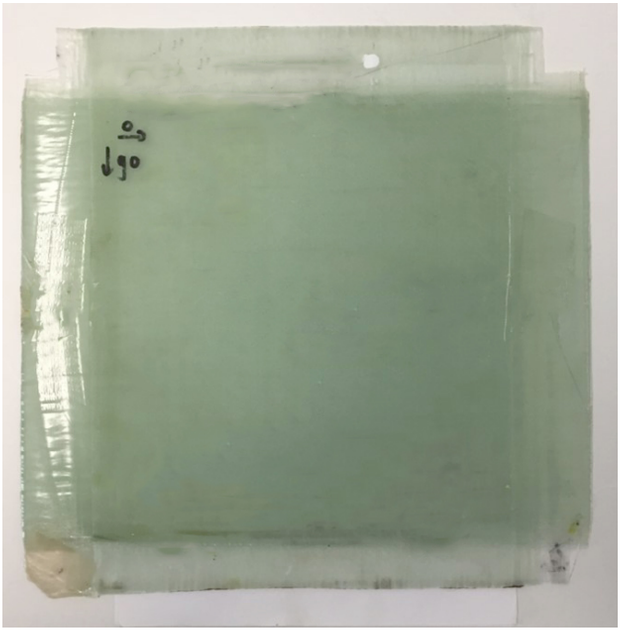

Figure 3.2.24. removed peel ply and written layer direction.

4. Cutting the cross ply

4.1 Materials and equipment

- Diamond cutter

4.2 Cutting

When the second curing is completed the cross ply is being cut using a diamond cutter.
The top side (T) and the bottom side (B) shall be cut separately.
After cutting the peel ply is removed.

5. Infusion assessment

When the peel ply is removed the infusion of the cross ply needs to be assessed.

Accepted
The surface of the cross ply needs to well infused.
No dry spots or non-infused areas shall be visible.
See figure 5.1.

Rejected
The surface of the cross ply is not well infused.
Dry spots or non-infused areas are visible.
See figure 5.2.


Figure 5.1 accepted

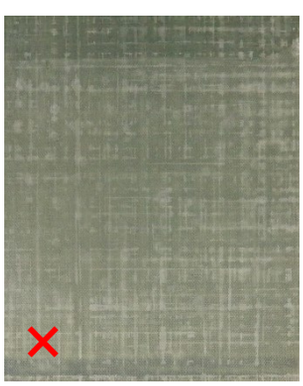
Figure 5.2 rejected

Appendix 4 Procedure of SB 0/90 test method

1. Scope

This test method describes the determination of the short beam 0/90 (SB 0/90) on cross ply with 0/90° roving orientation. SB 0/90 testing is used as a raw material control test on roving to measure resin fibre bonding.

The test is derived from ASTM D 2344 and ISO 14130.

2. Apparatus / Test equipment

- Water cooled diamond cutting machine. Cutting blade is a of fine grade quality.
- Testing machine: UTM equipped with a 3-point bending equipment. Reference ASTM 2344.
- Data logging system to measure the applied load at shear or failure.
- Vernier calliper suitable for measuring the dimensions within 0.01 mm.

3. Test Specimens

3.1 Sampling

The cross ply is made up of roving layers alternately in 0° direction and in 90° direction:

[0 / 90 / 0 / 90 / 0 / 90 / 0 / 90 / 0 /90 / 0]

Crack initiation will start at the layers in the 90° direction during the test. Layers in 0° direction have a supporting function. For specimen subjected to SB 0/90 testing the following is applicable:

- For specimen produced with Epikote 828 / IPD + Ethacure 100,
  Tg1 shall be between 130-140 °C.
  Tg2 shall be according WS QAC W001.
- SB 0/90 specimens are cut from a cross ply, parallel to the roving layers in 0° direction. See fig.1.
- SB 0/90 specimen thickness is preferable between 4 and 6 mm. Other thicknesses may be tested in accordance with this Test Method.

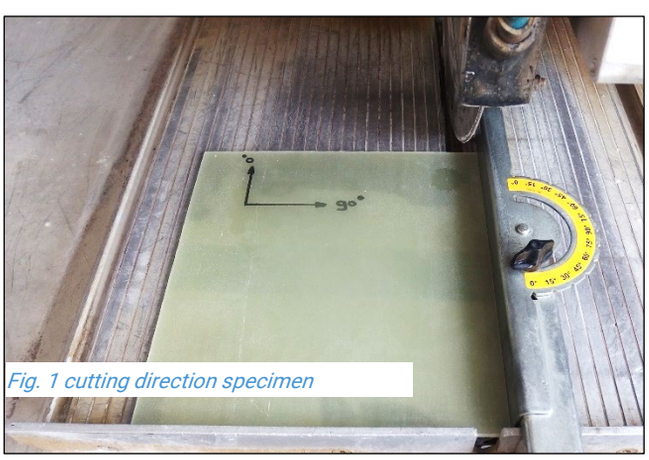

Fig. 1 cutting direction specimen

3.2 Sample cutting dimensions

SB 0/90 short beam testing requires the following specimen configuration for:

T x W x Beam x L

- T = Thickness test sample
- W = Specimen width = Thickness x 3 (ASTM 2344 = x 2 [1)])
- L = Specimen length[2)] = Thickness x 6
- Beam = Beam Span Length = Thickness x 4 (Deviates from ISO 14130)

The number of test specimen per pipe sample shall be 5 at minimum. It is recommended to cut the specimen using a cutting machine with water-cooled diamond cutting blade. The grade of diamond particles on the blade needs to be very fine.

[1)] **Note:** Specimen width shall be taken 3 x specimen thickness which deviates from ASTM 2344 Minimum width is 10 mm.

[2)] **Note:** Specimen can be cut from a plate in separate pieces where L = Thickness x 6.

Specimen can be cut from a plate as one piece. The distance (L) between the test positions shall be ≥ Thickness x 6. See figure 2.

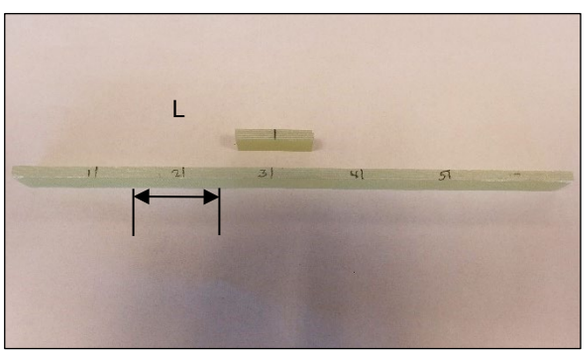

Fig. 2 Distance (L) between test positions

3.3 Test fixture (Example)

- Specimen thickness (T) : 4.6 mm
- Specimen width (W) : 13.8 mm (3 x T)
- Specimen length (L) : min. 27.6 mm (6 x T)
  (L = min. 27.6 mm between test positions when specimen is cut from a plate as one piece, see fig. 2)

- Beam span length : 18.4 mm (4 x T)
- Test speed : 1 mm per minute
- Loading Nose and Supports, as per ASTM 2344, shall be 6.0 mm and 3.0 mm diameter cylinders
  respectively. Or as per ISO 14130 Loading Nose and supports shall be 10.0 mm and 4.0 mm diameter cylinders respectively. See fig. 4.

3.4 Apparatus

- UTM Testing machine, properly calibrated, operating at a constant rate of crosshead motion. See figure 3.

  Error in the loading shall not exceed +/- 1%.

  Equipment loaded by compression mode. See figure 4

- Data logging system in N.
- Vernier calliper or micrometre suitable for measuring the dimensions within 0.01 mm.

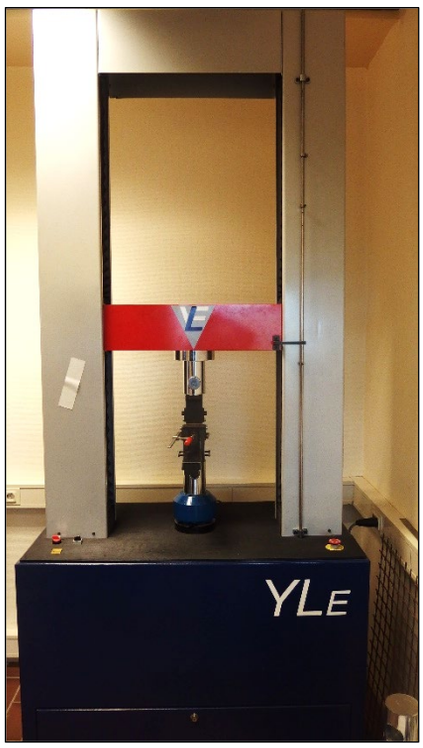

Fig. 3 Universal Testing Machine (UTM)

3.5 Conditioning

- The temperature in the laboratory test room shall be 23 °C ± 2 °C.

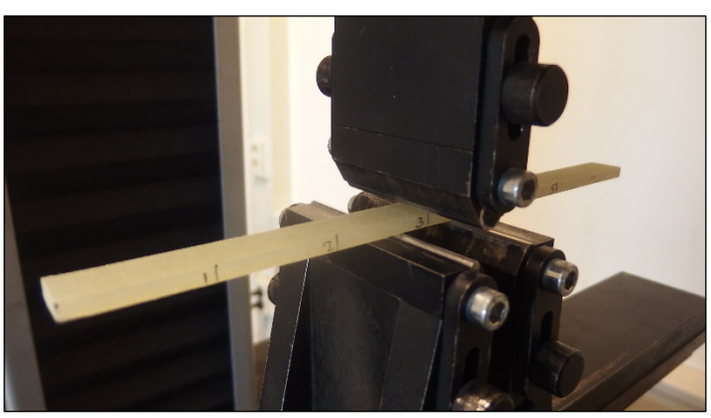

Fig. 4 Equipment for compression

4. Preparation

- Condition the test specimen at 23 °C ± 2 °C for a minimum of 2 hours.
- Reset the load sensor to zero.
- The crosshead movement speed should be set at 1 mm/min.

5. Procedure

- Measure and record the width and thickness of the test specimen at the specimen centre (loading nose position), to an accuracy of 0.01 mm. Thickness is measured at both sides. Take the mean value of both measurements as actual specimen thickness. Do not use specimens having a variation in thickness more than 0.2 mm.

- Centre the loading nose between the supports. Align the loading nose parallel to the supports. See figure 5.

- Align and centre the specimen such that its longitudinal axis is perpendicular to the loading nose and side supports, in accordance with ASTM 2344.
  See figure 6.

- Move the loading nose slowly to the supports until just above the specimen.

- Enter the relevant data in the input menu of the UTM.

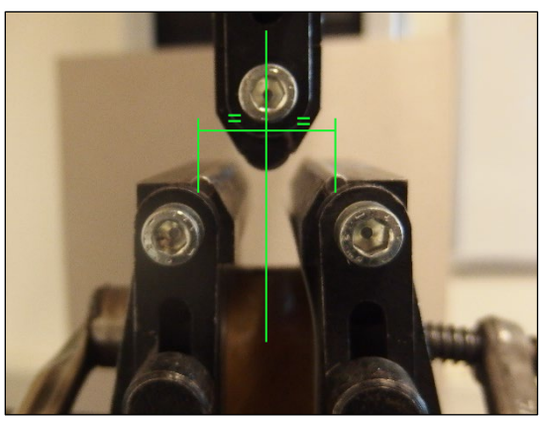

Fig. 5 centered and aligned load nose

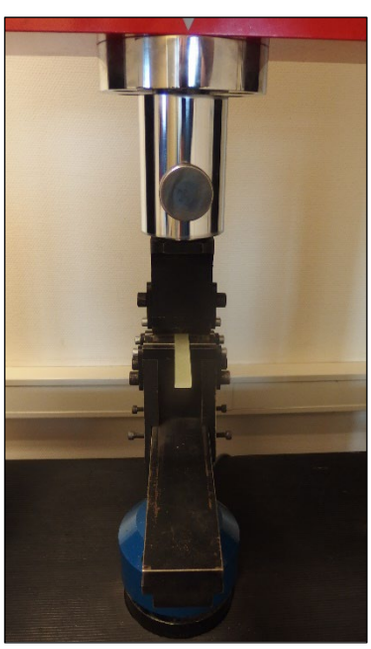

Fig. 6 centered and aligned specimen

Apply load to the specimen at the specified rate while recording data. Continue loading either of the following occurs:

- A load drop-off of 30%.
- Two-piece failure.
- The head travel exceeds the thickness of the specimen.

Record load versus crosshead displacement data throughout the test method. Record the maximum load and if required the final load, and the load at any obvious discontinuities in the load-displacement data.

Typical failure modes that can be identified visually and shall be included in the report are:

- Interlaminar Shear.
- Delamination in the specimen between the layers. See fig. 7.

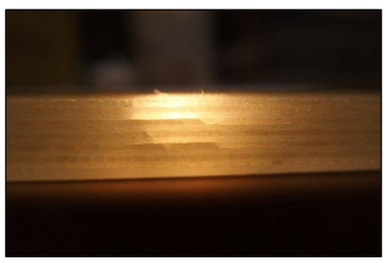

Fig. 7 Interlaminar shear

- Flexure by compression.
  Top side specimen. See fig. 8.

  (Example is a woven fabric laminate)

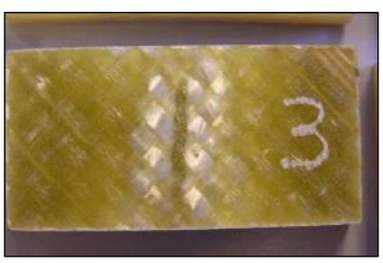

Fig. 8 Flexure by compression

- Cracking or breaking by tension.
  Back side specimen. See fig. 9.

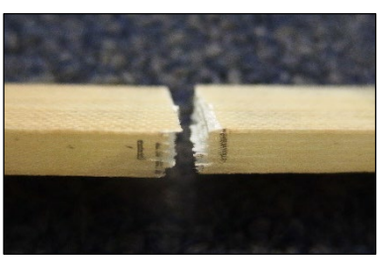

Fig. 9 Breaking by tension

Calculate the SB 0/90 strength using the formula given below:

$$\text{SB 0/90 strength} = 0.75 \cdot \frac{Pm}{T \cdot W}$$

Where:

SB 0/90 = short beam 0/90 strength (N/mm^2)

Pm = maximum load observed during the test (N)

T = measured thickness of the test specimen (mm)

W = measured width of the test specimen (mm)

- Calculate the average SB 0/90 strength from the individual results of 5 specimens.
- Measure and record the test temperature.

6. Report

The test report shall include the following particulars:

- Identification of the tested specimen.
- The thickness and width of each specimen.
- SB 0/90 strength of each specimen in N/mm^2 and the average of all the specimens and the standard deviation.
- Test temperature.

7. Reference documents

ASTM D 2344: Standard Test Method for Short-Beam Strength of Polymer Matrix Composite materials and Their Laminates.

ISO 14130: Fibre-reinforced plastic composites. Determination of apparent interlaminar shear strength by Short-Beam method.

Appendix 5 Procedure of polishing of GRE and CFRE samples

Preparation epoxy resin

1. Weight the resin and hardener in the mass ratio resin:hardener 25:3. Note that 50 grams:6 grams was just not enough for six samples.
2. Mix the components with a wooden spatula.
3. Use the degassing system (Stuers Citovac) to extract the air bubbles from the mixture.

Cutting sample for microscopy

1. Label embedding cups and add the corresponding sample
2. Use the saw to cut approx. 1-centimeter sample pieces (see figure below).

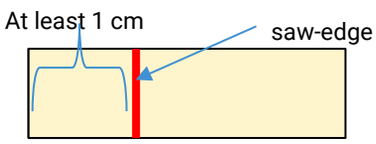

3. Dry the samples and the cups with a tissue.

Embedding samples in epoxy

1. Pour a thin layer of the resin mixture into each cup (see figure below)
2. Press the 1 cm piece of composite with the saw-edge up in the thin layer of resin.

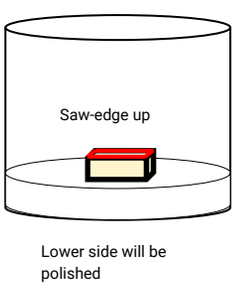

3. Cover the sample with resin
4. Place the samples in the desiccator.
5. Remove the samples from the cups after **at least** 24 hours.

Sanding and polishing

First sand the samples by hand gradually from a coarse grain (grain size 68 µm) to a medium grain (grain size 18 µm). The quality of every sanding step is checked using an optical microscope with a magnification of 4x. In case the surface shows sanding stripes in only one direction, the step is repeated until sanding stripes are evenly spread in all directions. Afterwards the samples are polished with the polishing machine from a medium grain (grain size 18 µm) to a fine grain (grain size 1 µm).

Sanding by hand

The table below shows the required sanding papers for the manual steps. Each step reduces the grain size by a factor of 2 approximately.

Table 1 Grain sizes – manual sanding

ISO number	Average particle diameter [µm]
P220	68
P500	30
P1000	18

Hint: Renew the sanding paper after three samples.

Steps:

1. Insert a P220 sanding paper in the sanding machine. Let the tap run to cover the paper with water. Grind the edge of the bottom (analysis side) in order to remove sharp edges. Sand all samples with this paper and check the quality using the optical microscope. Repeat followed by the P500 and the P1000 polishing paper in the following way:
2. **Gently** press the sample onto the rotating polishing paper. Rotate the samples 90 ° (quarter turn) clockwise and move the sample from the inside to the outside as shown in the figure. If the polishing paper turns white, you press too hard.

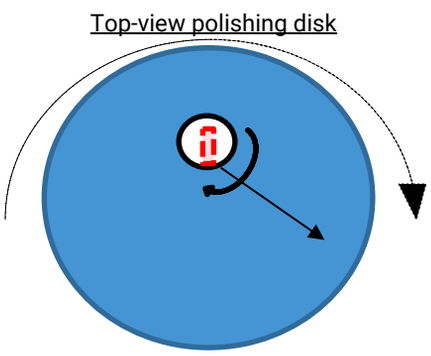

Polishing machine steps

1. Continue in the polishing machine with a polishing disc with grain size 9 µm.
2. Use a diamond suspension as polishing liquid.
3. After each polishing step, clean the samples with demineralised water and cotton wool (a new cotton wool for each sample). Clean the polishing disc with demineralised water and a brush. Clean the sample carousel holder with demi water and a brush.
4. Repeat the steps 1-3, but now for grain size 3 µm and 1 µm.
5. Rinse the "analysis side" of the samples with ethanol and dry it with a hairdryer.

Grain size [µm]	Disc	Diamond suspension	Disc rotation [rpm]	Sample holder speed [rpm]	Force single sample / sample holder	Duration [min]
9	MD-allegro magnetic disc	Struers Diapro Allegro/Largo 9 µm	150	140 (same turning direction as disc)	30 N / 180 N	5
3	MD-Dac 3 µm magnetic disc	Struers Diapro Dac 3 µm	150	140 (same turning direction as disc)	30 N / 180 N	5
1	MD-Dac 1 µm magnetic disc	Struers Dia Duo 1 µm	150	140 (same turning direction as disc)	10 N / 60 N	5

Appendix 6 Procedure of microscopic analysis method using the EVOS microscope

- Polished samples (appendix 5) were raster-scanned with the EVOS in a six-wells plate holder.
- The dimensions of 10 samples were measured using a calliper to determine area of the sample surface. All values were averaged what resulted in an area of 75 mm^2.
- The number of cracks was counted by scanning the layers per sample as schematically shown below.

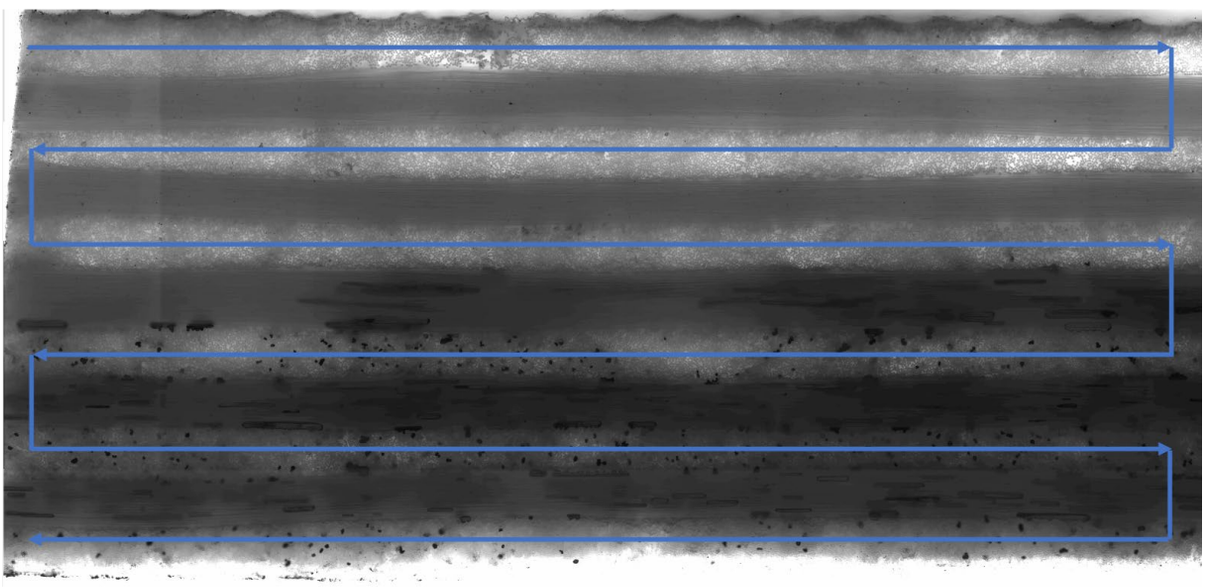

- In order to determine the number of point defects, an area of 300x300 px was magnified and the point defects were counted in that area. This area is 0.035 mm^2.

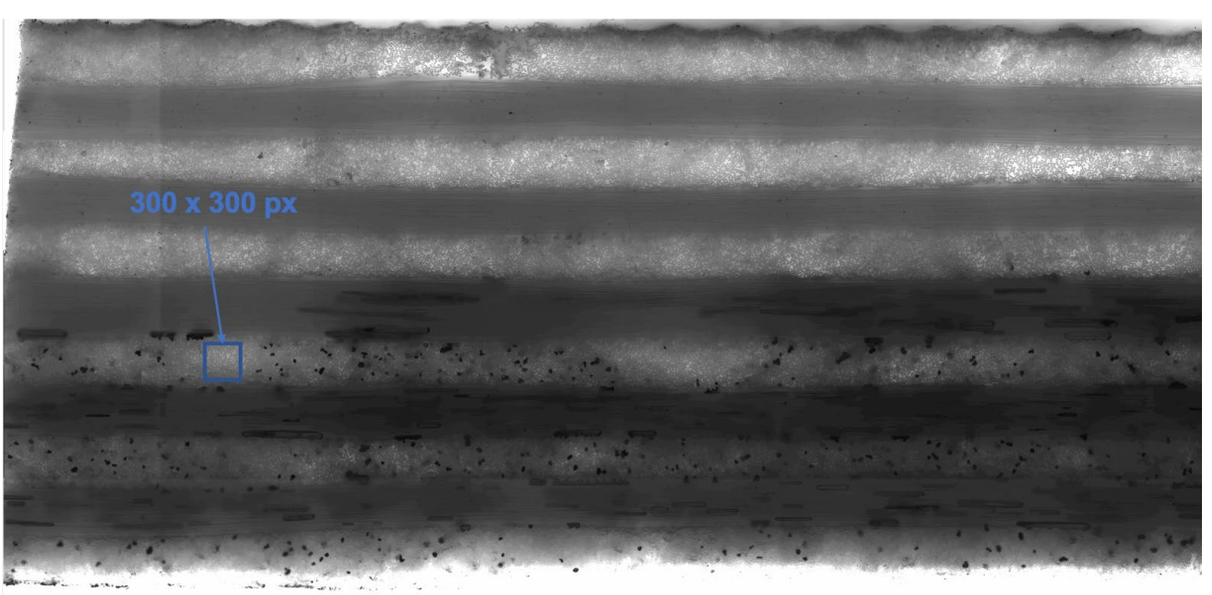

Appendix 7 Numerical test data of UEWS, ATS and SB 0/90 research rovings.

UEWS *roving type*		*hardener*	**dry** *0 hours (MPa)*	**wet 80 °C** *1500 hr (MPa)*
SUP3 GF1-A	Fresh	MDA	180	130
SUP3 GF1-A	Aged	MDA	100	n/a
SUP3 GF1-A	Aged	IPD	50	n/a
SUP3 GF1-B	Fresh	MDA	188	140
SUP3 GF1-B	Fresh	MDA	200	160
SUP1 GF2	Fresh	MDA	200	180
SUP1 GF2	Fresh	IPD	210	190
SUP1 GF2	Aged	MDA	210	195
SUP1 GF2	Aged	IPD	220	210
SUP2 GF3-A	Fresh	MDA	181	170
SUP2 GF3-A	Fresh	IPD	207	190
SUP2 GF3-A	Aged	MDA	180	188
SUP2 GF3-A	Aged	IPD	200	180
SUP2 GF3-B	Fresh	Basf 072#23	220	210
SUP2 GF3-B	Fresh	IPD	260	220
SUP3 GF4	Fresh	MDA	185	180
SUP3 GF4	Fresh	IPD	205	200
SUP3 GF4	Aged	MDA	160	140
SUP3 GF4	Aged	IPD	175	175

Ageing fingerprint rovings *roving type*	*storage*
SUP3 GF1-A Aged	6 months Abu Dhabi
SUP1 GF2 Aged	oven, 6 weeks 48 °C
SUP2 GF3-A Aged	oven, 6 weeks 48 °C
SUP3 GF4 Aged	oven, 6 weeks 48 °C

ATS on pipe *roving type*		*hardener*	**initial** *0 hours (MPa)*	**hot-wet 80°C** *1500 hr (MPa)*
SUP3 GF1-A	Fresh	MDA	68.5	48.9
SUP3 GF1-A	Aged	MDA	55.1	
SUP3 GF1-A	Aged	IPD	41.6	
SUP3 GF1-B	Fresh	MDA	65.5	54.5
SUP3 GF1-B	Fresh	MDA	65.5	52.2
SUP1 GF2	Fresh	MDA	68.1	56.1
SUP1 GF2	Fresh	IPD	71.7	57.5
SUP1 GF2	Aged	MDA	65.6	57.7
SUP1 GF2	Aged	IPD	68.9	57.6
SUP2 GF3-A	Fresh	MDA	72.9	61.1
SUP2 GF3-A	Fresh	IPD	73.4	63.4
SUP2 GF3-A	Aged	MDA	68.6	59.6
SUP2 GF3-A	Aged	IPD	68.1	59.9
SUP2 GF3-B	Fresh	Basf 072#23	84.7	73.4
SUP2 GF3-B	Fresh	IPD	83.4	74.9
SUP3 GF4	Fresh	MDA	69.2	69.6
SUP3 GF4	Fresh	IPD	70.0	64.3
SUP3 GF4	Aged	MDA	59.4	60.5
SUP3 GF4	Aged	IPD	59.5	57.0

ATS on strip *roving type*		*hardener*	**initial** *0 hours (MPa)*	**hot-wet 80°C** *1500 hr (MPa)*	**hot-wet 100°C** *250 hr (MPa)*	**hot-wet 100°C** *500 hr (MPa)*
SUP1 GF2	Fresh	MDA	68.2	60.5	61.0	60.9
SUP1 GF2	Fresh	IPD	70.0	58.4	57.6	56.9
SUP1 GF2	Aged	MDA	68.5	59.2	60.9	59.8
SUP1 GF2	Aged	IPD	73.9	59.8	60.1	60.4
SUP2 GF3-A	Fresh	MDA	71.1	63.7	66.6	66.1
SUP2 GF3-A	Fresh	IPD	75.4	63.6	69.6	68.4
SUP2 GF3-A	Aged	MDA	71.8	64.5	66.5	59.4
SUP2 GF3-A	Aged	IPD	70.9	62.6	64.3	63.7
SUP2 GF3-B	Fresh	Basf 072#23	82.2	n/a	70.9	69.4
SUP2 GF3-B	Fresh	IPD	80.9	n/a	73.5	72.5
SUP3 GF4	Fresh	MDA	71.9	70.9	68.8	70.5
SUP3 GF4	Fresh	IPD	69.9	68.4	67.0	65.6
SUP3 GF4	Aged	MDA	58.2	63.1	59.4	56.4
SUP3 GF4	Aged	IPD	59.3	58.3	57.1	57.2

Short Beam 0-90			initial	average	hot-wet 100°C	average
roving type		*hardener*	*0 hours (MPa)*		*250 hr (MPa)*	
SUP1 GF1	Fresh	Detda & IPD	64.7	63.6	31.7	32.1
SUP1 GF1	Fresh	Detda & IPD	62.4		32.4	
SUP1 GF1	Aged	Detda & IPD	52.8	50.4	36.1	35.0
SUP1 GF1	Aged	Detda & IPD	47.9		33.9	
SUP1 GF2	Fresh	Detda & IPD	63.9	61.8	31.8	32.4
SUP1 GF2	Fresh	Detda & IPD	59.7		32.9	
SUP1 GF2	Aged	Detda & IPD	61.3	62.3	37.4	37.2
SUP1 GF2	Aged	Detda & IPD	63.3		36.9	
SUP2 GF3	Fresh	Detda & IPD	63.3	62.6	52.4	53.3
SUP2 GF3	Fresh	Detda & IPD	63.5		53.2	
SUP2 GF3	Fresh	Detda & IPD	60.9		54.2	
SUP2 GF3	Aged	Detda & IPD	58.3	60.3	58.1	56.9
SUP2 GF3	Aged	Detda & IPD	62.3		55.7	
SUP3 GF4	Fresh	Detda & IPD	59.6	58.7	46.8	46.6
SUP3 GF4	Fresh	Detda & IPD	57.8		46.3	
SUP3 GF4	Aged	Detda & IPD	53.7	54.6	47.1	46.7
SUP3 GF4	Aged	Detda & IPD	55.4		46.3	

Short Beam 0-90, hot-wet		initial	average	hot-wet 100°C	average	hot-wet 115°C	average	hot-wet 125°C	average
roving type		*0 hours (MPa)*		*250 hr (MPa)*		*250 hr (MPa)*		*250 hr (MPa)*	
SUP1 GF1	Fresh	64.7	63.6	31.7	32.1	24.8	25.5	24.0	24.7
SUP1 GF1	Fresh	62.4		32.4		26.2		25.4	
SUP1 GF1	Aged	52.8	50.4	36.1	35.0	27.1	27.4	24.6	24.1
SUP1 GF1	Aged	47.9		33.9		27.7		23.5	
SUP1 GF2	Fresh	63.9	61.8	31.8	32.4	27.2	28.0	27.2	26.8
SUP1 GF2	Fresh	59.7		32.9		28.8		26.4	
SUP1 GF2	Aged	61.3	62.3	37.4	37.2	29.5	29.4	30.0	29.7
SUP1 GF2	Aged	63.3		36.9		29.3		29.3	
SUP2 GF3	Fresh	63.3	62.6	52.4	53.3	44.5	45.9	42.6	42.6
SUP2 GF3	Fresh	63.5		53.2		47.0		42.1	
SUP2 GF3	Fresh	60.9		54.2		46.2		43.2	
SUP2 GF3	Aged	58.3	60.3	58.1	56.9	48.6	48.9	44.1	39.5
SUP2 GF3	Aged	62.3		55.7		49.2		34.9	
SUP3 GF4	Fresh	59.6	58.7	46.8	46.6	42.4	40.5	40.8	36.2
SUP3 GF4	Fresh	57.8		46.3		38.5		31.5	
SUP3 GF4	Aged	53.7	54.6	47.1	46.7	37.0	36.6	37.7	37.0
SUP3 GF4	Aged	55.4		46.3		36.2		36.2	
SUP3 GF5	Fresh	61.5	64.7	46.6	47.3	40.8	39.3	36.1	37.2
SUP3 GF5	Fresh	67.8		47.9		37.7		38.2	
SUP3 GF5	Aged	61.9	63.0	45.6	45.9	37.5	35.9	33.1	34.1
SUP3 GF5	Aged	64.1		46.1		34.2		35.0	
SUP3 GF6	Fresh	56.1	55.5	45.9	43.1	33.1	31.5	28.2	28.8
SUP3 GF6	Fresh	54.9		40.3		29.9		29.4	
SUP3 GF6	Aged	55.3	57.9	41.4	42.3	28.8	30.3	30.1	30.6
SUP3 GF6	Aged	60.5		43.2		31.8		31.1	
SUP4 GF7	Fresh	52.7	55.1	39.0	40.6	33.6	34.0	30.9	31.6
SUP4 GF7	Fresh	55.3		44.5		36.1		31.0	
SUP4 GF7	Fresh	57.3		38.2		32.3		32.9	
SUP4 GF7	Aged	44.4	41.2	34.8	35.9	28.5	28.3	25.2	24.6
SUP4 GF7	Aged	38.0		37.0		28.0		24.0	
SUP5 GF8	Fresh	60.4	59.8	49.0	48.4	40.5	39.2	38.4	39.0
SUP5 GF8	Fresh	59.1		47.8		37.9		39.5	
SUP5 GF8	Aged	58.8	58.6	49.7	49.6	43.2	42.7	37.7	38.8
SUP5 GF8	Aged	58.4		49.4		42.2		39.8	

Appendix 8 Numerical test data of SB 0/90 rovings.

Short Beam 0/90, after drying		dried after hot-wet 100°C	average	dried after hot-wet 115°C	average	dried after hot-wet 125°C	average
roving type		*1 wk 80 °C (MPa)*		*1 wk 80 °C (MPa)*		*1 wk 80 °C (MPa)*	
SUP1 GF1	Fresh	41.5	41.1	32.9	31.8	31.5	31.8
SUP1 GF1	Fresh	40.6		30.6		32.0	
SUP1 GF1	Aged	43.8	44.7	33.4	33.4	31.9	32.3
SUP1 GF1	Aged	45.6		33.4		32.7	
SUP1 GF2	Fresh	37.3	41.2	33.5	34.3	31.2	31.5
SUP1 GF2	Fresh	45.0		35.1		31.7	
SUP1 GF2	Aged	46.8	46.3	33.6	34.2	33.3	33.7
SUP1 GF2	Aged	45.7		34.7		34.0	
SUP2 GF3	Fresh	54.9		41.8		40.9	
SUP2 GF3	Fresh	54.3	54.8	47.1	44.6	42.0	41.7
SUP2 GF3	Fresh	55.1		44.9		42.1	
SUP2 GF3	Aged	59.3	58.0	43.9	47.1	40.3	41.9
SUP2 GF3	Aged	56.7		50.2		43.5	
SUP3 GF4	Fresh	48.0	49.0	37.5	37.9	37.4	34.3
SUP3 GF4	Fresh	49.9		38.2		31.2	
SUP3 GF4	Aged	47.4	46.8	41.0	41.3	42.4	40.8
SUP3 GF4	Aged	46.1		41.6		39.1	
SUP3 GF5	Fresh	49.0	47.3	34.0	36.8	38.7	37.8
SUP3 GF5	Fresh	45.6		39.6		36.8	
SUP3 GF5	Aged	49.6	49.8	38.0	38.0	35.1	34.6
SUP3 GF5	Aged	49.9		38.0		34.1	
SUP3 GF6	Fresh	41.5	40.6	30.3	31.3	28.7	29.8
SUP3 GF6	Fresh	39.7		32.3		30.8	
SUP3 GF6	Aged	41.9	41.6	32.7	32.6	31.5	32.3
SUP3 GF6	Aged	41.3		32.5		33.1	
SUP4 GF7	Fresh	42.5		34.9		32.0	
SUP4 GF7	Fresh	45.5	44.0	33.0	34.1	31.2	32.0
SUP4 GF7	Fresh	44.1		34.3		32.7	
SUP4 GF7	Aged	35.7	35.9	30.8	29.2	42.0	41.2
SUP4 GF7	Aged	36.1		27.5		40.3	
SUP5 GF8	Fresh	52.1	51.5	39.7	39.6	37.2	37.1
SUP5 GF8	Fresh	50.9		39.5		36.9	
SUP5 GF8	Aged	48.7	49.8	42.2	42.1	27.4	27.7
SUP5 GF8	Aged	50.8		41.9		27.9	

Appendix 9 Numerical test data SB 0/90 long term exposure to 121 °C (250 °F) water.

Short Beam 0-90 *roving type*		**initial** *0 hours (MPa)*	**hot-wet 121°C** *500 hrs (MPa)*	**hot-wet 121°C** *1000 hrs (MPa)*	**hot-wet 121°C** *3000 hrs (MPa)*	**hot-wet 121°C** *5000 hrs (MPa)*
SUP1 GF1	Fresh	64.7	21.6	20.3	18.8	19.2
SUP1 GF1	Aged	52.8	23.2	22.7	19.8	20.1
SUP1 GF2	Fresh	63.9	26.2	23.5	18.6	18.1
SUP1 GF2	Aged	63.3	26.0	25.9	19.8	19.0
SUP2 GF3	Fresh					
SUP2 GF3	Aged	62.3	38.2	35.2	23.5	21.4
SUP3 GF4	Fresh	59.6	38.5	32.8	17.9	17.4
SUP3 GF4	Aged	55.4	31.5	30.1	20.7	17.3
SUP3 GF5	Fresh					
SUP3 GF5	Aged	61.9	31.7	28.5	23.4	22.2
SUP3 GF6	Fresh	54.9	28.0	27.9	23.8	23.1
SUP3 GF6	Aged	60.5	29.1	24.5	18.7	16.6
SUP4 GF7	Fresh	52.7	28.3	24.3	17.3	15.0
SUP4 GF7	Aged					
SUP5 GF8	Fresh	60.4	38.4	34.2	23.8	22.8
SUP5 GF8	Aged	54.0	34.3	33.0	24.7	22.5

Appendix 10 Numerical test data SB 0/90 carbon tow and selected roving.

Short Beam 0-90 *roving type*		**initial** *0 hours (MPa)*	**average** *(MPa)*	**hot-wet 100°C** *250 hr (MPa)*	**average** *(MPa)*	**hot-wet 150°C** *250 hr (MPa)*	**average** *(MPa)*
SUP6 CF1	Fresh	44.8	44.8	36	36	21.9	21.9
SUP6 CF1	Fresh	44.1	41.2	38.8	35.6	24.5	23.7
SUP6 CF1	Fresh	38.2		32.3		22.8	
SUP6 CF1	Aged	40.7	44.1	36.1	40.1	22.5	22.2
SUP6 CF1	Aged	47.5		44.1		21.8	
SUP6 CF1	Fresh	39.8	39.8	44.6	44.6	24.4	24.4
SUP2 GF3	Fresh	59.8	59.8	57.2	57.2	12.2	12.2

Appendix 11 Graphical data on crack and point defect numbers of glass-matrix systems after ageing and hot-wet exposure, research rovings.

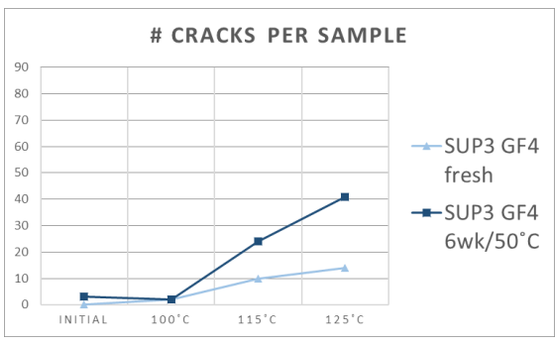

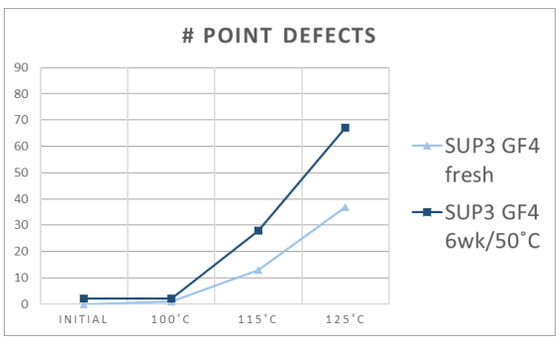

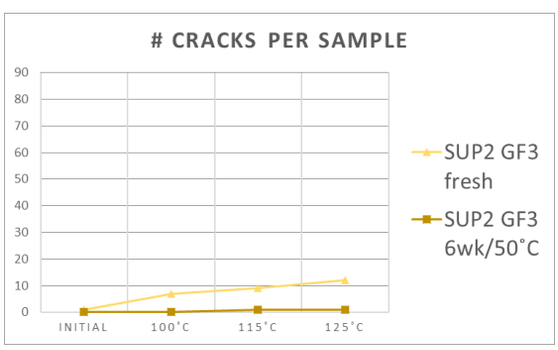

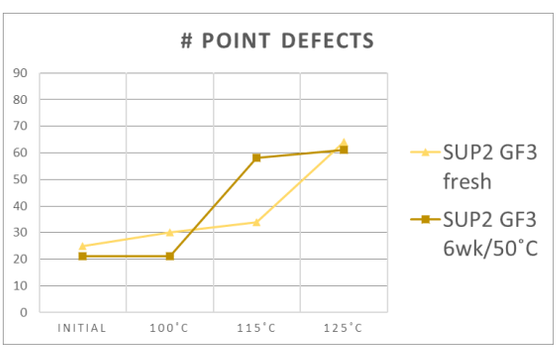

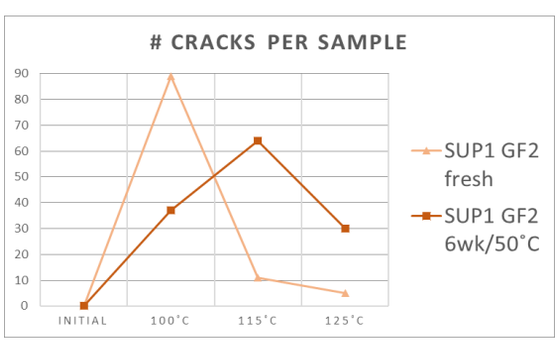

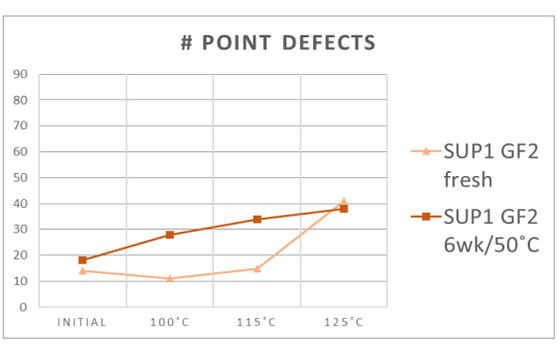

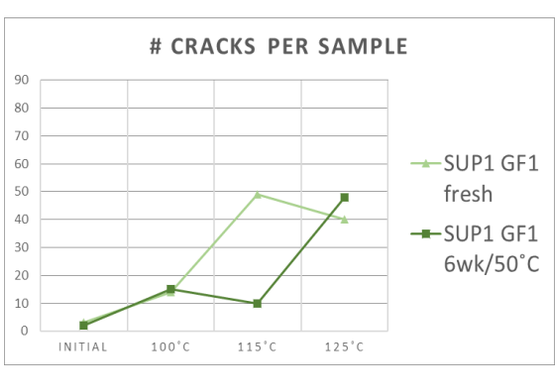

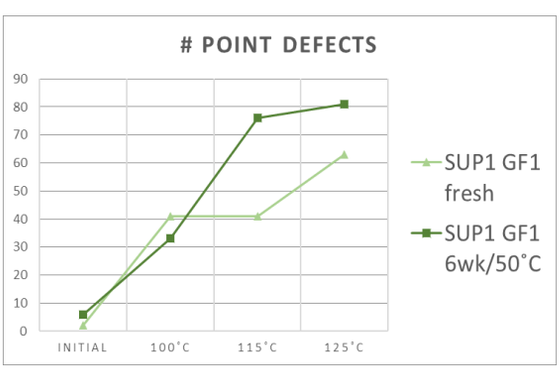

Appendix 12 Graphical data on crack and point defect numbers of glass-matrix systems after ageing and hot-wet exposure for 250 hours, test rovings.

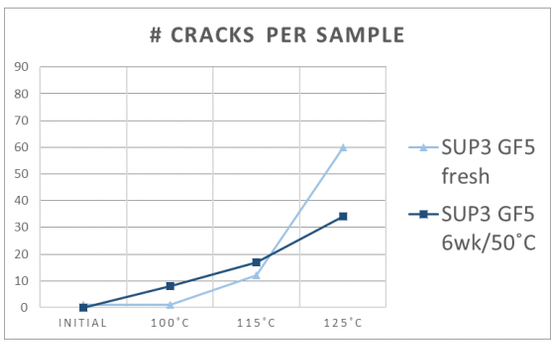

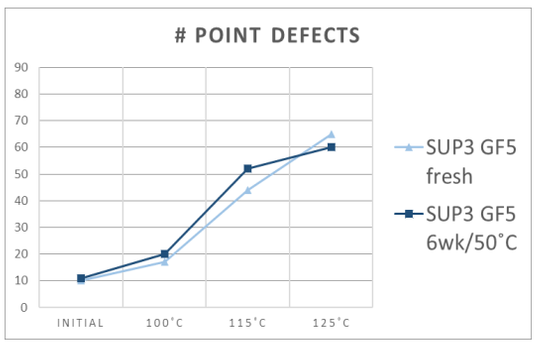

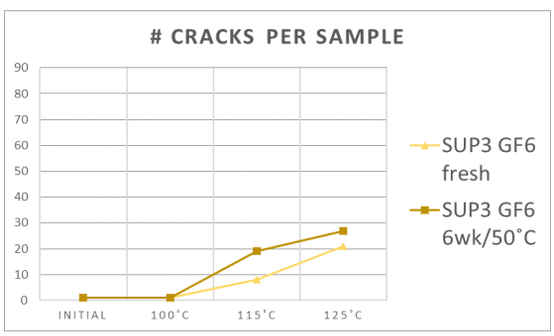

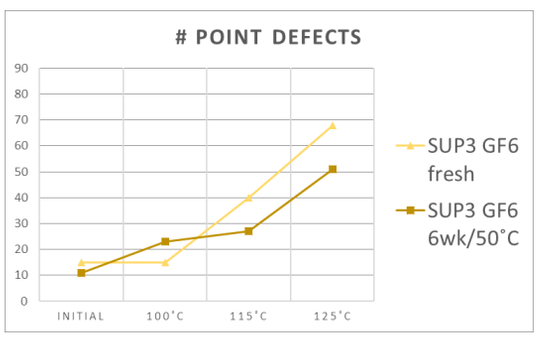

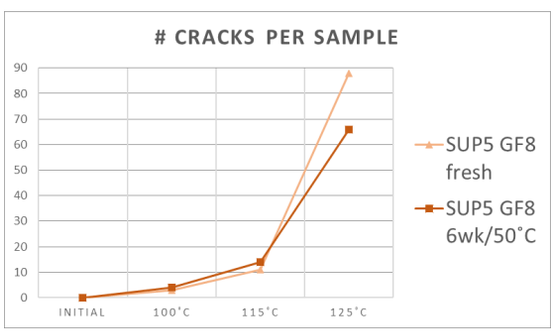

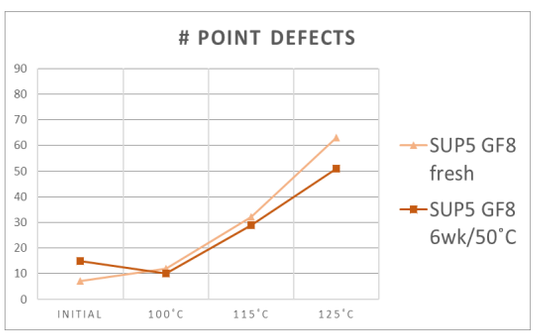

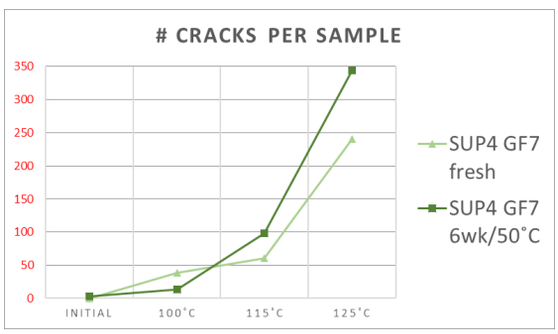

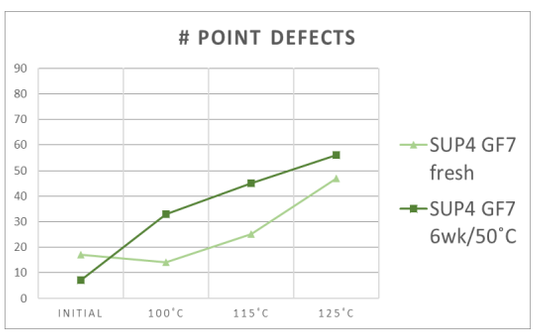

Appendix 13 Graphical data on crack and point defect numbers of glass-matrix systems after long term exposure to 121 °C (250 °F) water.

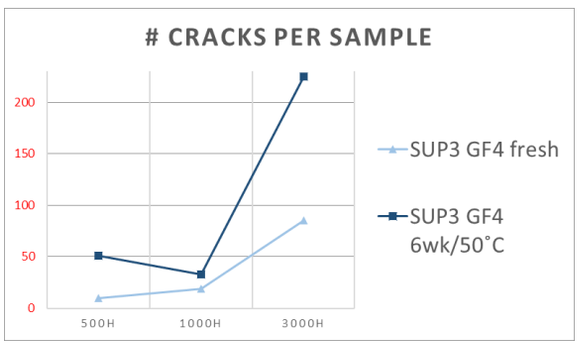

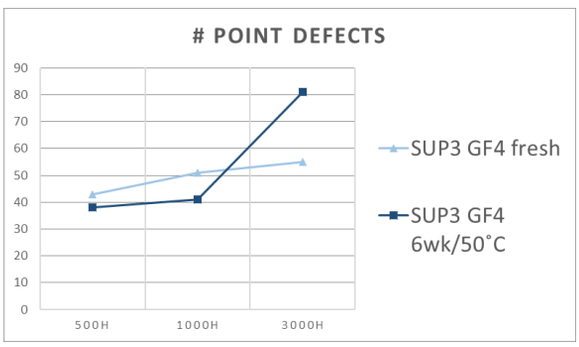

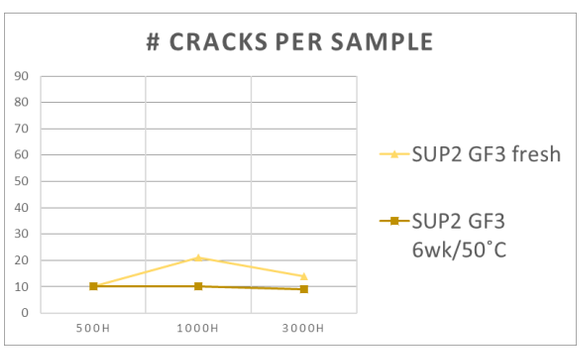

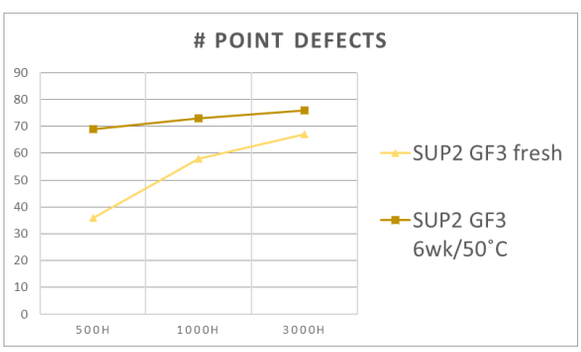

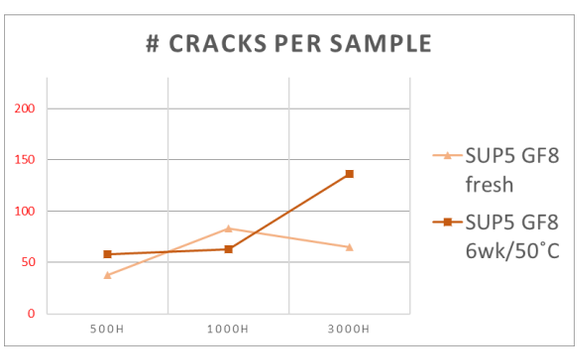

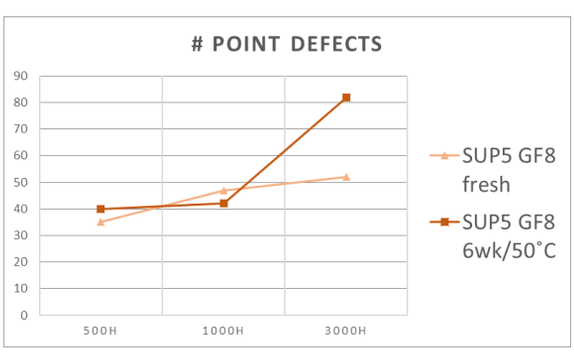

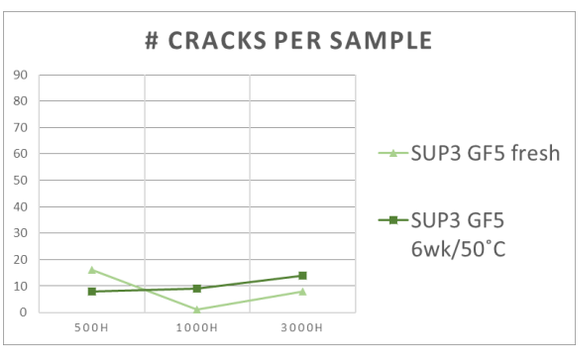

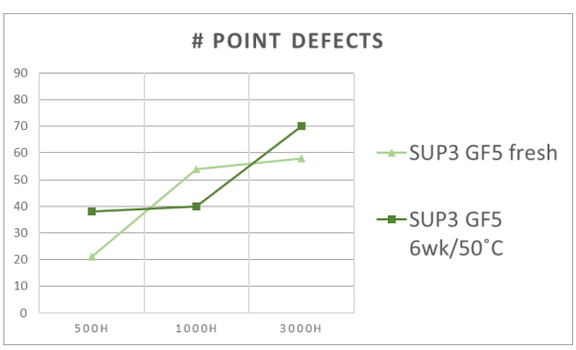

Appendix 14 Overview stitched EVOS optical microscope images

The stitched microscope images obtained with the EVOS are available via Future Pipe Industries BV or via the Saxion Research Cloud. For more information please contact k.rookus@futurepipe.com.

Test series 1:

Sample name	Roving ageing	Hot/wet conditions	EVOS data file name
SUP3 GF4	fresh	initial	s1_104_initial.TIF
	6 weeks @ 50 ˚C	initial	s1_96_initial.TIF
	fresh	250 hours @ 100 ˚C	s1_104_100.TIF
	6 weeks @ 50 ˚C	250 hours @ 100 ˚C	s1_96_100.TIF
	fresh	250 hours @ 115 ˚C	s1_104_115.TIF
	6 weeks @ 50 ˚C	250 hours @ 115 ˚C	s1_96_115.TIF
	fresh	250 hours @ 125 ˚C	s1_104_125.TIF
	6 weeks @ 50 ˚C	250 hours @ 125 ˚C	s1_96_125.TIF
SUP2 GF3	fresh	initial	s1_99_initial.TIF
	6 weeks @ 50 ˚C	initial	s1_120_initial.TIF
	fresh	250 hours @ 100 ˚C	s1_99_100.TIF
	6 weeks @ 50 ˚C	250 hours @ 100 ˚C	s1_120_100.TIF
	fresh	250 hours @ 115 ˚C	s1_99_115.TIF
	6 weeks @ 50 ˚C	250 hours @ 115 ˚C	s1_120_115.TIF
	fresh	250 hours @ 125 ˚C	s1_99_125.TIF
	6 weeks @ 50 ˚C	250 hours @ 125 ˚C	s1_120_125.TIF
SUP1 GF2	fresh	initial	s1_106_initial.TIF
	6 weeks @ 50 ˚C	initial	s1_112_initial.TIF
	fresh	250 hours @ 100 ˚C	s1_106_100.TIF
	6 weeks @ 50 ˚C	250 hours @ 100 ˚C	s1_112_100.TIF
	fresh	250 hours @ 115 ˚C	s1_106_115.TIF
	6 weeks @ 50 ˚C	250 hours @ 115 ˚C	s1_112_115.TIF
	fresh	250 hours @ 125 ˚C	s1_106_125.TIF
	6 weeks @ 50 ˚C	250 hours @ 125 ˚C	s1_112_125.TIF
SUP1 GF1	fresh	initial	s1_103_initial.TIF
	6 weeks @ 50 ˚C	initial	s1_109_initial.TIF
	fresh	250 hours @ 100 ˚C	s1_103_100.TIF
	6 weeks @ 50 ˚C	250 hours @ 100 ˚C	s1_109_100.TIF
	fresh	250 hours @ 115 ˚C	s1_103_115.TIF
	6 weeks @ 50 ˚C	250 hours @ 115 ˚C	s1_109_115.TIF
	fresh	250 hours @ 125 ˚C	s1_103_125.TIF
	6 weeks @ 50 ˚C	250 hours @ 125 ˚C	s1_109_125.TIF

Test series 2:

Sample name	Roving ageing	Hot/wet conditions	EVOS data file name
SUP3 GF5	fresh	initial	s2_116_initial.TIF
	6 weeks @ 50 ˚C	initial	s2_114_initial.TIF
	fresh	250 hours @ 100 ˚C	s2_116_100.TIF
	6 weeks @ 50 ˚C	250 hours @ 100 ˚C	s2_114_100.TIF
	fresh	250 hours @ 115 ˚C	s2_116_115.TIF
	6 weeks @ 50 ˚C	250 hours @ 115 ˚C	s2_114_115.TIF
	fresh	250 hours @ 125 ˚C	s2_116_125.TIF
	6 weeks @ 50 ˚C	250 hours @ 125 ˚C	s2_114_125.TIF
SUP3 GF6	fresh	initial	s2_110_initial.TIF
	6 weeks @ 50 ˚C	initial	s2_128_initial.TIF
	fresh	250 hours @ 100 ˚C	s2_110_100.TIF
	6 weeks @ 50 ˚C	250 hours @ 100 ˚C	s2_128_100.TIF
	fresh	250 hours @ 115 ˚C	s2_110_115.TIF
	6 weeks @ 50 ˚C	250 hours @ 115 ˚C	s2_128_115.TIF
	fresh	250 hours @ 125 ˚C	s2_110_125.TIF
	6 weeks @ 50 ˚C	250 hours @ 125 ˚C	s2_128_125.TIF
SUP5 GF8	fresh	initial	s2_118_initial.TIF
	6 weeks @ 50 ˚C	initial	s2_126_initial.TIF
	fresh	250 hours @ 100 ˚C	s2_118_100.TIF
	6 weeks @ 50 ˚C	250 hours @ 100 ˚C	s2_126_100.TIF
	fresh	250 hours @ 115 ˚C	s2_118_115.TIF
	6 weeks @ 50 ˚C	250 hours @ 115 ˚C	s2_126_115.TIF
	fresh	250 hours @ 125 ˚C	s2_118_125.TIF
	6 weeks @ 50 ˚C	250 hours @ 125 ˚C	s2_126_125.TIF
SUP4 GF7	fresh	initial	s2_124_initial.TIF
	6 weeks @ 50 ˚C	initial	s2_130_initial.TIF
	fresh	250 hours @ 100 ˚C	s2_124_100.TIF
	6 weeks @ 50 ˚C	250 hours @ 100 ˚C	s2_130_100.TIF
	fresh	250 hours @ 115 ˚C	s2_124_115.TIF
	6 weeks @ 50 ˚C	250 hours @ 115 ˚C	s2_130_115.TIF
	fresh	250 hours @ 125 ˚C	s2_124_125.TIF
	6 weeks @ 50 ˚C	250 hours @ 125 ˚C	s2_130_125.TIF

Test series 3:

Sample name	Roving ageing	Hot/wet conditions	EVOS data file name
SUP3 GF5	fresh	500 hours @ 121 ˚C	s3_104_121_500.TIF
	6 weeks @ 50 ˚C	500 hours @ 121 ˚C	s3_96_121_500.TIF
	fresh	1000 hours @ 121 ˚C	s3_104_121_1000.TIF
	6 weeks @ 50 ˚C	1000 hours @ 121 ˚C	s3_96_121_1000.TIF
	fresh	3000 hours @ 121 ˚C	s3_104_121_3000.TIF
	6 weeks @ 50 ˚C	3000 hours @ 121 ˚C	s3_96_121_3000.TIF
SUP2 GF3	fresh	500 hours @ 121 ˚C	s3_99_121_500.TIF
	6 weeks @ 50 ˚C	500 hours @ 121 ˚C	s3_120_121_500.TIF
	fresh	1000 hours @ 121 ˚C	s3_99_121_1000.TIF
	6 weeks @ 50 ˚C	1000 hours @ 121 ˚C	s3_120_121_1000.TIF
	fresh	3000 hours @ 121 ˚C	s3_99_121_3000.TIF
	6 weeks @ 50 ˚C	3000 hours @ 121 ˚C	s3_120_121_3000.TIF
SUP5 GF8	fresh	500 hours @ 121 ˚C	s3_118_121_500.TIF
	6 weeks @ 50 ˚C	500 hours @ 121 ˚C	s3_125_121_500.TIF
	fresh	1000 hours @ 121 ˚C	s3_118_121_1000.TIF
	6 weeks @ 50 ˚C	1000 hours @ 121 ˚C	s3_125_121_1000.TIF
	fresh	3000 hours @ 121 ˚C	s3_118_121_3000.TIF
	6 weeks @ 50 ˚C	3000 hours @ 121 ˚C	s3_125_121_3000.TIF
SUP3 GF5	fresh	500 hours @ 121 ˚C	s3_116_121_500.TIF
	6 weeks @ 50 ˚C	500 hours @ 121 ˚C	s3_114_121_500.TIF
	fresh	1000 hours @ 121 ˚C	s3_116_121_1000.TIF
	6 weeks @ 50 ˚C	1000 hours @ 121 ˚C	s3_114_121_1000.TIF
	fresh	3000 hours @ 121 ˚C	s3_116_121_3000.TIF
	6 weeks @ 50 ˚C	3000 hours @ 121 ˚C	s3_114_121_3000.TIF

Additional tests:

Sample name	Roving ageing	Hot/wet conditions	EVOS data file name
SUP2 GF3	fresh	500 hours @ 150 ˚C	additional_134_150_500.TIF additional_134_150_500zoom.TIF
SUP6 CF1 carbon tow	fresh	500 hours @ 150 ˚C	additional_141_150_500a.TIF additional_141_150_500b.TIF
	6 weeks @ 50 ˚C	500 hours @ 150 ˚C	additional_138_150_500a.TIF additional_138_150_500b.TIF additional_138_150_500c.TIF

10. Literature

Micromechanical Modelling of the Transverse Strengths of Unidirectional Glass Fibre Reinforced Polyester.
PhD-thesis Albert ten Busschen, Delft University Press 1996
ISBN 90-407-1354-5

Prüfung von UD-Ringen. Eine neue Methode zur Charakterisierung der Glas-Harz-Kompatibilität.
28. Internationale AVK-Tagung 1997.
Albert ten Busschen

Korrosion von GFK-Laminaten: Einfluß von Aufbau, Glasfaserverstärkung und Versuchsmethode.
Erfahrungen mit GFK im Anlagenbau. 2. Tagung 1998
Albert ten Busschen

Composites – An introduction
Introductory composites book, 2015
ISBN 978-90-77812-471
R.P.L. Nijssen

Effects of aging of glass fibres on the mechanical properties of the composite pipe systems
TFF-Report, December 2016
Jan Bosch, Sander Fokkes, Jan ten Brinke, Kees Rookus, Martin Bennink

Glass Fibre Strength—A Review with Relation to Composite Recycling
Fibers 2016, 4, 18; doi:10.3390/fib4020018
James Thomason, Peter Jenkins and Liu Yang

Influence of Glass Fibre Sizing and Storage Conditions on Composite Properties
Proceedings Conference on Durability of Composites in a Marine Environment 2, 2017
Luc Peters, 3B Fibreglass

XPS and AFM study of interaction of organosilane and sizing with e-glass fibre surface
Journal of Adhesion, 84 (4). pp. 322-338. ISSN 0021-8464
Liu, X.M. and Thomason, J.L. and Jones, F.R. (2008)

Characterisation of interphase nanoscale property variations in glass fibre reinforced polypropylene and epoxy resin composites
Composites Part A: Applied Science and Manufacturing
Volume 33, Issue 4, April 2002, Pages 559-576
Shang-Lin Gao, Edith Mäder

Experimental mechanics of fiber reinforced composite materials
SEM Monograph No. 4, USA, 1984
Whitney, J.M., Daniel, I.M., Pipes, R.B.

AFM characterization of the interfacial properties of carbon fiber reinforced polymer composites subjected to hygrothermal treatments.
Composites Science and Technology
Volume 67, Issue 1, January 2007, Pages 92-101
Ying Wang, Thomas H. Hahn

11. Standards

International standards (ISO)

ISO 527 ‘Plastics – Determination of tensile properties’

Part 1: General Principles
Part 2: Test conditions for mouldings and extrusion parts
Part 3: Test conditions for films and sheets
Part 4: Test conditions for isotropic and orthotropic fibre-reinforced plastic composites
Part 5: Test conditions for unidirectional fibre-reinforced plastic composites

ISO 178 ‘Plastics – Determination of flexural properties’

ISO 3597 ‘Textile-glass-reinforced plastics – Determination of mechanical properties on rods made or roving-reinforced resin.’

Part 1: General considerations and preparation of rods
Part 2: Determination of flexural strength
Part 3: Determination of compressive strength
Part 4: Determination of apparent interlaminar shear strength

ISO 14125 ‘Fibre-reinforced Plastics – Determination of flexural properties’

ISO 14130 ‘Fibre-reinforced Plastics – Determination of the apparent shear strength by short-beam method’

ISO 14692 ‘Petroleum and natural gas industries – Glass-reinforced plastics (GRP) piping’

Part 1: Vocabulary, symbols, application and materials
Part 2: Qualification and manufacture
Part 3: System design
Part 4: Fabrication, installation and operation

American standards (ASTM)

ASTM D2344 – 00 ‘Standard Test Method for Short-Beam Strength of Polymer Matrix Composite Materials and Their Laminates.’

ASTM D2992 – 18 ‘Standard Practice for Obtaining Hydrostatic or Pressure Design Basis for ‘Fiberglas’ (Glass-Fiber-Reinforced Thermosetting Resin) Pipe and Fittings’

Professorship for Polymer Engineering

The Professorship for Polymer Engineering of University of Applied Sciences Windesheim was founded in 2009; the groep's objective is to improve the knowledge base on sustainable processing of plastics and composites within and through the higher education system. Its primary function is as a research group in Polymer Engineering, delivering output in the field of applied science. The team operates within market based projects and comprises lecturers from Civil Engineering, Industrial Product Design and Mechanical Engineering. The output of the projects is integrated into the curriculum of these study programmes.

Characterisation of Glass Fibre Reinforced Epoxy (GRE) Composites in hot/wet Conditions.

The project described in this report, was commissioned by the company Future Pipe Industries (FPI) and was funded by TechForFuture (TFF). In this project, FPI worked together with the Universities of Applied Sciences Saxion and Windesheim. The objective of the project was to investigate the long-term hot/wet performance of Glass fibre Reinforced Epoxy composites used for industrial pipe systems. A large part of the work consisted of the development of test methods for both macroscopic and microscopic level. This resulted in new test methods that were found to be as discriminative as the proven internal 'finger-print tests' of FPI, a much more elaborative test. A series of glass fibre products was evaluated both for their resistance to storage in hot environments ('thermal ageing') and to long-term hot-wet exposure up to temperatures of 125 C. Furthermore, Carbon Fibre Reinforced Epoxy (CFRP) and Glass Fibre Reinforced Epoxy (GRE) were monitored for their response to long-term hot/wet exposure up to a temperature of 150 C.

TECH FOR FUTURE

FPI FUTURE PIPE INDUSTRIES

SAXION

University of Applied Sciences Windesheim